Calhoun: The NPS Institutional Archive

DSpace Repository

Theses and Dissertations | 1. Thesis and Dissertation Collection, all items

1998-06

Human male and female biodynamic response to underwater explosion events.

Oglesby, Douglas B.

Monterey, California. Naval Postgraduate School

http://hdl.handle.net/10945/8481

Downloaded from NPS Archive: Calhoun

http://www.nps.edu/library

Calhoun is the Naval Postgraduate School's public access digital repository for research materials and institutional publications created by the NPS community. Calhoun is named for Professor of Mathematics Guy K. Calhoun, NPS's first appointed -- and published -- scholarly author.

Dudley Knox Library / Naval Postgraduate School
411 Dyer Road / 1 University Circle
Monterey, California USA 93943

NPS ARCHIVE
1998.06
OGLESBY, D.

DUDLEY KNOX LIBRARY
NAVAL POSTGRADUATE SCHOOL
MONTEREY CA 93943-5101

NAVAL POSTGRADUATE SCHOOL
MONTEREY, CALIFORNIA

THESIS

HUMAN MALE AND FEMALE BIODYNAMIC RESPONSE TO UNDERWATER EXPLOSION EVENTS

by

Douglas B. Oglesby

June 1998

Thesis Advisor: Young S. Shin

Approved for public release; distribution is unlimited.

REPORT DOCUMENTATION PAGE

Form Approved OMB No. 0704-0188

Public reporting burden for this collection of information is estimated to average 1 hour per response, including the time for reviewing instruction, searching existing data sources, gathering and maintaining the data needed, and completing and reviewing the collection of information. Send comments regarding this burden estimate or any other aspect of this collection of information, including suggestions for reducing this burden, to Washington Headquarters Services, Directorate for Information Operations and Reports, 1215 Jefferson Davis Highway, Suite 1204, Arlington, VA 22202-4302, and to the Office of Management and Budget, Paperwork Reduction Project (0704-0188) Washington DC 20503.

1. AGENCY USE ONLY *(Leave blank)*	2. REPORT DATE	3. REPORT TYPE AND DATES COVERED
	June 1998.	Engineer's and Master's Thesis

4. TITLE AND SUBTITLE:
HUMAN MALE AND FEMALE BIODYNAMIC RESPONSE TO UNDERWATER EXPLOSION EVENTS

5. FUNDING NUMBERS

6. AUTHOR(S)
Oglesby, Douglas B.

7. PERFORMING ORGANIZATION NAME(S) AND ADDRESS(ES)
Naval Postgraduate School
Monterey CA 93943-5000

8. PERFORMING ORGANIZATION REPORT NUMBER

9. SPONSORING/MONITORING AGENCY NAME(S) AND ADDRESS(ES)

10. SPONSORING/MONITORING AGENCY REPORT NUMBER

11. SUPPLEMENTARY NOTES
The views expressed here are those of the authors and do not reflect the official policy or position of the Department of Defense or the U.S. Government.

12a. DISTRIBUTION/AVAILABILITY STATEMENT
Approved for public release; distribution is unlimited.

12b. DISTRIBUTION CODE

13. ABSTRACT ***(maximum 200 words)*** Ship survivability is a complex issue. For a ship to remain a viable warfighting asset following damage resulting from enemy munitions such as mines or torpedoes, the ship's crew must remain sufficiently uninjured to be capable of employing the ship's weapons systems. Sophisticated computer simulations of human response, such as those made possible by the Articulated Total Body (ATB) Model, may be used to estimate injury potentials, and thus crew survivability, during underwater explosion events. With this goal in mind, accelerometer data and video footage recorded during live fire testing were used to generate and validate ATB models for both a seated and a standing Hybrid III Anthropomorphic Test Device (ATD). Subsequently, these models were used to estimate the biodynamic response and injury potentials for both male and female human subjects in a vessel subjected to underwater explosion events. This established a method for evaluating crew survivability for a given underwater explosion induced deck excitation.

14. SUBJECT TERMS
Biodynamic Response, Underwater Explosion, Articulated Total Body Model

15. NUMBER OF PAGES
163

16. PRICE CODE

17. SECURITY CLASSIFICATION OF REPORT	18. SECURITY CLASSIFICATION OF THIS PAGE	19. SECURITY CLASSIFICATION OF ABSTRACT	20. LIMITATION OF ABSTRACT
Unclassified	Unclassified	Unclassified	UL

NSN 7540-01-280-5500

Standard Form 298 (Rev. 2-89)
Prescribed by ANSI Std. 239-18 298-102

Approved for public release; distribution is unlimited.

HUMAN MALE AND FEMALE BIODYNAMIC RESPONSE TO UNDERWATER EXPLOSION EVENTS

Douglas B. Oglesby
Lieutenant, United States Navy
B.S.A.E., University of Missouri-Rolla, 1990

Submitted in partial fulfillment of the
Requirements for the degree of

MECHANICAL ENGINEER

and

MASTER OF SCIENCE IN MECHANICAL ENGINEERING

from the

NAVAL POSTGRADUATE SCHOOL
June 1998

DUDLEY KNOX LIBRARY
NAVAL POSTGRADUATE SCHOOL
MONTEREY CA 93943-5101

ABSTRACT

Ship survivability is a complex issue. For a ship to remain a viable warfighting asset following damage resulting from enemy munitions such as mines or torpedoes, the ship's crew must remain sufficiently uninjured to be capable of employing the ship's weapons systems. Sophisticated computer simulations of human response, such as those made possible by the Articulated Total Body (ATB) Model, may be used to estimate injury potentials, and thus crew survivability, during underwater explosion events. With this goal in mind, accelerometer data and video footage recorded during live fire testing were used to generate and validate ATB models for both a seated and a standing Hybrid III Anthropomorphic Test Device (ATD). Subsequently, these models were used to estimate the biodynamic response and injury potentials for both male and female human subjects in a vessel subjected to underwater explosion events. This established a method for evaluating crew survivability for a given underwater explosion induced deck excitation.

TABLE OF CONTENTS

LIST OF FIGURES

LIST OF TABLES

ACKNOWLEDGMENTS

I would like to express my sincerest appreciation to Professor Young S. Shin for his dedicated support throughout this endeavor. His wisdom and technical guidance significantly enhanced my education at the Naval Postgraduate School.

I extend my gratitude to Dr. Louise Obergefell of the Harry G. Armstrong Aerospace Medical Research Laboratory for her training and assistance concerning the use of the ATB, GEBOD, VIEW, and IMAGE programs. I would like to thank Mr. Tom Sides and Mr. Fred Costanzo of UERD for providing the accelerometer data and video footage from the live fire tests, and for providing all needed background information concerning the test setup. I would also like to thank Dr. Matthew Koebbe of the Scientific Visualization Laboratory at the Naval Postgraduate School for his tremendous assistance with all aspects of video capture and production.

I would like to thank my wife, Julie, for her patience, support, and understanding.

I. INTRODUCTION

Ship survivability is a complex issue. Typically, when survivability is spoken of, it is in reference to the susceptibility and vulnerability of a ship's engineering and combat systems suites. However, for a ship to remain capable of fighting following damage resulting from enemy munitions such as mines or torpedoes, the ship's crew must remain sufficiently uninjured to be able to employ the weapons systems and fight the ship. This research concentrated on investigating the effects of underwater explosions on crew vulnerability using the Articulated Total Body (ATB) Program.

Live Fire Test and Evaluation (LFT&E) of naval systems, such as the SITE Phase III series of tests conducted at the Aberdeen Test Center during the summer of 1996, provide a reference from which simulations of shipboard environments and shock induced excitations may be developed. In this research, two cases from the SITE Phase III tests were simulated. In each case, the test subject was a 50^{th} percentile male Hybrid III Anthropomorphic Test Device (ATD). In the first case, the ATD was seated in a standard operator's chair. In the second case, the ATD was in a standing position.

Models of the shipboard environment, of the ATD's, and of the input excitation were developed based on videotape footage and accelerometer data recorded during the test events. These models were validated by comparing the predicted and recorded gross body motion of the ATD's and by comparing the predicted and measured accelerations of the ATD's head, thorax, and pelvis. Following validation, the models of the environment and shock induced excitation were used in conjunction with models of human beings (a 50^{th} percentile male and a 5^{th} percentile female) in various positions. From these simulations, predicted accelerations, forces, and torques were compared against injury tolerance values and injury estimates were made.

II. OVERVIEW OF COMPUTATION AND VISUALIZATION PROGRAMS

Several programs were used to simulate and visualize the biodynamic response of the test subjects to underwater explosion induced excitations. The Articulated Total Body (ATB) program was used to perform all computations required for the simulations. The Generator of Body Data (GEBOD) program was used to generate the models of the test subjects used in the ATB program. The VIEW and IMAGE programs were used, respectively, for two- and three-dimensional visualization of the motion of the test subjects as predicted using the ATB program.

A. ARTICULATED TOTAL BODY (ATB) PROGRAM

The ATB program was primarily designed to simulate the three-dimensional response of a system of rigid bodies subjected to dynamic applied and interactive contact forces and was originally developed to model the response of crash test dummies.

Within the ATB program, test subjects are represented by rigid lumped mass elements connected to each other by joints of various configurations (pin, ball-and-socket, Euler, etc.) having user defined torque properties based upon the particular bodily joint being modeled. Each element has user defined mass and inertia properties, again based upon the particular body segment being modeled, and the volume it occupies is represented by an ellipsoid. The contact surfaces defined by these ellipsoids provide the basis for interaction with the environment, which is composed of contact planes, ellipsoids, and hyperellipsoids with user specified properties of force-deflection, energy absorption, rate dependence, etc. By evaluating the penetration of the body segment ellipsoids into the contact surfaces representing the environment, the dynamic interactive forces are computed and then applied to the body segments. The motion of these body segments is then determined by solving Newton's equations of motion. Excitation may be provided by prescribing the motion of the vehicle to which the contact surfaces of the environment are attached. The ATB program may be used to provide tabular time histories of segment accelerations, velocities, or displacements, joint forces, joint torques,

and contact forces between body segments and other body segments or the contact surfaces representing the environment. In addition, the ATB program may be used to generate data files for use by the VIEW and/or IMAGE programs for visualization.

For more detailed information concerning the capabilities of the ATB program, consult Refs. [1] and [2]. For more technical information concerning the validation of the ATB program itself, consult Ref. [3].

B. GENERATOR OF BODY DATA (GEBOD) PROGRAM

The GEBOD program is used to provide the input data sets for use with the ATB program for modeling ATD's or human beings. Each input data set contains the geometric and mass properties of the body segments as well as the locations and mechanical properties of the joints connecting the body segments. The GEBOD program may be used to generate body data sets for the Hybrid II Dummy (50^{th} percentile male), the Hybrid III Dummy (50^{th} percentile male with either seated or standing pelvis), adult human males and females, and human children. The body data sets for the human subjects are based on body measurement survey data and stereophotometric data.

For more detailed information concerning the capabilities and use of the GEBOD program, consult Refs. [1] and [4].

C. VIEW PROGRAM

The VIEW program is used to visualize the body motions as computed using the ATB program. This is accomplished through simple line drawings of the planes and contour drawings of the ellipsoids that make up the test subject and the environment. The user of the VIEW program specifies a camera position, a viewing direction, and the colors for all rendered elements. The images produced by the VIEW program may be displayed to a screen or printed for comparison against videotaped footage of the actual test.

For more information concerning the use and capabilities of the VIEW program, consult Refs. [1] and [5].

D. IMAGE PROGRAM

The IMAGE program is also used to visualize the body motions as computed using the ATB program. However, the IMAGE program uses shaded ellipsoids and planes to produce three-dimensional images of the test subject and environment. The user still specifies a camera position, a viewing direction, and the colors for all rendered elements. However, since the IMAGE program is interactive, the user may vary the camera position and viewing direction while the images are being displayed. The images produced by the IMAGE program may be recorded onto videotape or to a movie file.

For more information concerning the use and capabilities of the IMAGE program, consult Ref. [1].

III. ORIGINAL TEST SETUP

The simulations performed during this research were based on a portion of the SITE Phase 3 test series conducted during the summer of 1996. This live fire test series was conducted on a submerged shock test vehicle in the test pond at the Aberdeen Test Center, Aberdeen, Maryland. Three Hybrid III ATD's were aboard the test vehicle during the tests. Two of these ATD's were 50^{th} percentile males (one standing and one seated) and the third was a seated 5^{th} percentile female. In this research, one simulation was performed for each of the male ATD's. No film or video record was made of the female ATD during the tests, thus no simulations were performed for this ATD.

A. SUBMARINE SHOCK TEST VEHICLE (SSTV)

The test platform used during the SITE Phase 3 test series was the Submarine Shock Test Vehicle (SSTV). This vehicle was designed in the late 1960s by the Naval Ship Engineering Center (NAVSEC) and the Underwater Explosions Research Division (UERD) of the Naval Ship Research and Development Center (NSRDC). Its purpose was to serve as a shock platform for testing submarine systems and shock-hardened submarine equipment under conditions simulating combat shock. The SSTV was constructed by the Electric Boat Division, Groton, Connecticut, and the Fore River Division, Quincy, Massachusetts, of the General Dynamics Corporation, under joint sponsorship by the Defense Atomic Support Agency (DASA) and the Navy. Figure 1 shows the SSTV as configured during the 1996 SITE Phase 3 test series. [Ref. 6].

1. Description of the SSTV

The SSTV is based on a missile compartment from a USS LAFAYETTE (SSBN-616) Class submarine, but portions of the crown were modified with TRIDENT hull plating and framing for the second SSTV test series conducted in 1977. The SSTV hull is a constant diameter cylinder containing a test compartment, comprised of two platforms, and several ballast tanks. The vehicle is towed to the test site, submerged using the ballast tanks, subjected to a shock test, surfaced, and given a post-test

inspection. All required services must be provided by off-hull sources. The basic dimensions for the SSTV are shown in Table 1. [Ref. 6].

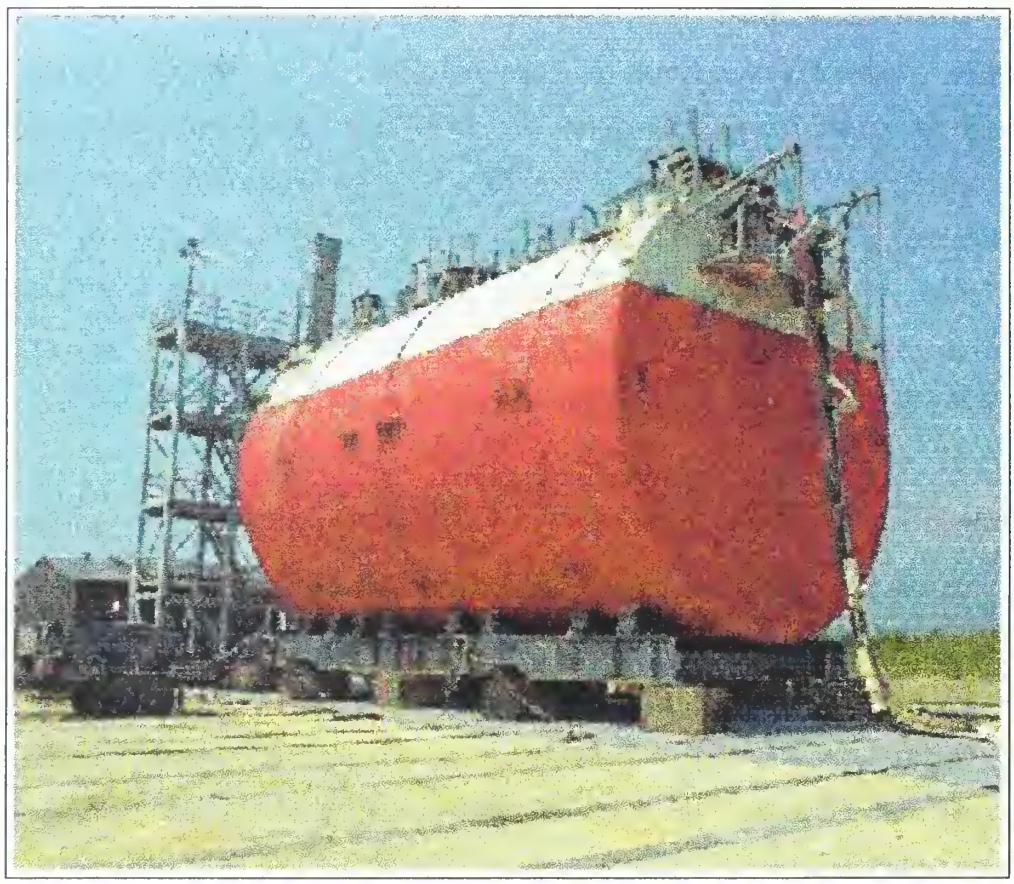

Figure 1. Submarine Shock Test Vehicle (SSTV). From Ref. [6]

Table 1. Basic SSTV Dimensions. After Ref. [6]

Item	Dimension
Overall length	53 ft 3 in
Test compartment length	35 ft
Diameter	33 ft
Ballast tank length (each)	9 ft
Hull plate thickness	2 inches nominal
Frame spacing	35 inches nominal
Displacement	900 – 1300 tons

2. Test Compartment Instrumentation

While the SSTV was extensively instrumented during the test series, the only instruments of particular concern to this research were the linear accelerometers. Figure 2 and Figure 3 show the locations of the accelerometers mounted on the first and second platforms, respectively, of the SSTV test compartment. In each case, the last letter of the identifying code refers to the orientation of the accelerometer: A for athwartships, V for vertical, and F for fore-and-aft.

In all cases, the accelerometer data was sampled at 20 kHz, then processed through a 2-pole bessel low pass filter of 1000 Hz with an associated decimation of the sample rate to 5000 Hz.

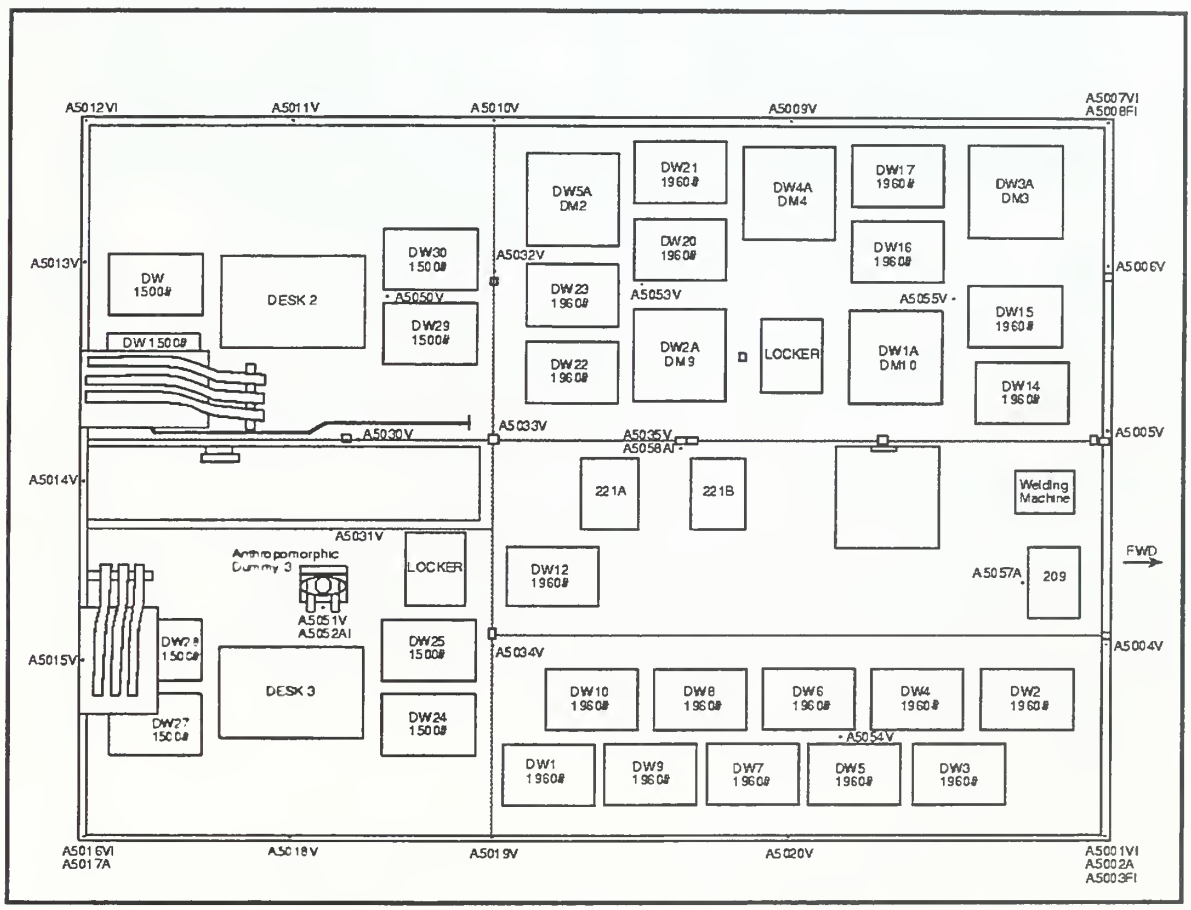

Figure 2. SSTV First Platform Accelerometer Locations. From Ref. [7]

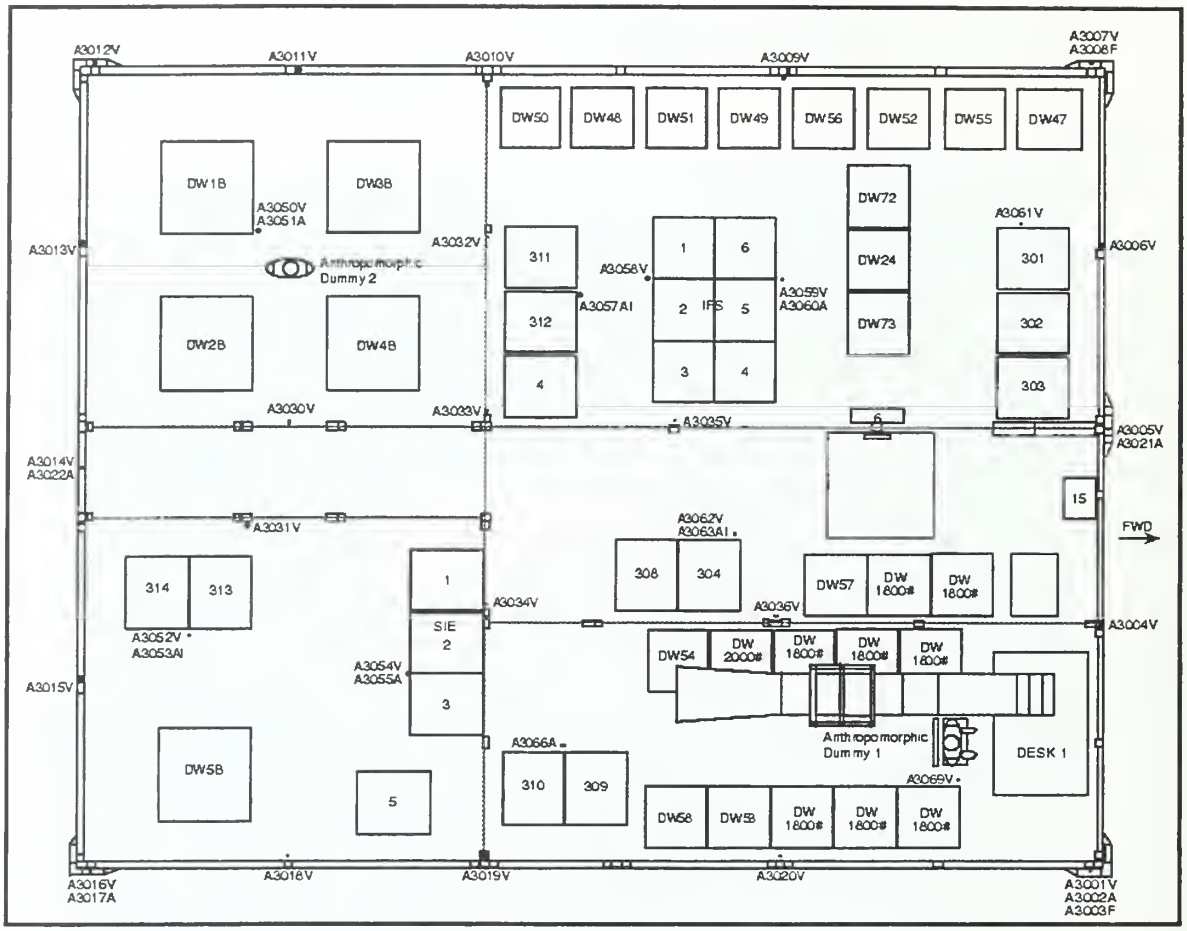

Figure 3. SSTV Second Platform Accelerometer Locations. From Ref. [7]

B. HYBRID III DUMMY

All of the anthropomorphic test devices used in the SITE Phase 3 test series were Hybrid III dummies. The Hybrid III dummy is widely used as an occupant crash protection assessment device by car manufacturers, automotive suppliers, and various other test centers throughout the world [Ref. 8].

1. Overview

The 50th percentile adult male Hybrid III dummy was developed in 1976 by the General Motors Corporation. The Hybrid III dummy is human-like in shape, as can be seen in Figure 4, and has improved head, neck, chest, and knee impact response biofidelity as compared to its predecessor, the Hybrid II dummy. [Ref. 8].

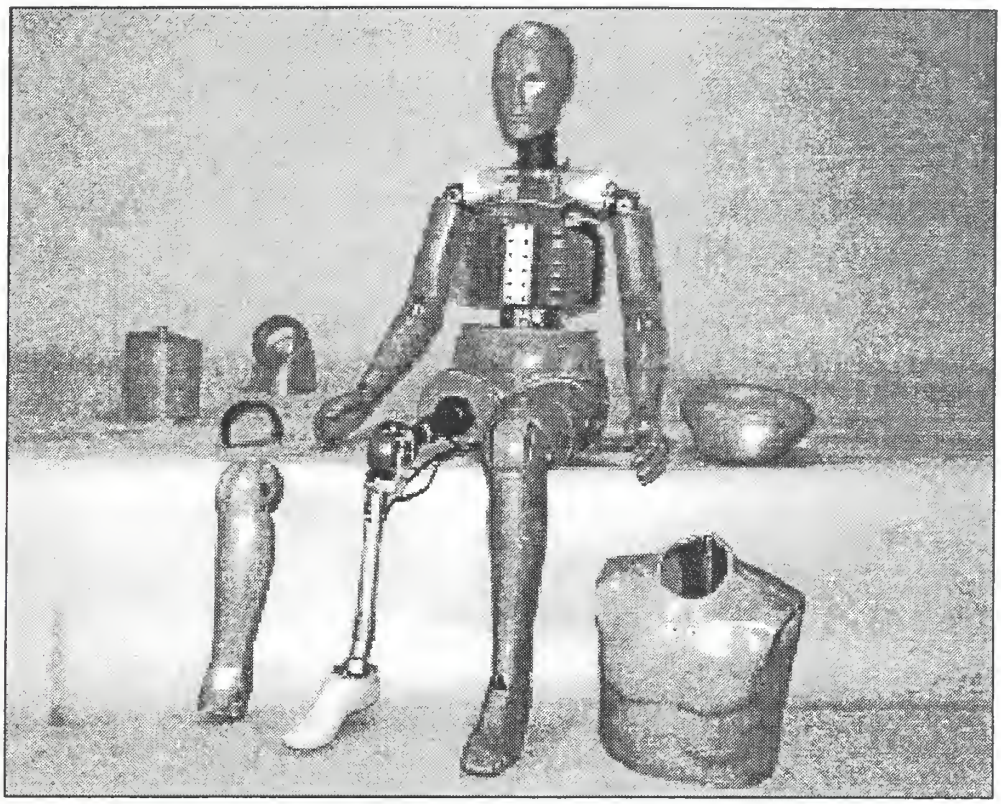

Figure 4. Hybrid III Dummy. From Ref. [9]

The head of the Hybrid III dummy is made from an aluminum shell covered by a vinyl skin and has a human-like impact response in the forehead area. The head is connected to the torso by an articulated neck composed of four rubber segments bonded to aluminum disks and end plates and having a braided steel cable running through the center. The chest contains six steel ribs, each of which is covered with damping material and is connected on one end to a rigid spine and on the other end to a leather part representing the sternum. This design allows for a distribution of the loading during chest impacts and has compliance comparable to that of a human. The lumbar spine of the Hybrid III dummy is made from two braided steel cables encased in a curved rubber piece and connected to end plates on each end. The pelvis is an aluminum casting in the shape of a human pelvis and covered with a vinyl skin. The legs, which have ball joints at the hip and ankle, are made of steel shafts covered with a vinyl skin and there are rubber pads inserted under the skin in the knee areas. [Ref. 8].

2. Instrumentation

The Hybrid III dummy is capable of being extensively instrumented. Figure 5 shows common sensor locations for an adult Hybrid III dummy. The ATD's used in the SITE Phase III series had triaxial linear accelerometers mounted at the center's of gravity of the head, chest, and pelvis, as illustrated by the boxes around the respective labels in Figure 5. For more information concerning the instrumentation capabilities of the Hybrid III dummies, consult References [8] and [9].

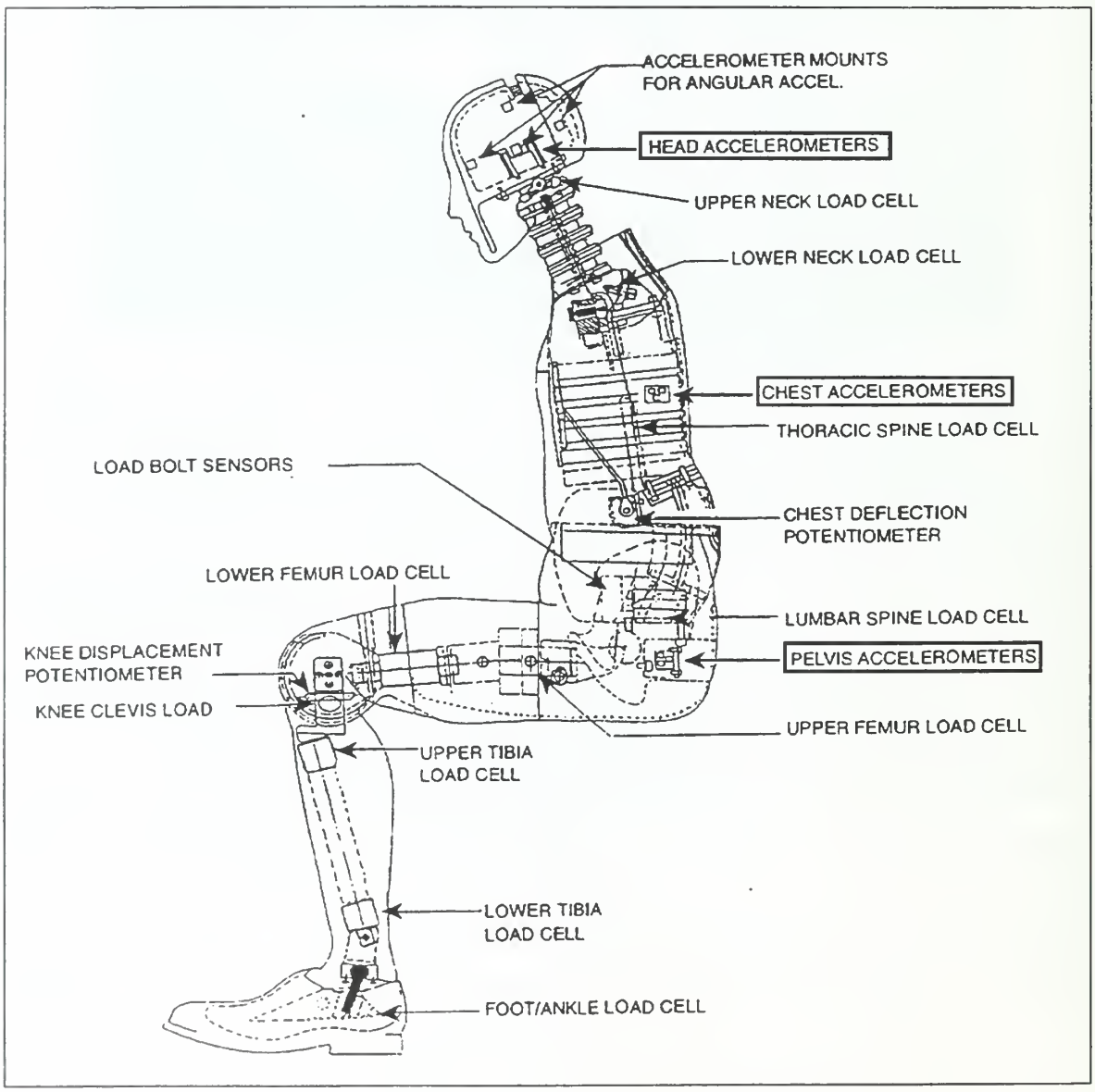

Figure 5. Hybrid III Dummy Sensor Locations. After Ref. [8]

C. SEATED HYBRID III DUMMY SETUP

The seated Hybrid III dummy, located on the first platform of the SSTV as shown in Figure 2, was the subject of the first simulation. The shock excitation for this simulation, as well as the recorded video footage and dummy accelerometer data, were from Shot 9991. This particular shot was chosen because of the combination of relatively clear video footage and significant dummy motion.

1. Physical Environment

The Hybrid III dummy was seated facing starboard, lap belt securely fastened, in a standard operator's chair. In front of the ATD was a desk with a computer, monitor, and keyboard. Figure 6 is a still image captured from the videotape of the actual test event and shows the setup of the seated Hybrid III dummy. Note the lap belt securing the ATD in the seat and the instrumentation cables running over the top of the seat back.

Figure 6. Seated Hybrid III Dummy Setup

2. Instrumentation

As was previously discussed, the Hybrid III dummy was instrumented with triaxial linear accelerometers located at the centers of gravity of the head, thorax, and pelvis, as illustrated in Figure 5. As was the case for the SSTV accelerometers, the dummy accelerometer data was sampled at 20 kHz, then processed through a 2-pole

bessel low pass filter of 1000 Hz with an associated decimation of the sample rate to 5000 Hz. During the shot, a recorder channel failure led to the loss of the Y-oriented accelerometer data for the pelvis. This was not of particular concern since the predominant motion occurred in the X-Z plane. Figure 7 shows the sign conventions used in reporting the accelerations, velocities, and displacements of various body segments.

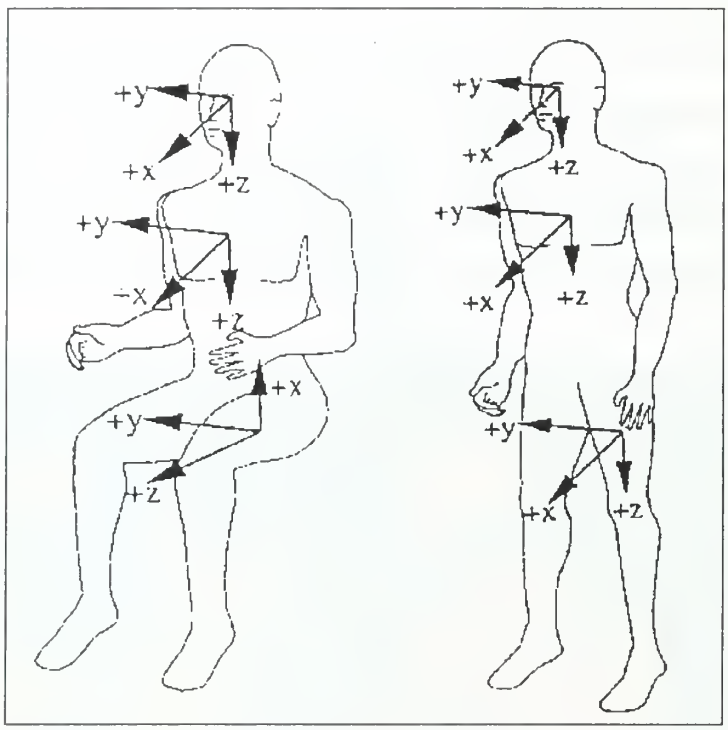

Figure 7. Dummy Coordinate System. After Ref. [8]

D. STANDING HYBRID III DUMMY SETUP

The standing Hybrid III dummy, located on the second platform of the SSTV as shown in Figure 3, was the subject of the second simulation. The shock excitation for this simulation, as well as the recorded video footage and dummy accelerometer data, were from Shot 9993. As was the case for the seated dummy, the particular shot used for the simulation was chosen based on the combination of relatively clear video footage and significant dummy motion.

1. Physical Environment

The Hybrid III dummy was standing, facing starboard, on the second platform of the SSTV. A harness was placed around the ATD's lower chest to provide tie points for the elastic cords used to keep the ATD standing until the shock event. Four sets of elastic cords, with four strands per set, were attached to the chest harness of the ATD and to the overheard of the second platform of the SSTV. Figure 8 is a still image captured from the videotape of the actual test event and shows the setup of the standing Hybrid III dummy. Note the chest harness and four sets of restraining elastic cords. In addition to the cords supporting the ATD, there are four safety lines to restrain the ATD in the event that one or more of the elastic cords fails. These safety lines are the untensioned lines shown in Figure 8.

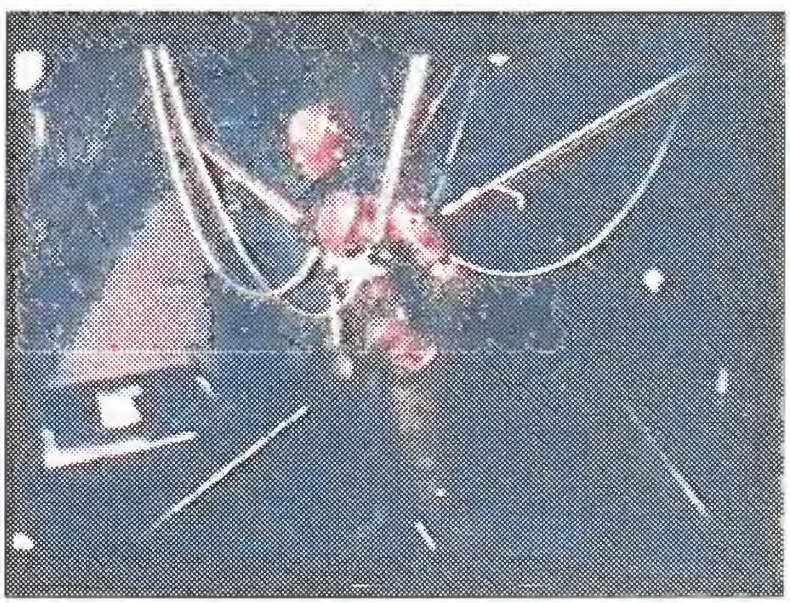

Figure 8. Standing Hybrid III Dummy Setup

2. Instrumentation

The instrumentation used in the standing dummy was identical to that used in the seated dummy. No instrumentation failures occurred during the test, thus all nine components of the head, thorax, and pelvis linear accelerations were captured for the duration of the event.

IV. MODEL GENERATION AND VALIDATION

Generating and validating a model of the shipboard physical environment and the shock induced deck excitation was the first step towards performing estimates of injury potentials for male and female human subjects in various positions. Both the model of the physical environment and the one of the deck excitation were created in the input file for the ATB program. The simulation of the underwater explosion event was then performed and the predicted motion of the model of the Hybrid III dummy was compared to the motion of the actual dummy recorded during live shock testing. Once the predicted and recorded motions were in acceptably close agreement, the models of the environment and deck excitation were considered validated.

A. SEATED HYBRID III DUMMY

The first simulation performed was of the seated 50th percentile male Hybrid III dummy for the excitation induced during the SITE Phase III shock test series, Shot 9991.

1. Model of Physical Environment

For the seated Hybrid III dummy, the relevant shipboard environment consisted solely of the chair in which the ATD was seated. There was no apparent contact between the ATD and the desk as seen in Figure 6, thus the desk was not modeled. The ATB model of the chair was constructed using planar and ellipsoidal contact surfaces based upon physical measurements taken of the actual chair used during the shock test series. The chair's lap belt was modeled using the simple belt feature in the ATB program. The force deflection characteristics for the lap belt and the contact surfaces of the chair were based upon an existing ATB simulation of an ejection seat. The ATB model of the Hybrid III dummy, generated using the GEBOD program, was positioned in the model of the chair so as to match the initial position of the ATD as seen in Figure 6 as closely as possible. For more detailed information concerning the construction of the model of the chair used in the simulation of the seated Hybrid III dummy, consult Ref. [1].

2. Input Excitation

Within the ATB program, the excitation can be specified in several different ways. For the simulations performed in this research, the tabulated six degree of freedom deceleration option was used. The three linear and three angular components of the deceleration of the vehicle were specified at each time interval. Decelerations, vice accelerations, are used because the ATB program was originally developed to model ATD response to car crashes.

The vertical and athwartships components of the linear decelerations were taken directly from the recorded accelerations located at the base of the operator's chair (accelerometers A5051V and A5052A, respectively, as seen in Figure 2). The only changes made to these input signals were to account for differences in sign conventions and to convert accelerations to decelerations as required by the ATB program. No fore-and-aft accelerations were measured at the base of the chair. By examination of the measured accelerations in that direction at the forward end of the test vessel, this component of acceleration was determined to be minor and not of interest, and as such was not included in the model's excitation signal. The vertical and athwartships components of the excitation signal are shown in Figure 9 and Figure 10, respectively.

No angular accelerations were measured at the base of the operator's chair, so estimates were made from comparison of two linear accelerometers separated by an athwartships distance, in the case of roll, and by a fore-and-aft distance in the case of pitch. The roll angular deceleration signal was constructed from the vertical accelerations recorded by accelerometers A5018V and A5011V located as seen in Figure 2. Similarly, the pitch angular deceleration signal was constructed from the vertical accelerations recorded by accelerometers A5051V and A5015V located as seen in Figure 2. A yaw angular deceleration signal was constructed from the fore-and-aft accelerations recorded by accelerometers A5003F and A5008F located as seen in Figure 2, but this signal was considered to be minor and was not included in the model's excitation signal. The roll and pitch components of the angular excitation signal are shown in Figure 11 and Figure 12, respectively. For more detailed information concerning the construction of the excitation signal, consult Ref. [1].

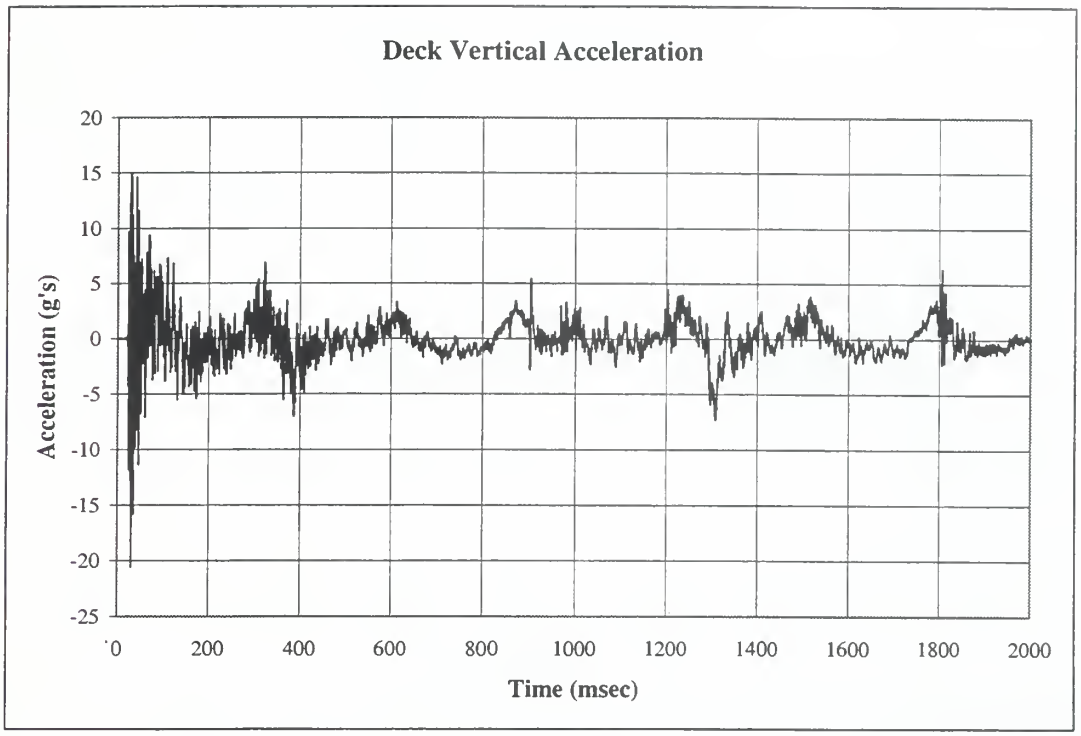

Figure 9. Deck Vertical Acceleration for Shot 9991

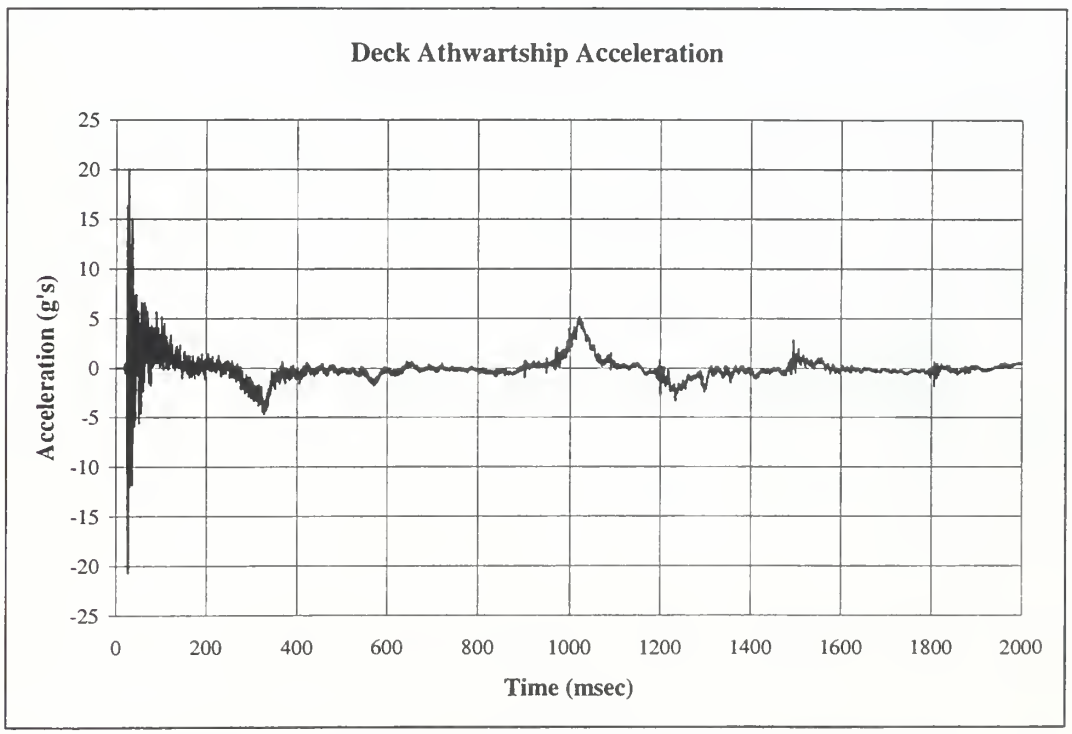

Figure 10. Deck Athwartships Acceleration for Shot 9991

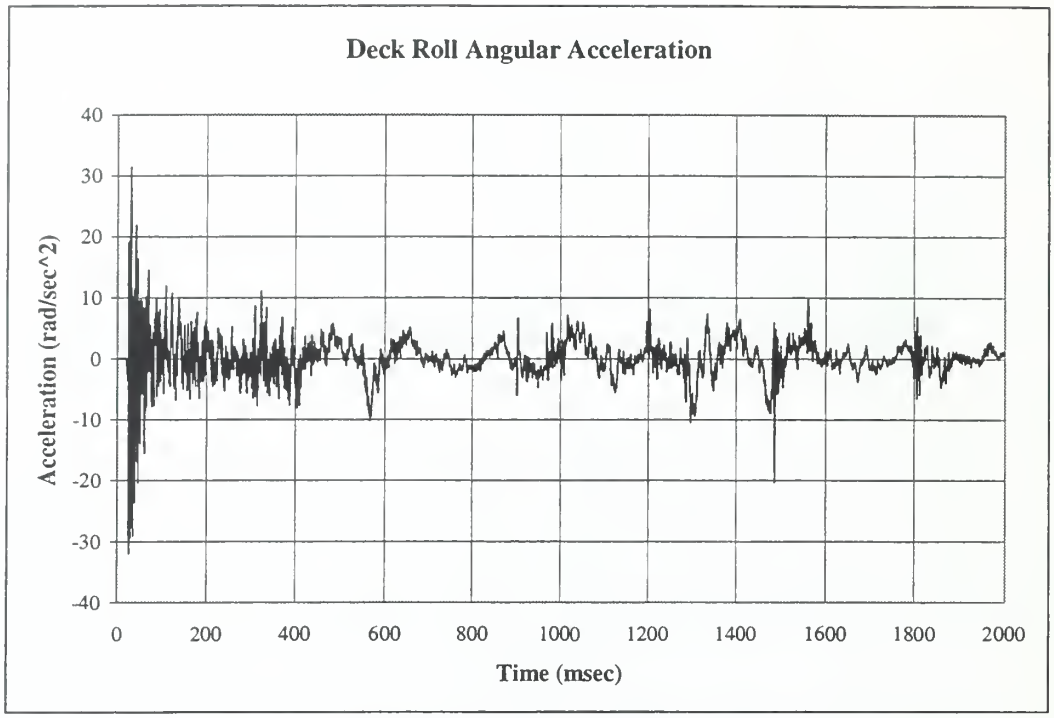

Figure 11. Deck Roll Angular Acceleration for Shot 9991

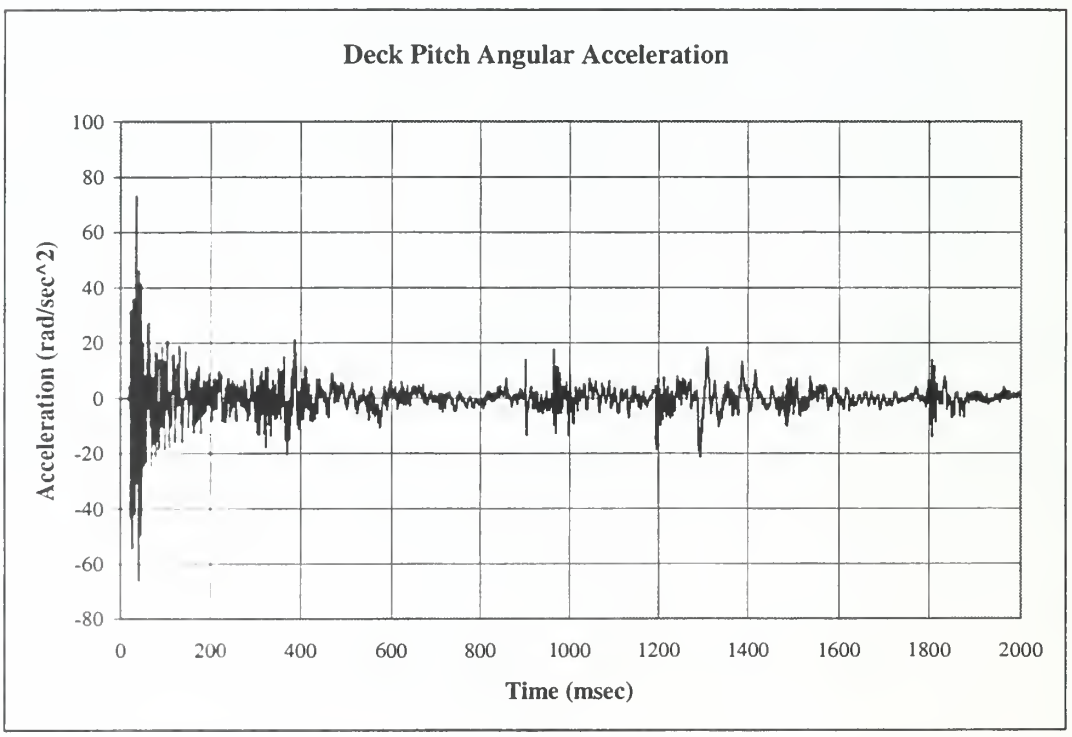

Figure 12. Deck Pitch Angular Acceleration for Shot 9991

3. Validation Results

In order to validate the models of the physical environment and deck excitation, the predicted motion and accelerations were compared against the motion recorded on videotape and the accelerometer data from the Hybrid III dummy. Small changes were made to the initial positioning of the body segments of the ATD model and to the force-deflection characteristics of the contact surfaces until an adequate match between predicted and recorded motion and accelerations was obtained. Only the X and Z components of the dummy accelerations were considered (see Figure 7 for sign convention). The predominant motion of the ATD was in the X-Z plane, thus the Y component was not of particular interest.

The comparison between the predicted and measured accelerations for the head X and Z directions are shown in Figure 13 and Figure 14, respectively. The overall agreement is quite good, with the phasing consistent and many of the amplitudes closely matched. The agreement between predicted and measured thorax X and Z accelerations, shown in Figure 15 and Figure 16, respectively, is not as close as for the head. The phasing of the thorax Z response is still good, but the magnitudes of the peaks are generally under-estimated. Similarly, the pelvis X accelerations, shown in Figure 17, are not in as close agreement as the pelvis Z accelerations, shown in Figure 18, which show good agreement both in phasing and amplitude. Overall, the predicted head, thorax, and pelvis accelerations show very acceptable agreement, particularly in the Z direction. The phasing of the predicted response is nearly identical to the measured response, and the predicted amplitudes are acceptably close to those measured during testing.

The predicted gross bodily motion of the ATD is also in reasonably good agreement with the images captured from the video of the test event. Figure 19 and Figure 20 show several frames comparing the test video with the predicted motion generated using the IMAGE program. Basic phasing of the motion agrees well with the video although the arm motion is significantly different. One source of differing motion is the seat back. As can be seen in the images from the test, the angle that the seat back makes with the seat pan is increased after the first recoiling of the dummy into the seat back. However, the seat back was not modeled as being able to rotate in the simulations.

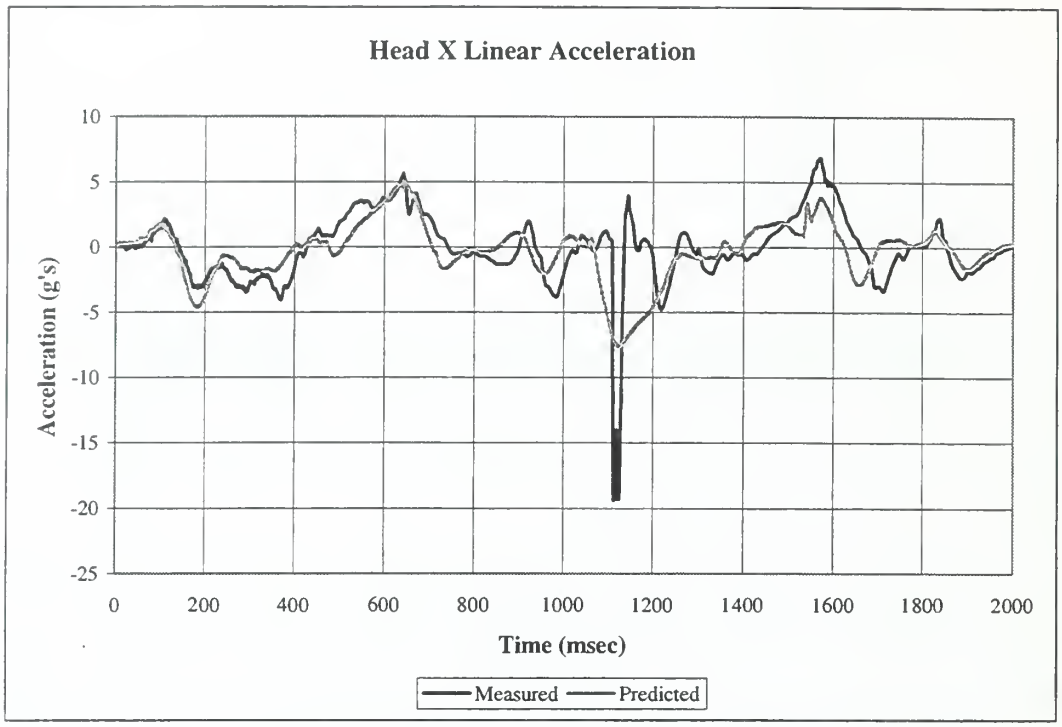

Figure 13. Head X-Acceleration Validation for Shot 9991

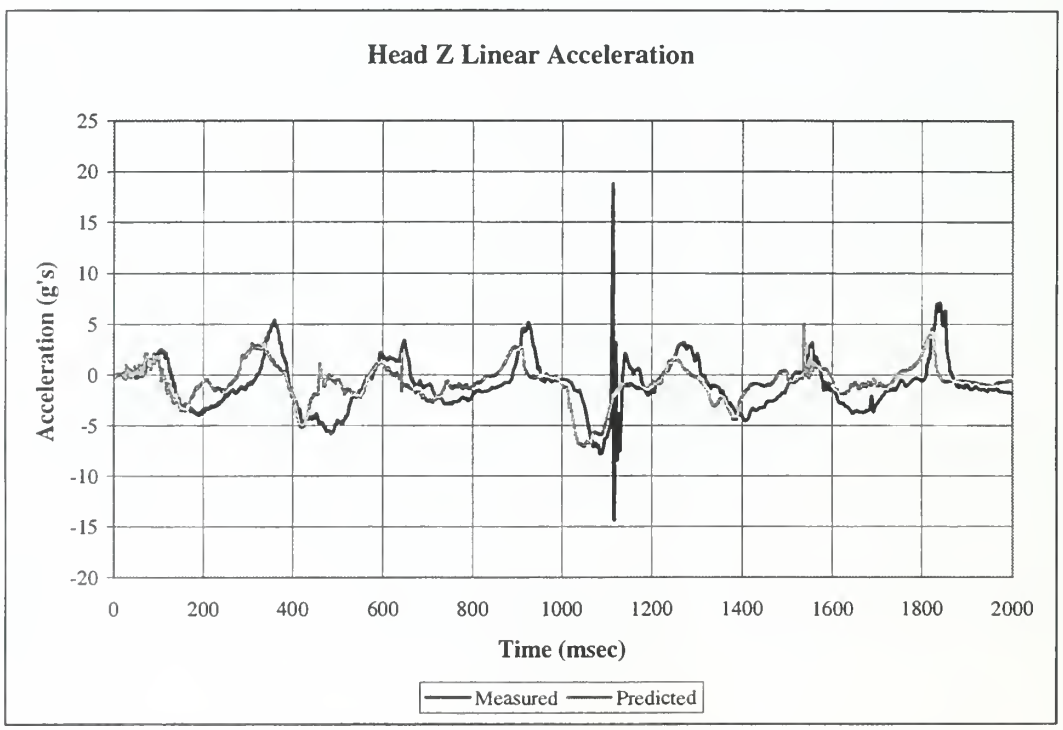

Figure 14. Head Z-Acceleration Validation for Shot 9991

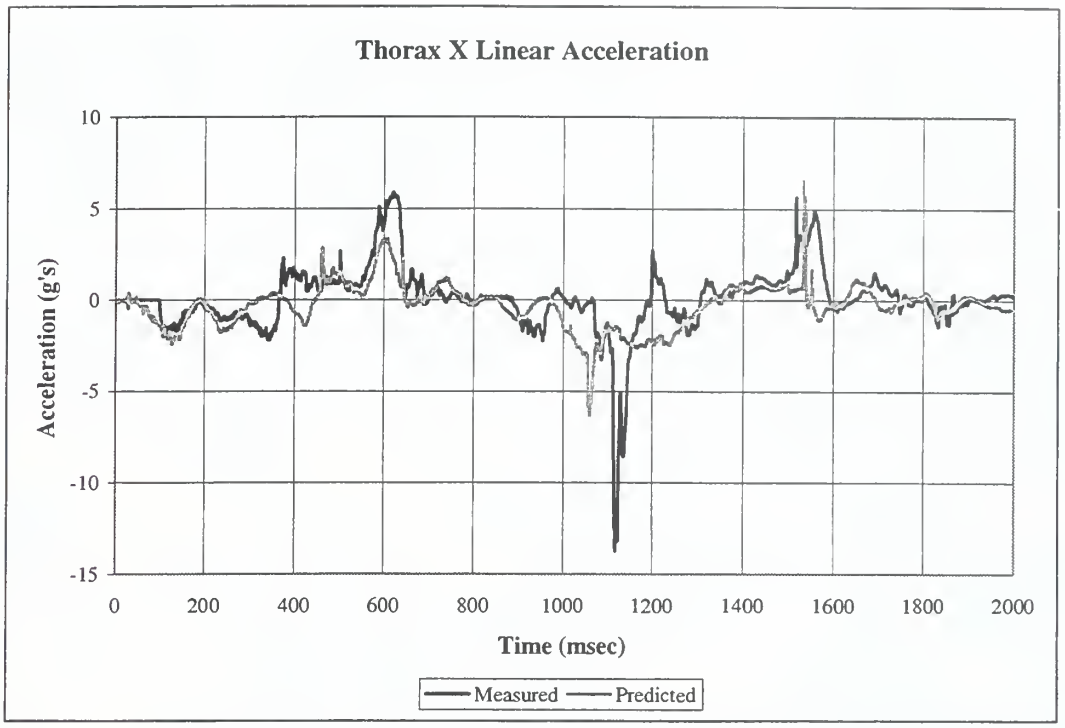

Figure 15. Thorax X-Acceleration Validation for Shot 9991

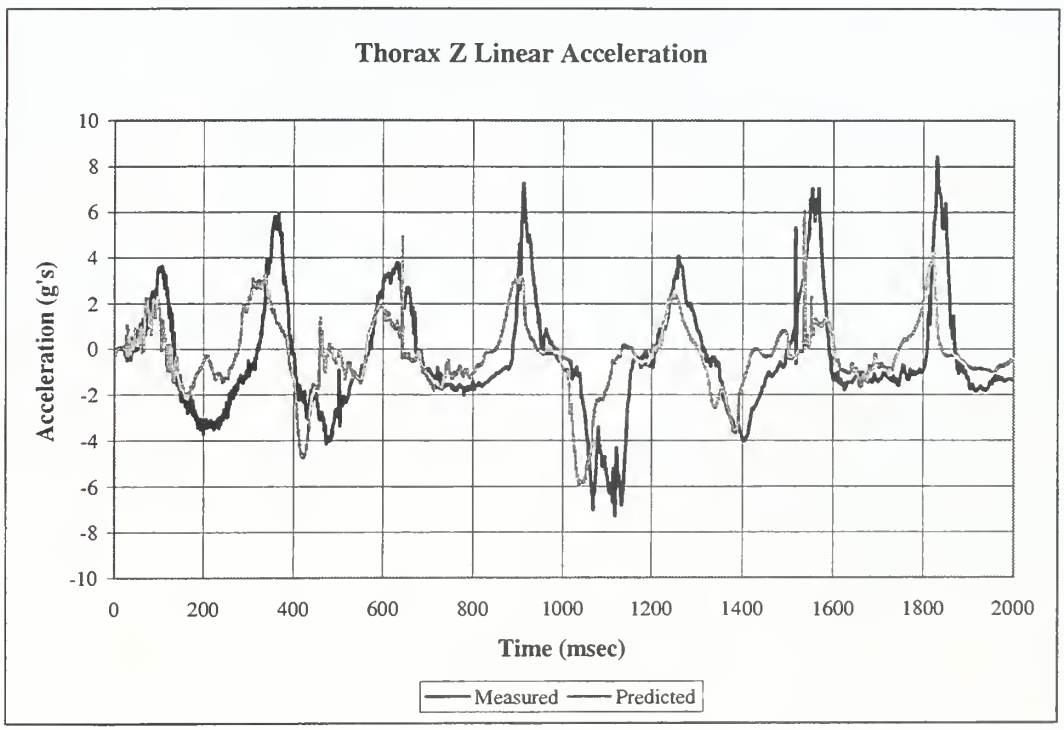

Figure 16. Thorax Z-Acceleration Validation for Shot 9991

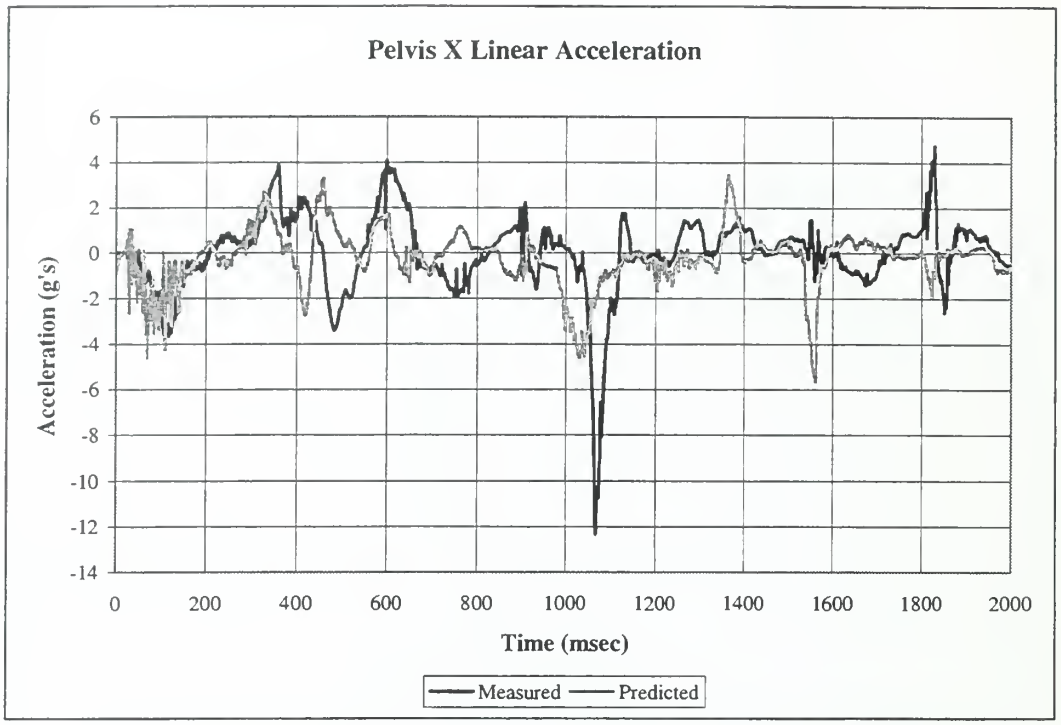

Figure 17. Pelvis X-Acceleration Validation for Shot 9991

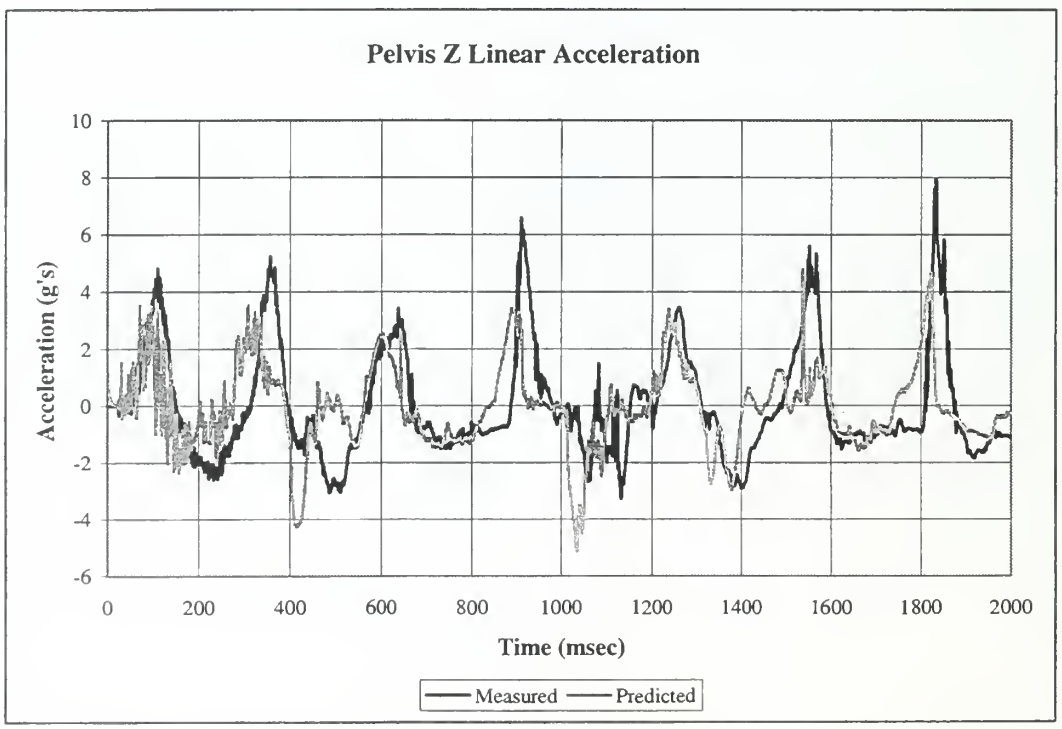

Figure 18. Pelvis Z-Acceleration Validation for Shot 9991

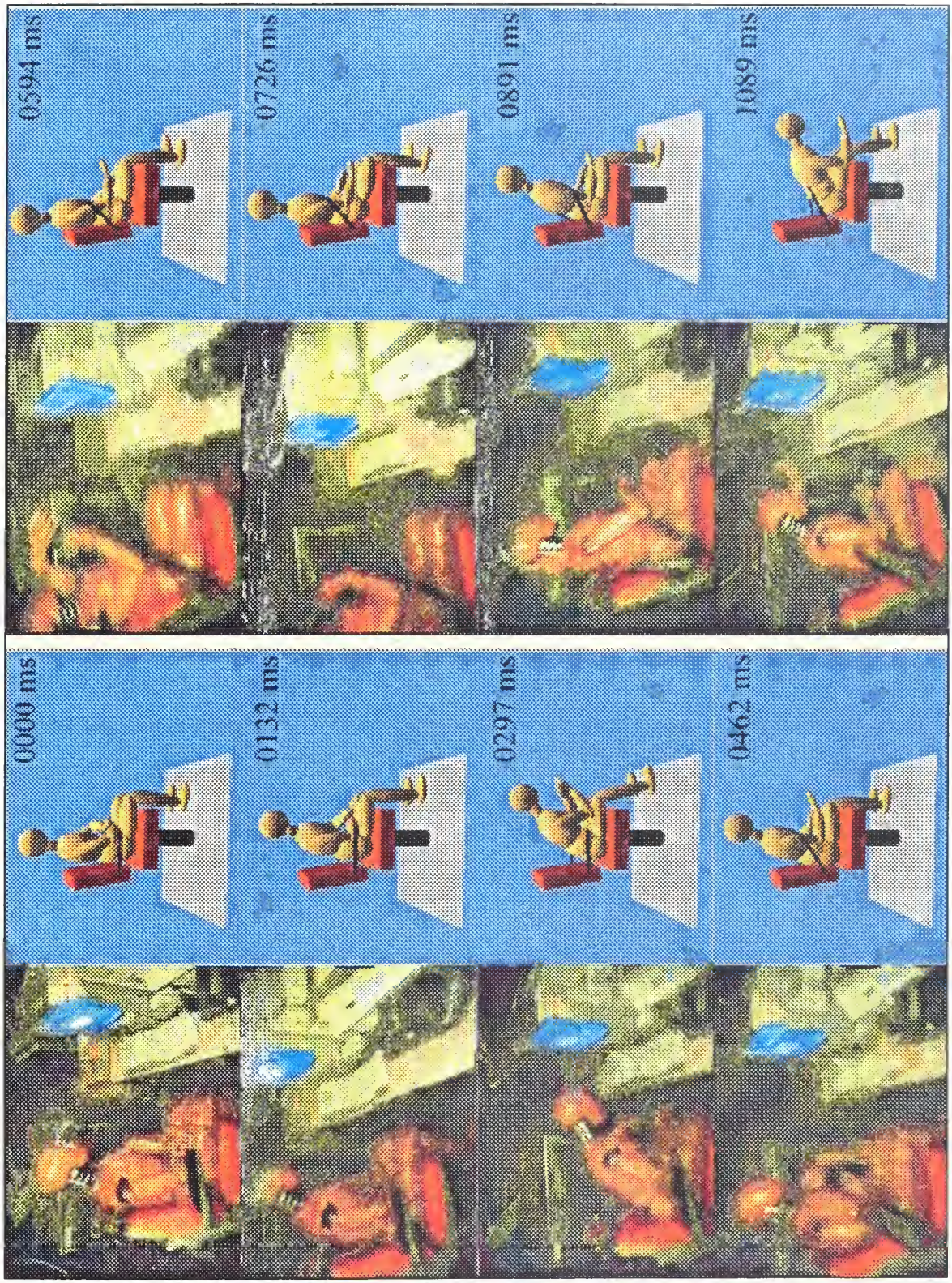

Figure 19. Motion Validation for Shot 9991 (Part 1)

Figure 20. Motion Validation for Shot 9991 (Part 2)

B. STANDING HYBRID III DUMMY

The second simulation performed was of the standing 50th percentile male Hybrid III dummy for the excitation induced during the SITE Phase III shock test series, Shot 9993.

1. Model of Physical Environment

For the standing Hybrid III dummy, the relevant shipboard environment consisted of the deck upon which the ATD was standing as well as the elastic cords partially supporting the ATD. The deck was simply modeled as a plane with the same force-deflection characteristics used for the deck in the simulation of the seated ATD. For more information concerning the manner in which this force-deflection characteristic was determined, consult Ref. [1].

The standing Hybrid III dummy was partially supported by elastic cords as previously described and as can be seen in Figure 8. These sets of elastic cords were modeled using the ATB program's harness belt feature. This feature was chosen over the simple belt feature because it allows belt pretensioning and contact with multiple segments. Each set of elastic cords was modeled as a single belt connected at one end to a fixed point on the upper torso of the dummy and at the other end to a fixed point on the vehicle. For each belt, contact was allowed between the belt and the closest upper arm segment. The locations of the contact points on the ATD and of the anchor points on the vehicle were estimated by examining the orientations of each set of cords with respect to the ATD as seen in the footage of the test. The model was adjusted to attempt to match these angles. For this portion of the simulation, the VIEW program was used for visualization of the model since the IMAGE program does not render belts. Figure 21 shows the initial position of the ATD and supporting belts as seen in the footage from the actual test and the ATB model of the ATD and supporting belts as rendered using the VIEW program. Note that as previously stated, the untensioned safety lines used in the test are not modeled for the simulation.

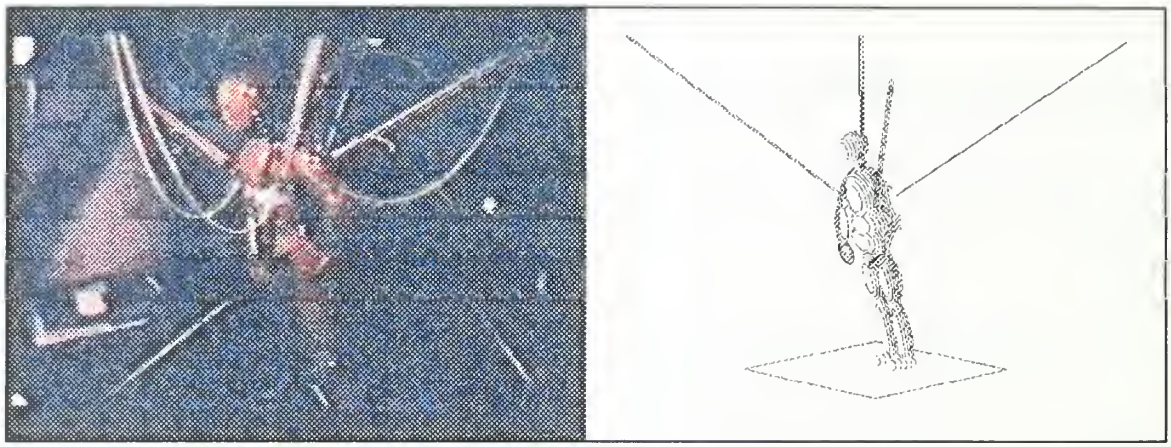

Figure 21. Belt Locations for Standing ATD

The force-deflection characteristics for each of these belts was determined from a small segment of the elastic cord used during the test series. The single strand of elastic cord was doubled over to produce a two-strand segment. One end was anchored while static loads were applied to the other end. The change in length, as measured between two intermediate points, led to a strain value associated with the applied loading. Since the standing Hybrid III dummy was supported by sets of four strands of elastic cord, the load associated with the measured strains in the two-strand segment were doubled to produce an estimated force-deflection (strain) characteristic for the ATB model. The measured strains and associated loads for both the two- and four-strand segments are shown in Table 2.

Table 2. Force Deflection Characteristics for Elastic Cord

Measured Strain	Applied Load for 2 Strands (lbf)	Force Associated with 4 Strands (lbf)
0.0000	0	0
0.047	5.5	11
0.243	11	22
0.533	16.5	33
0.907	22	44
1.300	29.5	59

2. Input Excitation

The input excitation for the standing Hybrid III dummy was specified in the same manner as the excitation for the seated dummy. The vertical and athwartships components, with appropriate sign changes, were taken directly from the accelerometers located on the deck near the dummy (accelerometers A3050V and A3051A, respectively, as seen in Figure 3). Since there were no fore-and-aft accelerometers located near the standing dummy, the two fore-and-aft accelerometers (A3003F and A3008F, as seen in Figure 3) located at the forward end of the SSTV were averaged to provide a single signal. Figure 22, Figure 23, and Figure 24 show the vertical, athwartships, and fore-and-aft components, respectively, of the excitation signal.

Again, no angular accelerations were measured at the base of the standing dummy, so estimates were made in the same manner as for the seated dummy. The roll angular deceleration signal was constructed from the vertical accelerations recorded by accelerometers A3030V and A3050V located as seen in Figure 3. Similarly, the pitch angular deceleration signal was constructed from the vertical accelerations recorded by accelerometers A30302V and A3050V located as seen in Figure 3. The yaw angular deceleration, included in the excitation signal, was constructed from the fore-and-aft accelerations recorded by accelerometers A3003F and A3008F located as seen in Figure 3. Figure 25, Figure 26, and Figure 27 show the roll, pitch, and yaw components, respectively, of the excitation signal.

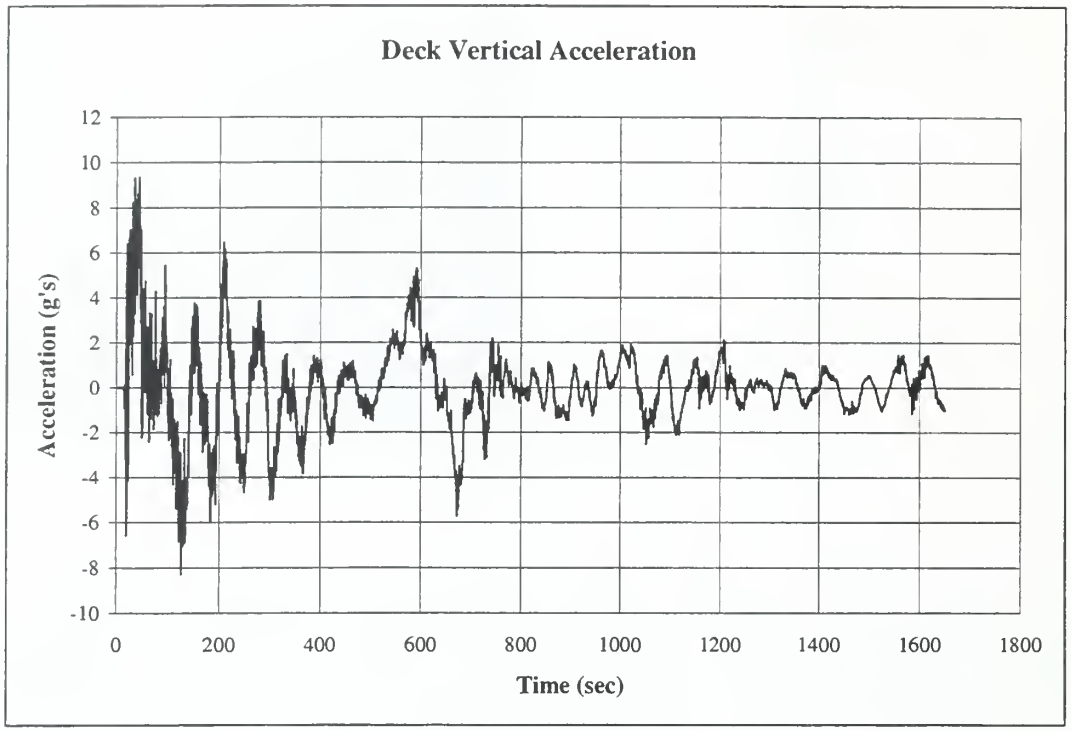

Figure 22. Deck Vertical Acceleration for Shot 9993

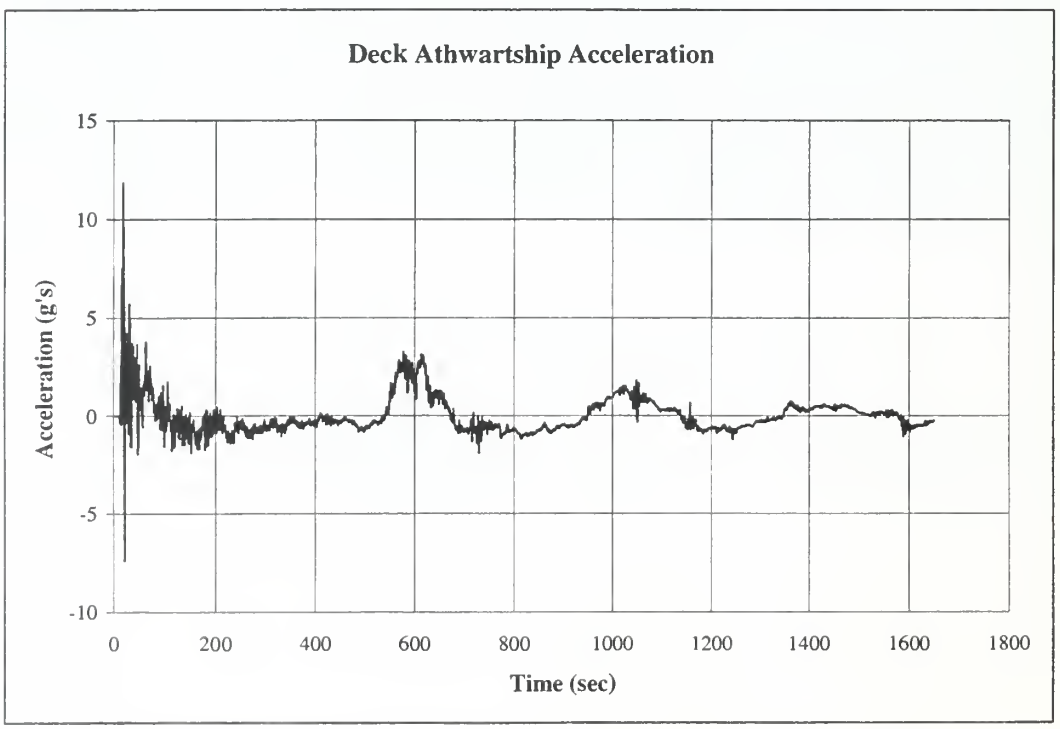

Figure 23. Deck Athwartships Acceleration for Shot 9993

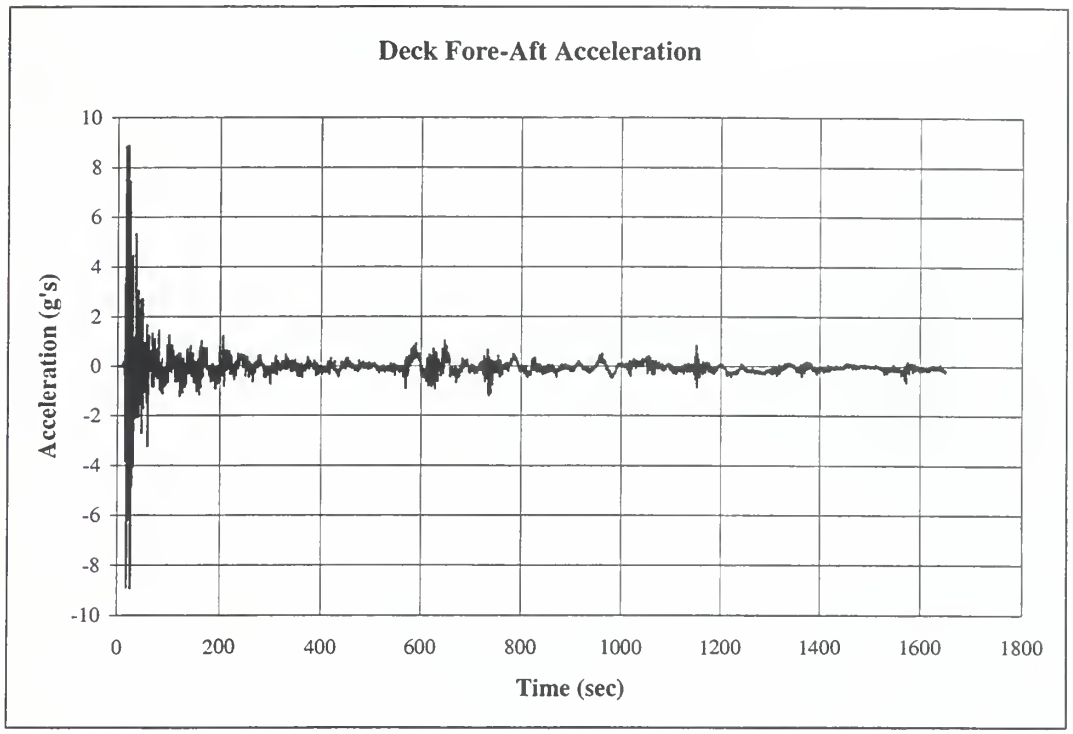

Figure 24. Deck Fore-and-Aft Acceleration for Shot 9993

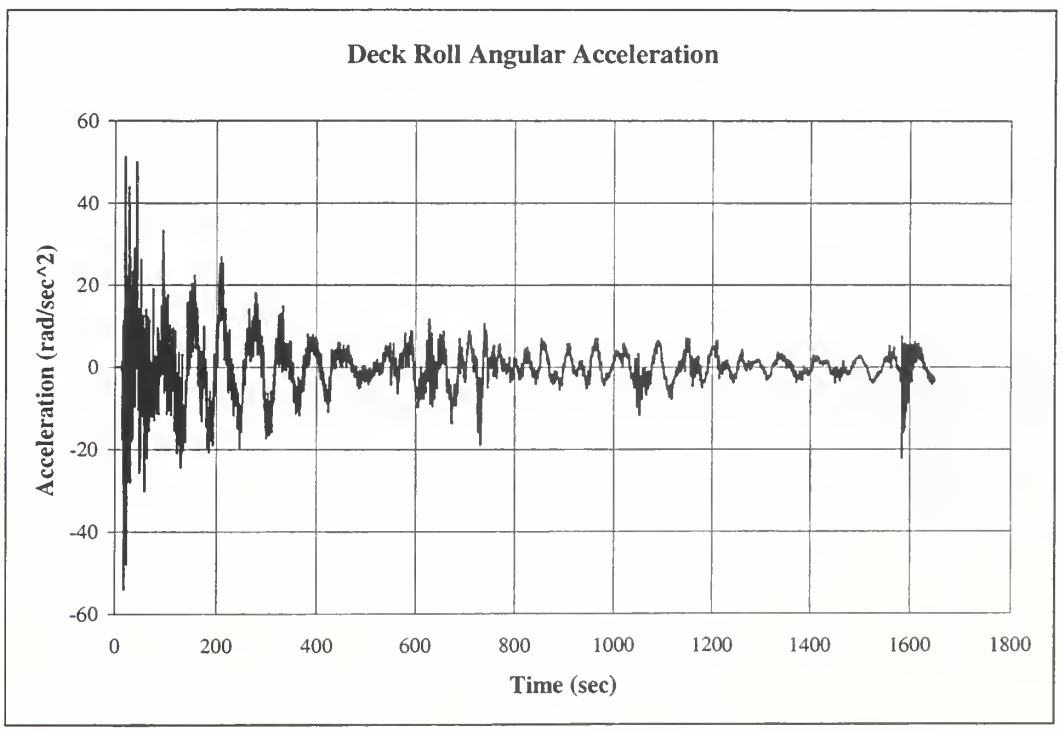

Figure 25. Deck Roll Angular Acceleration for Shot 9993

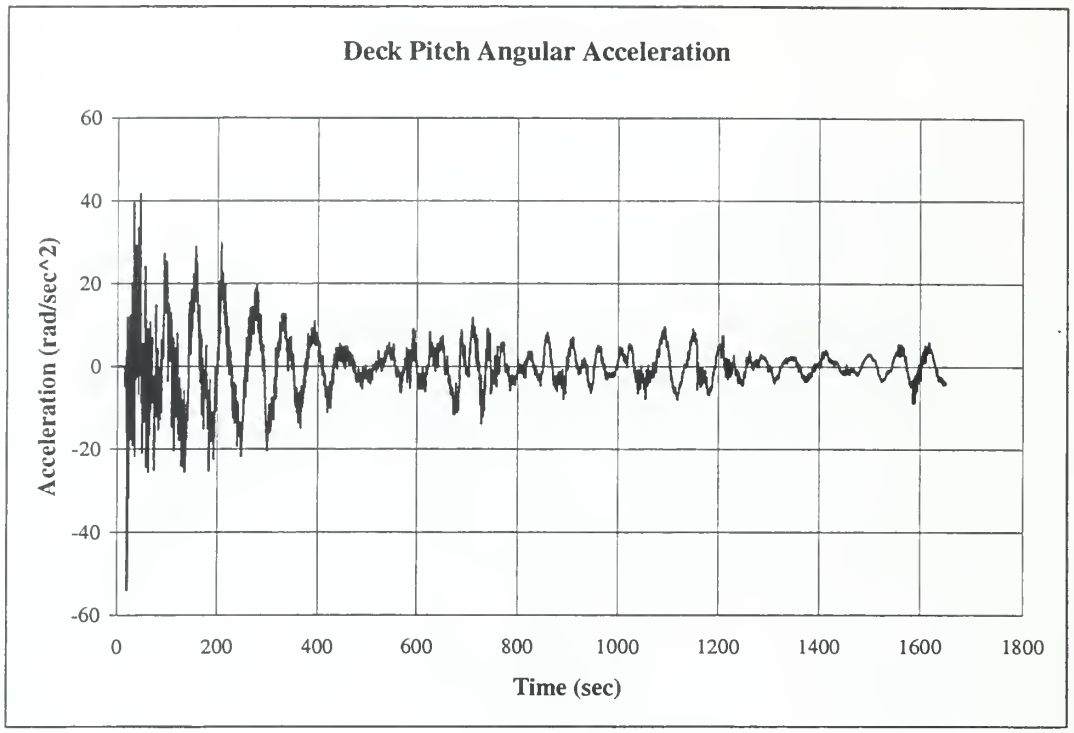

Figure 26. Deck Pitch Angular Acceleration for Shot 9993

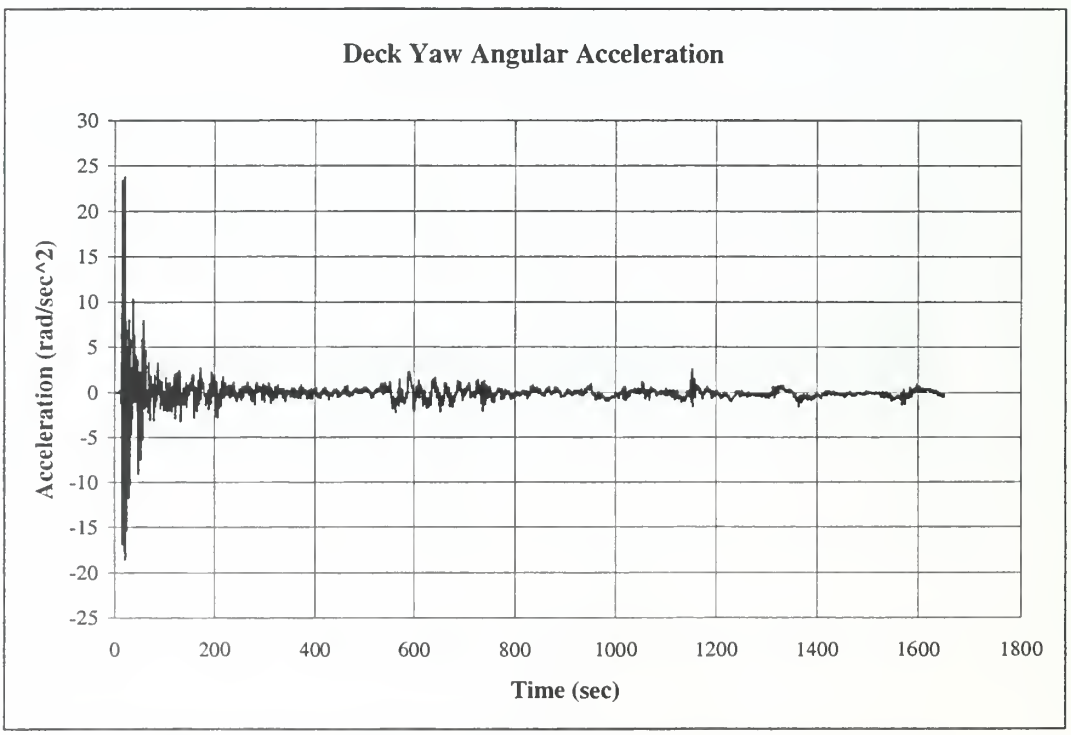

Figure 27. Deck Yaw Angular Acceleration for Shot 9993

3. Validation Results

As was the case for the simulation of the seated Hybrid III dummy, the model of the physical environment and deck excitation for the standing ATD was validated by comparing the predicted motion and accelerations against the motion recorded on high-speed film (transferred to videotape) and the accelerometer data from the ATD. Small changes were made to the initial positions of the body segments of the ATD and to the degree of pretension in the elastic cords supporting the ATD until an adequate match between the predicted and recorded motion and accelerations was obtained. It was found that the initial angle of lean of the ATD tended to affect the predicted peak accelerations and, to a lesser extent, the time of occurrence of those peaks. This time of occurrence was greatly affected, however, by the degree of pretensioning, with longer intervals between peaks resulting when a larger percentage of the ATD's weight was supported by the elastic cords. The degree of pretensioning was also found to affect the magnitudes of the predicted peak accelerations, but to a lesser extent than did the initial lean angle. Only the X and Z components of the dummy accelerations were considered (see Figure 7 for sign convention) since the predominant motion of the ATD was in the X-Z plane.

The predicted accelerations in the Z direction showed excellent phasing with the measured accelerations for the head, thorax, and pelvis. In particular, the initial acceleration peak, and the first two peaks resulting from bounces of the ATD on the deck, show nearly exact agreement in phasing with varying agreement in magnitudes. As was the case for the seated ATD, the agreements between predicted and recorded accelerations were better for the Z direction than for the X direction.

Figure 28 and Figure 29, respectively, show the comparisons between predicted and recorded accelerations for the head in the X and Z directions. The X direction shows reasonably good agreement in phasing up through the second bounce, which occurred at approximately 1050 msec, although with a tendency to underestimate peak magnitudes. The Z direction shows excellent phasing agreement, as previously noted, and good agreement of magnitudes. The first peak is overestimated by approximately 30 percent, the second peak by approximately 10 percent, and the third peak is underestimated by approximately 50 percent.

Figure 30 and Figure 31, respectively, show the comparisons between predicted and recorded accelerations for the thorax in the X and Z directions. Similar to the head X direction, the predicted thorax accelerations in the X direction do not match the recorded values as well as do those in the Z direction. The predicted thorax Z accelerations, possessing excellent phasing agreement with the recorded values, also match the recorded peak magnitudes quite well. The first and second peaks are overestimated by approximately 10 percent, but the third peak is underestimated by nearly 50 percent.

Figure 32 and Figure 33, respectively, show the comparisons between predicted and recorded accelerations for the pelvis in the X and Z directions. The predicted pelvis X accelerations match the recorded values significantly better than do the head or thorax X accelerations. The phasing is quite good through the second bounce and the predicted peak accelerations are reasonably close to the recorded values. Again the predicted Z accelerations show excellent phasing, but the agreement between the peak values is not as close for the pelvis as for the thorax. The first peak is underestimated by approximately 10 percent, but the second peak is underestimated by approximately 50 percent and the third peak by approximately 70 percent.

Overall, the predicted accelerations show quite good agreement with the recorded values, particularly in the phasing of the response. The predicted phasing for the Z accelerations is nearly identical to the recorded values through the second bounce of the ATD on the deck (approximately 1050 msec). The predicted amplitudes are acceptably close, particularly for the head and thorax Z directions.

Comparing the predicted gross motion of the ATD to that recorded during the test was neither as easy, nor as useful, as it was in the case of the seated ATD. The lighting was poor and the camera platform was also in motion as a result of the shock excitation. Nevertheless, Figure 34 shows several frames comparing the test footage with the predicted motion generated using the IMAGE program. Basic phasing of the motion is in good agreement although the ATB model of the Hybrid III dummy tends to buckle at the knees and waist when the dummy's feet strike the deck on the second bounce. This could account for the noted disagreements between the predicted and recorded accelerations following the second bounce.

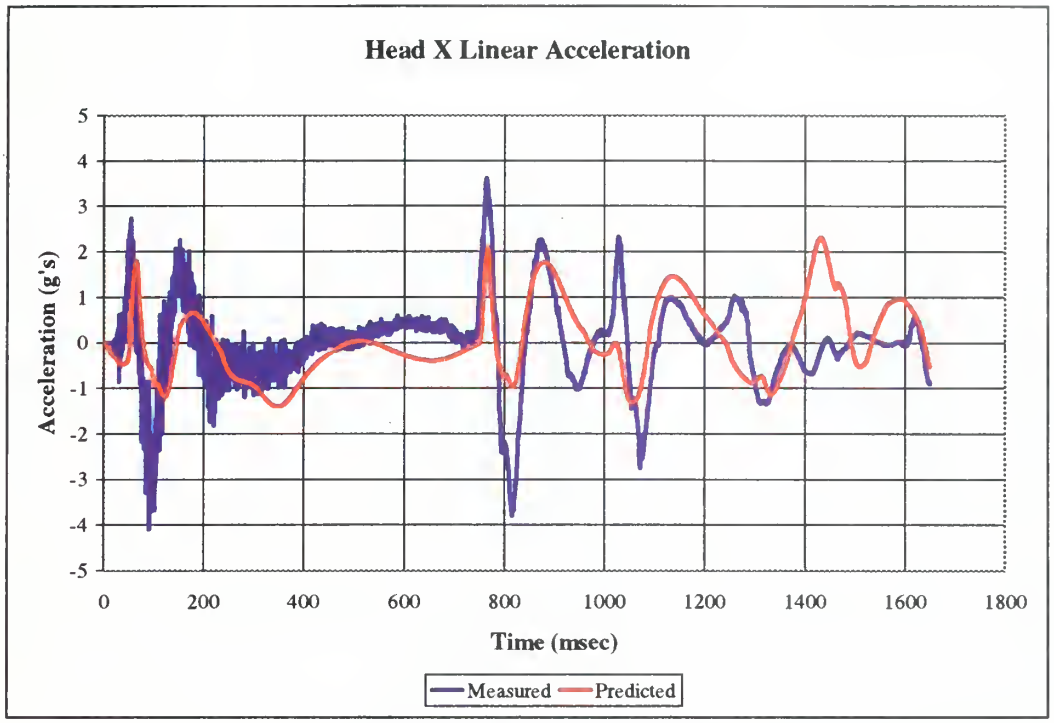

Figure 28. Head X-Acceleration Validation for Shot 9993

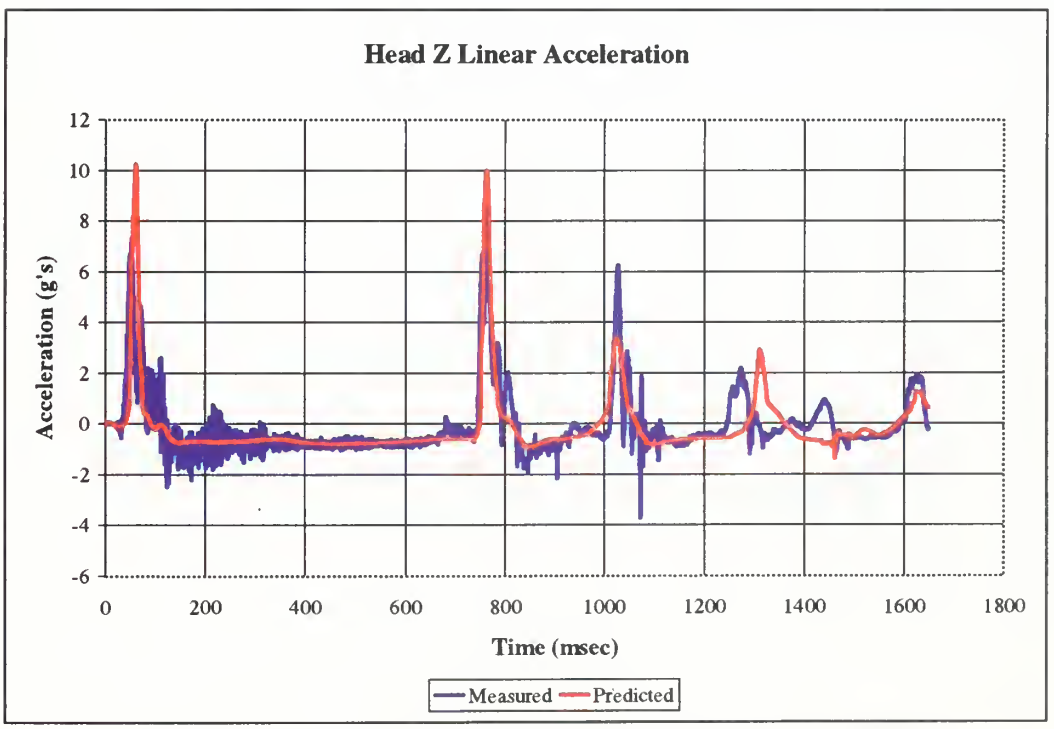

Figure 29. Head Z-Acceleration Validation for Shot 9993

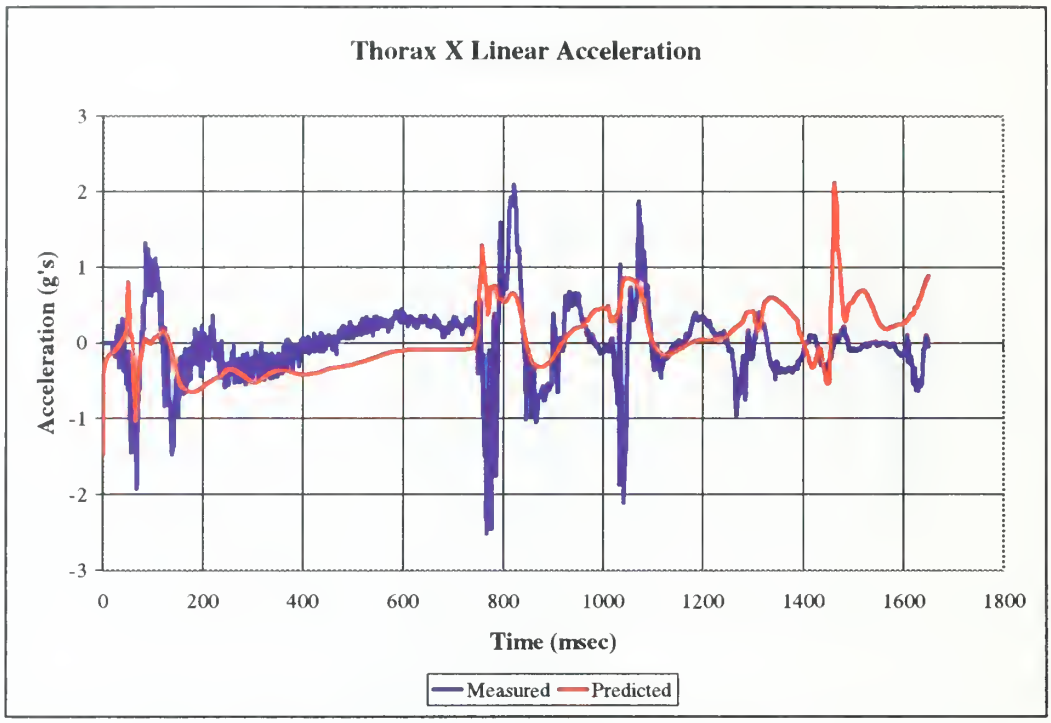

Figure 30. Thorax X-Acceleration Validation for Shot 9993

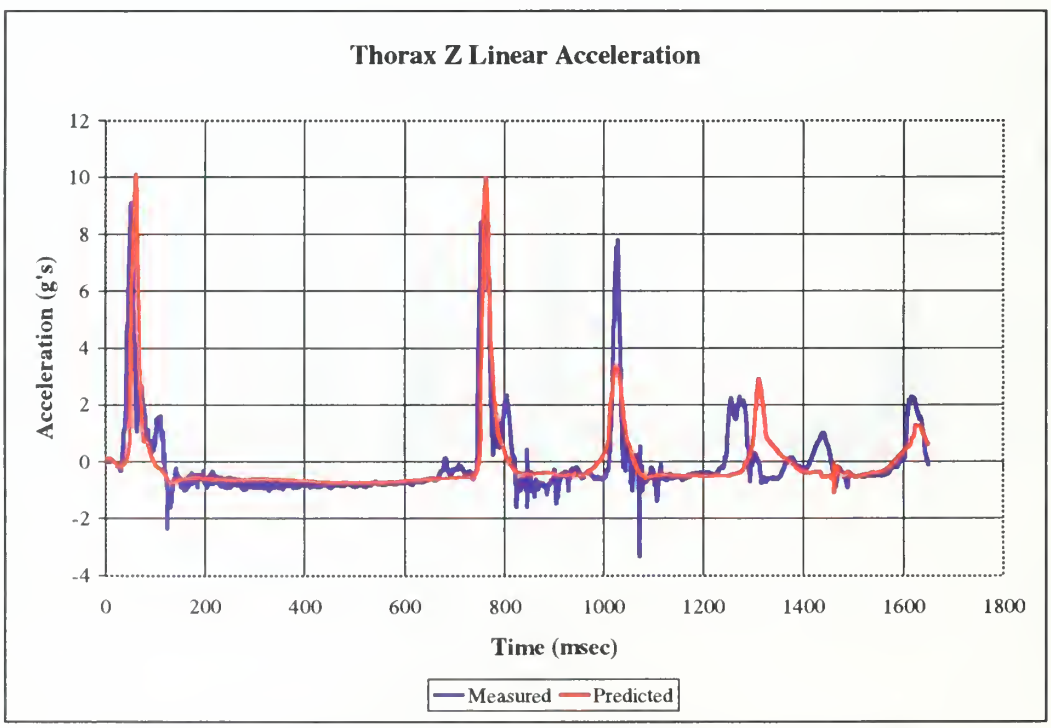

Figure 31. Thorax Z-Acceleration Validation for Shot 9993

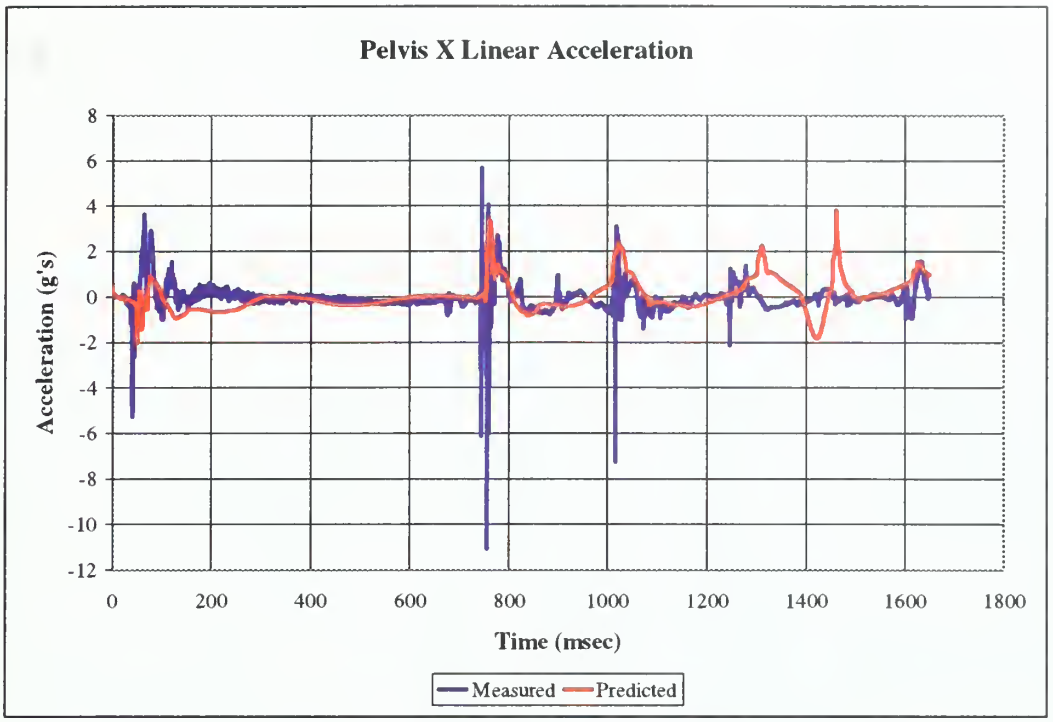

Figure 32. Pelvis X-Acceleration Validation for Shot 9993

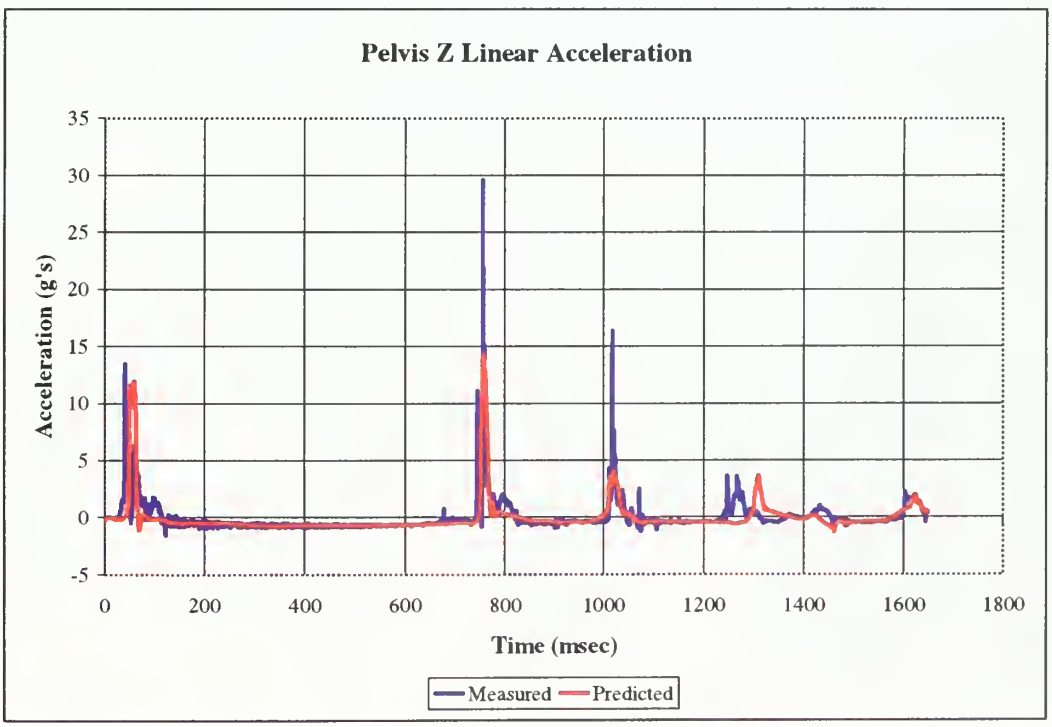

Figure 33. Pelvis Z-Acceleration Validation for Shot 9993

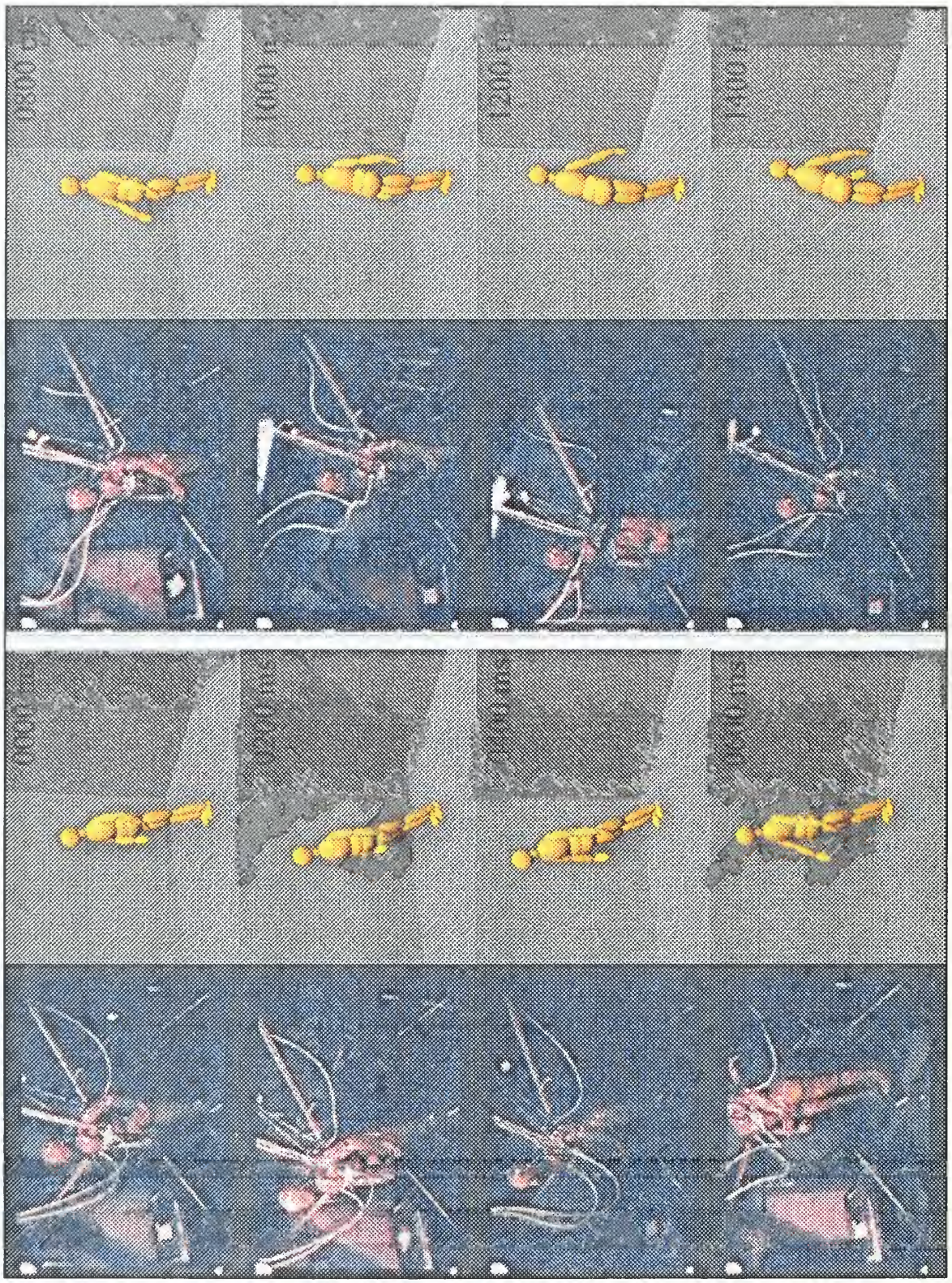

Figure 34. Motion Validation for Shot 9993

V. INJURY CRITERIA

Evaluating the potential for injury associated with measured or predicted bodily response (accelerations, forces, etc.) is an extremely complex task. The values against which these measured or predicted bodily responses are compared are generally referred to as injury criteria, injury tolerances, or injury assessment reference values (IARV's), and determining the appropriate tolerance levels is exceedingly difficult. Part of the difficulty arises from the fact that human beings are widely varied, and thus have widely varied tolerances to applied loading. More difficulty arises from the large number of possible injuries and their highly situational nature.

There has been a tremendous amount of research in the area of the biomechanics of injuries and the associated tolerance levels. Since much of this work has been performed by the automobile industry, the types of injuries for which the most information is available are those that tend to arise from car crashes. Whiplash, head impact, axial loading of the femur through knee impact with a dashboard, and loading of the foot/ankle complex through floor pan intrusion are just a few examples of the types of injuries which have received considerable attention.

For the purposes of this research, only those injuries most likely to arise from the particular ship shock situations modeled were examined. The associated tolerances have been grouped into two broad categories. The first of these categories is acceleration induced trauma. These are injuries that are the result not of impact, but of inertial loading, the most common example of which being whiplash. The second category is injury resulting from impact and includes injuries such as concussion and bone fracture.

A. ACCELERATION INDUCED TRAUMA

1. Head and Spine Anatomy

In order to interpret injury criteria, it is necessary to posses a rudimentary knowledge of the construction of the human spinal column and of some basic medical terminology. Table 3 provides a listing of some of the more common terms used in

describing orientations and directions with respect to the human body. Figure 35 illustrates the meanings of the terms flexion and extension when used in reference to the head-neck complex. The prefix 'hyper' indicates that the motion is "above, excessive, or beyond" [Ref. 11]. Thus, as shown in Figure 35, hyperextension of the cervical spine is an excessive extension beyond the normal.

Table 3. Orientation and Directional Terms. After Ref. [10]

Term	Definition	Example
Superior	Toward the head end or upper part of a structure or the body, above	The forehead is superior to the nose
Inferior	Away from the head end or toward the lower part of a structure or the body, below	The navel is inferior to the breastbone
Anterior	Toward or at the front of the body; in front of	The breastbone is anterior to the spine
Posterior	Toward or at the back of the body, behind	The heart is posterior to the breastbone
Medial	Toward or at the midline of the body; on the inner side of	The groin is medial to the thigh
Lateral	Away from the midline of the body; on the outer side of	The eye is lateral to the bridge of the nose

The spinal column is divided up into three main regions as shown in Figure 36. The upper most of these sections, consisting of seven vertebrae, is the cervical spine, or neck. Below the cervical spine is the thoracic spine, made up of the twelve thoracic vertebrae. These vertebrae articulate (join together as a joint [Ref. 11]) with the ribs and form the mid-back. Finally, the lower back is composed of the five lumbar vertebrae forming the lumbar spine. Each of the vertebrae in the spine may be referred to by an abbreviation such as "C5" that uniquely identifies its location within the spine as shown in Figure 36.

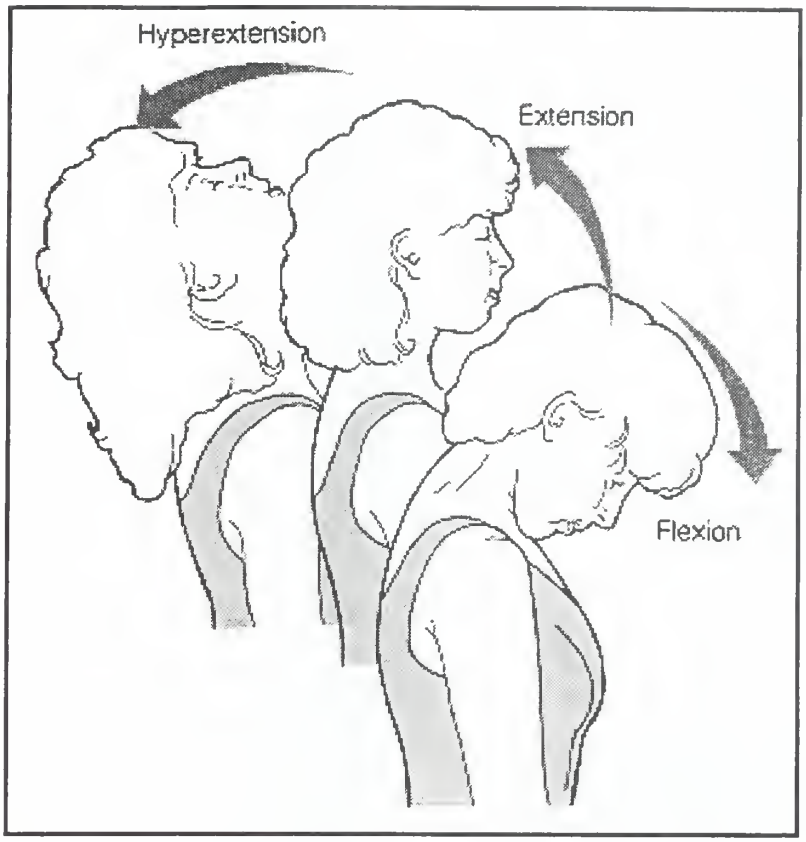

Figure 35. Motions of the Head. After Ref. [10]

The cervical spine forms the connection between the head and the torso, protecting the spinal cord, and, as such, is a very important structure. Figure 37 illustrates the manner in which the seven vertebrae make up the cervical spine to form this connection. The two uppermost cervical vertebrae, C1 and C2, are constructed differently from the remaining vertebrae. C1, also known as the atlas, and C2, also known as the axis, together form the joint between the spinal column and the skull. The two vertebrae are shown in Figure 38 and the joint between the skull and the atlas is shown in Figure 39. Flexion and extension motion of the skull is provided for by the articulation of the occipital condyles, located on the posteroinferior surface of the skull, with the superior articular facets on the atlas. Rotational motion of the skull is provided for by pivoting of the skull-atlas complex around the superior protruding portion of the axis, called the dens. Not shown in any of the illustrations are the vitally important muscles, ligaments, and cartilage that connect and control the motion of head and spine.

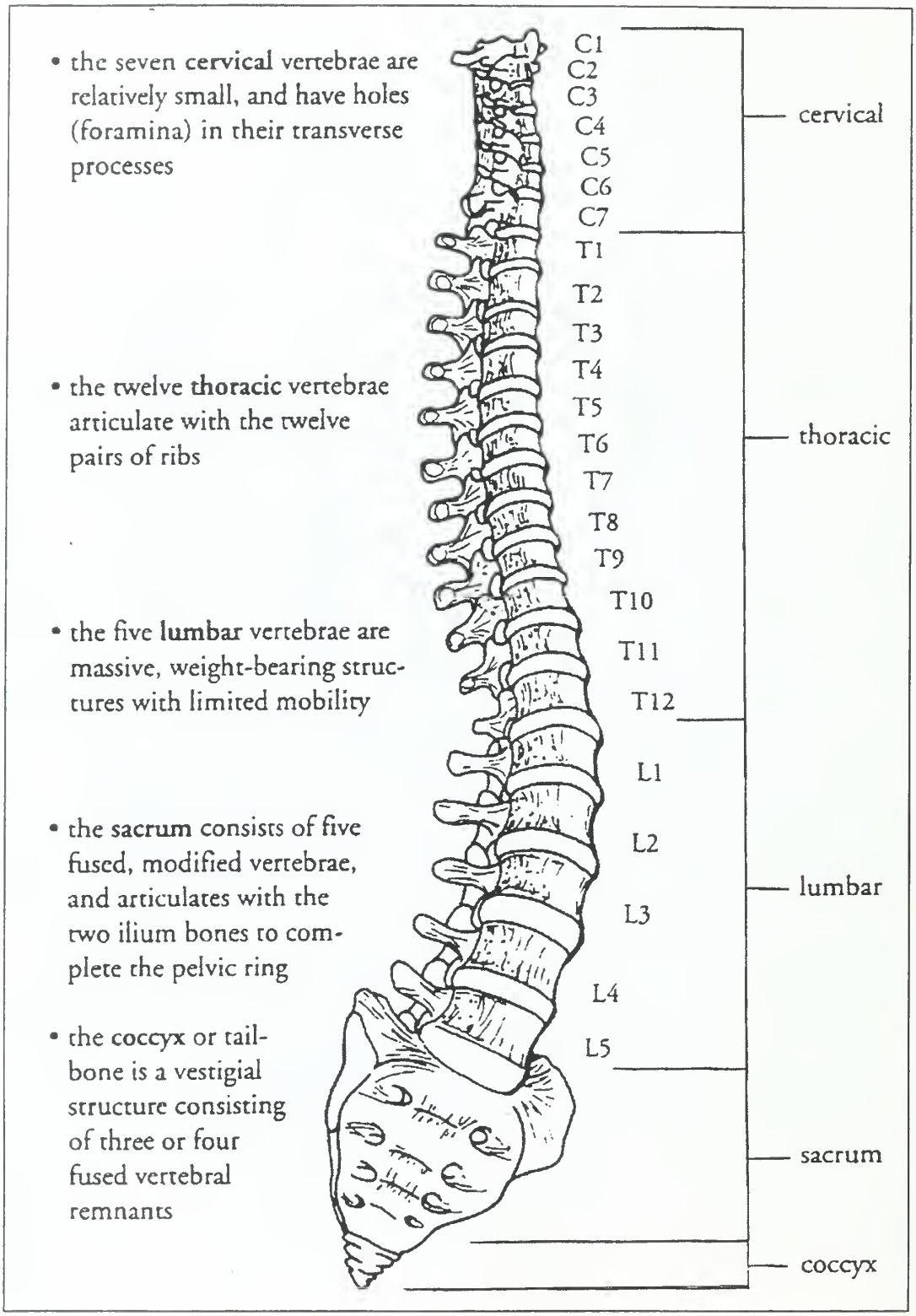

Figure 36. Spinal Column. From Ref. [12]

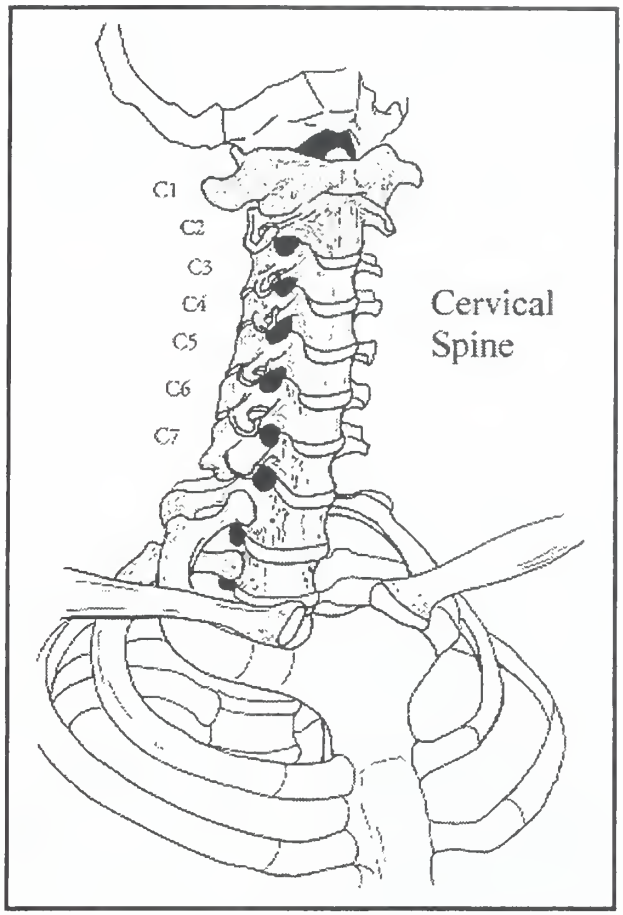

Figure 37. Cervical Spine. After Ref. [12]

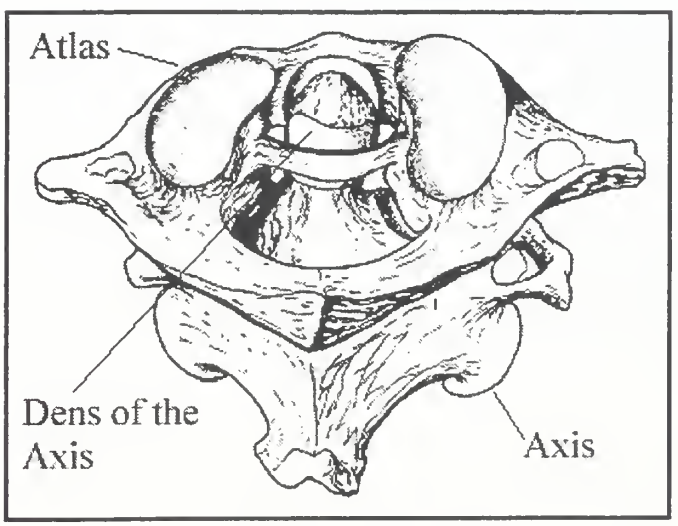

Figure 38. Atlas and Axis. After Ref. [12]

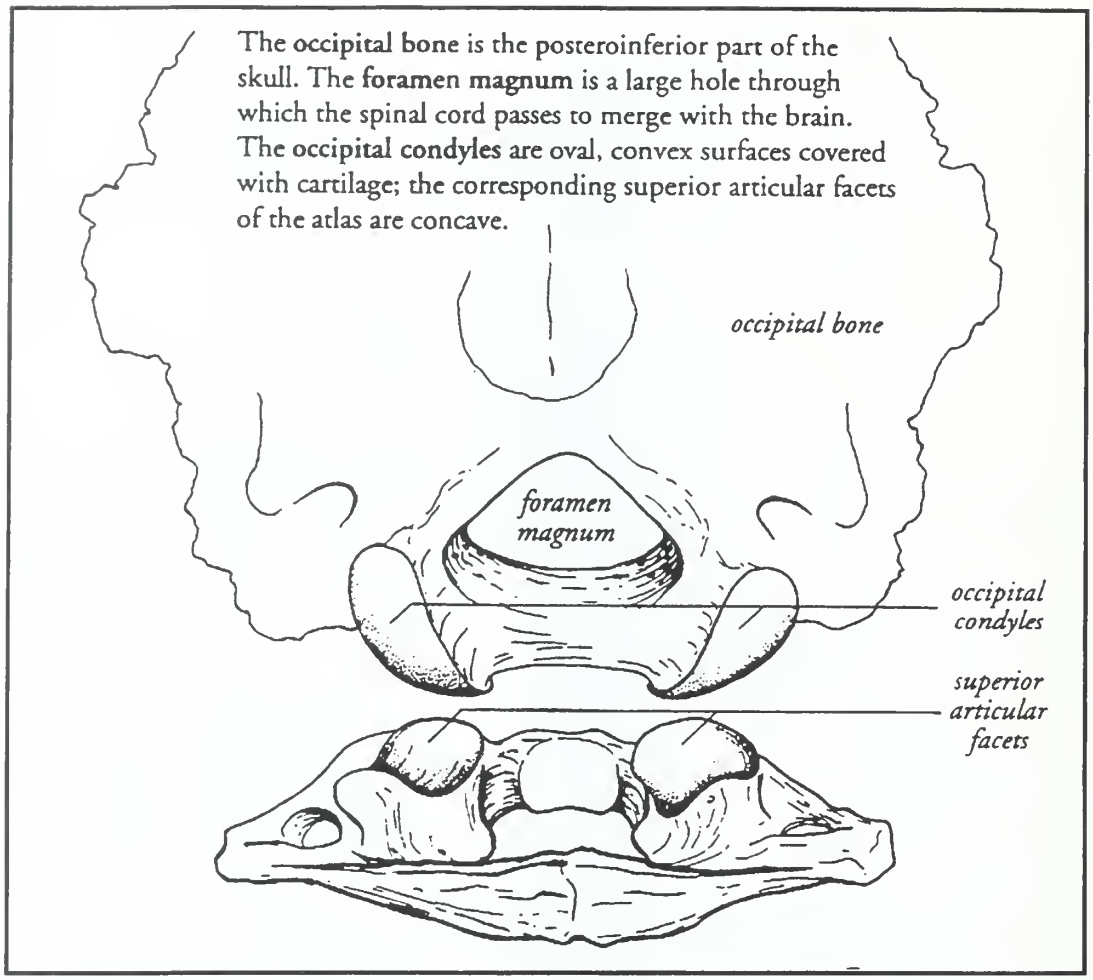

Figure 39. Occipital Condyles. After Ref. [12]

2. Whiplash Injury

Taber's Cyclopedic Medical Dictionary [Ref. 11] gives the following definition for whiplash injury:

> Imprecise term for injury to the cervical vertebrae and adjacent soft tissues. Produced by a sudden jerking or relative backward or forward acceleration of the head with respect to the vertebral column. Injury may occur to those in a vehicle that is suddenly and forcibly struck from the rear.

In an automobile, whiplash typically arises during a rear end collision. The body experiences an anterior acceleration, while the inertia of the head keeps it stationary. The force applied by the torso to the lower portion of the head causes a rotation of the head, resulting in an extension of the cervical spine. If the acceleration is sufficient, the inertial

loading of the cervical spine can result in hyperextension and a whiplash injury. This injury can also arise from flexion of the cervical spine as a result of a sudden deceleration of the body, followed by an extension due to recoil [Ref. 13]. Additionally, restraining the torso during a deceleration event (such as a frontal collision), can lead to a hyperflexion of the head-neck and an associated whiplash injury [Ref. 14].

a. Symptoms and Effects of Whiplash Injuries

Acceleration induced injuries to the soft tissues of the cervical spine can include injuries to the muscles, nerves, ligaments, and vessels. The exact location of the injury is nearly impossible to identify and can be difficult to treat. Hyperflexion can result in damaging the intraspinous (between the vertebrae) ligaments or the posterior longitudinal (along the posterior side of the vertebrae) ligament. Hyperextension can damage the anterior longitudinal (along the anterior side of the vertebrae) ligament. Traction (tension within the cervical spine) frequently accompanies acceleration induced hyperextension or hyperflexion and can result in further injuries to the ligaments. Similarly, muscles can be stretched or torn, with those located along the posterior and anterior portions of the neck being those most commonly damaged. [Ref. 15]

The pain associated with an acceleration induce trauma is usually not immediate, but rather develops over a period of hours or days. The inflammatory response, which take some time to develop, sensitizes the associated tissues and the process may continue for months or even years. Headaches, dizziness, and neck pain are common symptoms. In severe cases, these symptoms become chronic, enduring for years, and can become intrusive on the victim's life. [Ref. 15]

b. Injury Criteria

Since the exact mechanism of injury is not known and the clinical diagnosis is vague, it is difficult to define a specific tolerance level for whiplash injuries. One response parameter that may be examined is the relative angle made between the head and the torso. It has been reported [Ref. 13] that a primary consideration in seat design for protection against acceleration induced trauma is to limit the extension angle of the neck to below 80 degrees and preferably below 60 degrees. A study of frontal collisions yielded the conclusion that a whiplash type injury could be expected for flexion

angles exceeding 58 degrees or for angular accelerations of the head exceeding 950 rad/sec^2 [Ref. 14].

The position of the head relative to the torso may not be the best physical measurement for use in evaluating neck trauma, according to Ref. [16]. Rather, the moment about the occipital condyles would be a better indicator. Through studies involving both volunteers and cadavers, Ref. [16] has developed a both a proposed response envelope and a set of injury criteria for both flexion and extension. Figure 40 and Figure 41 show the proposed response envelopes and torque levels associated with various injuries for the flexion and extension, respectively. In each of the figures, the heavy black lines illustrate the response corridors proposed in Ref. [16]. For a mechanical neck, the torque-angle path traced during both loading and unloading should fall within these bounds. For this research, the corridors are not of particular interest, but the various torque levels will be used as injury criteria for acceleration induced loading of the cervical spine. As seen in Figure 40, the pain threshold in flexion is 44 ft-lb, the injury threshold derived from volunteer testing is 65 ft-lb, and the threshold for ligamentous or bone damage derived from cadaver testing is 140 ft-lb. Reference [16] cautions that the 140 ft-lb limit should be used with caution since there is no guarantee that severe muscle injuries would not be produced at lower torque levels. Figure 41 shows torque levels for extension similar to the flexion thresholds shown in Figure 40. The injury threshold in extension is 35 ft-lb and the threshold for ligament damage in extension is 42 ft-lb. Reference [16] also notes that these values and response corridors are for 50th percentile male subjects and that the corresponding torque thresholds for female subjects tend to be lower. No specific information concerning the tolerance values for small females was found, and, as such, the limits for the 50th percentile male were used for the 5th percentile female subjects as well. Thus, the predicted whiplash injuries for the small female have a tendency to be underestimated.

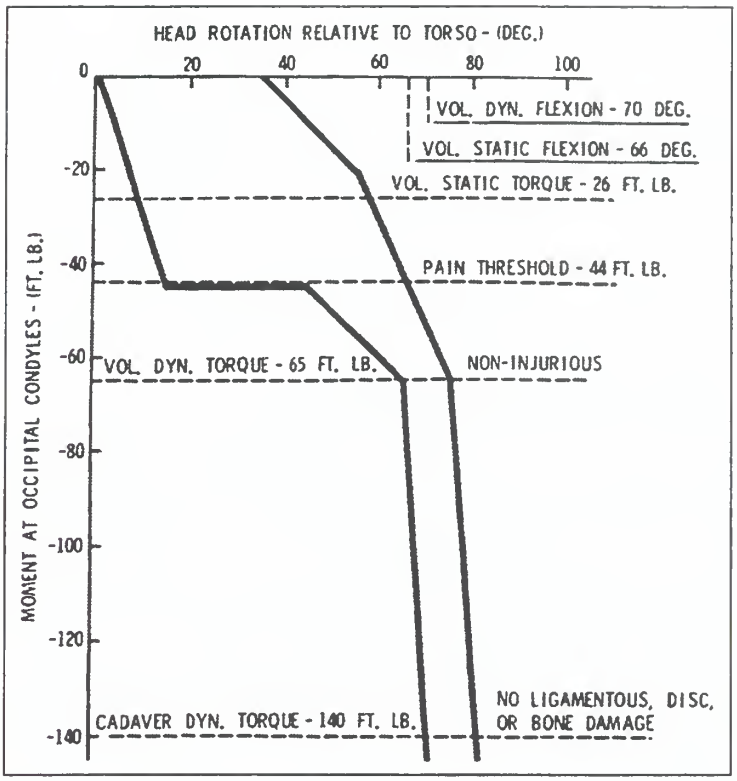

Figure 40. Flexion Response Envelope. From Ref. [16]

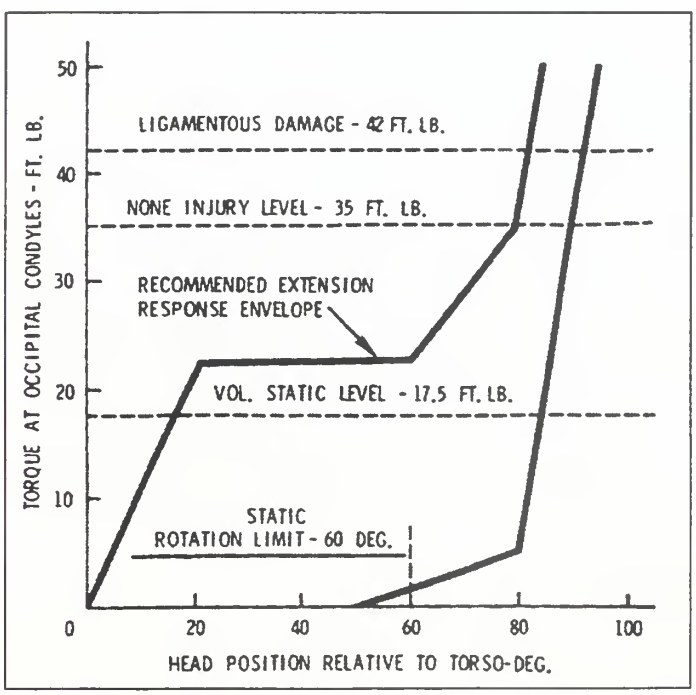

Figure 41. Extension Response Envelope. From Ref. [16]

B. INJURY RESULTING FROM IMPACT

While inertial loading of the cervical spine can result in acceleration induced trauma, more serious injuries are likely to result from loads caused by impact of portions of the body with surfaces in the environment. There are many possible injuries and associated injury tolerances, but only those most relevant to the specific cases studied in this research are presented here.

1. The Abbreviated Injury Scale (AIS)

Some injury criteria, such as the Head Injury Criteria (HIC), refer not to a specific injury, but rather to a certain level on a scaled injury description such as the Abbreviated Injury Scale (AIS). The AIS was developed in the early 1970's to serve as a single comprehensive system for rating tissue damage associated with crash injuries. An AIS code number on a scale of 1-6 is assigned to a specific injury description. It should be noted that the AIS rates the severity of an injury, but does not provide information concerning the outcome or fatality of that injury. The AIS scale is not a linear progression, but rather simply a means of distinguishing between the levels of severity for different injuries. Thus, an AIS 2 injury is not twice as severe as an AIS 1 injury. The basic descriptive terms for the six levels are shown in Table 4.

Table 4. Abbreviated Injury Scale Severity Codes. After Ref. [17]

AIS	Severity Code
1	Minor
2	Moderate
3	Serious
4	Severe
5	Critical
6	Virtually unsurvivable

2. The Head Injury Criteria (HIC)

In the early 1970's, a criterion for head injuries was proposed based upon an averaged value of the resultant acceleration of the center of gravity of the head. This criterion, the Head Injury Criteria (HIC), is computed using Equation (1).

$$HIC = \left[\left(\frac{1}{t_2 - t_1} \right) \int_{t_1}^{t_2} a(t)\, dt \right]^{2.5}_{\text{maximum}} (t_2 - t_1) \qquad (1)$$

The acceleration is expressed in G's and the times t_1 and t_2 are any two points in the acceleration time history that maximize the value of the expression. [Ref. 18]

The Federal Motor Vehicle Safety Standard (FMVSS) 208 limits the maximum time interval for the calculation of the HIC to 36 msec, but the International Organization for Standardization (ISO) limits the time interval to 15 msec. This limitation is imposed to prevent unrealistically high HIC values during air-bag interactions and three-point restraint system testing. The FMVSS 208 limits the value of HIC to 1000, corresponding to a 16 percent risk of an injury of at least AIS 4. Figure 42 shows the variation of risk of at least an AIS 4 injury with the HIC computed using a 15 msec (maximum) time interval. These values are used with the Hybrid III 50th percentile male dummy. The small (5th percentile) female Hybrid III dummy has a HIC limit of 1113, while the large (95th percentile) male Hybrid III dummy has a HIC limit of 957. [Ref. 8]

It is important to bear in mind the fact that an AIS 4 injury is classified as "severe." Some examples of AIS 4 injuries to the head are listed below [Ref. 17]:

1. Skull fracture with leak of cerebrospinal fluid
2. Laceration of the cerebellum or cerebrum
3. Hematoma (epidural, subdural, intracerebral, or intracerebellar)
4. Unconsciousness between 1 and 24 hours

Thus, the limit of 1000 (for the mid-sized adult male) still allows for significant chance of fairly serious injuries. Unfortunately, no correlation between HIC values and the likelihood of injuries with lower AIS ratings could be located.

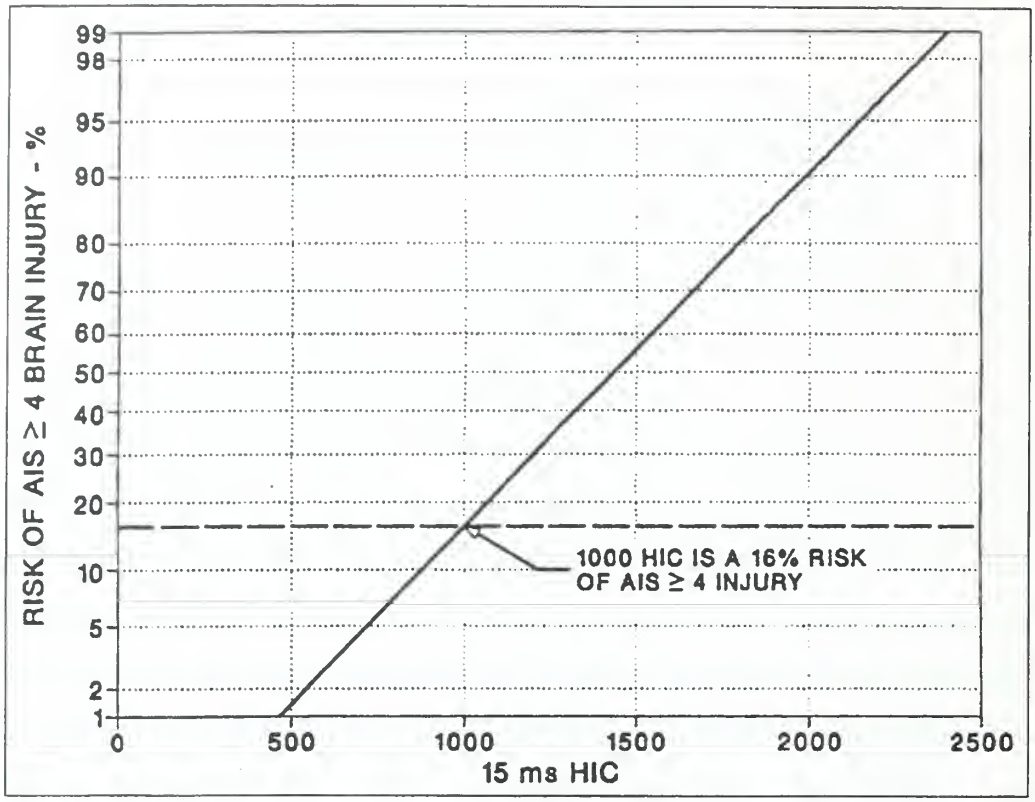

Figure 42. Injury Risk Associated with HIC Values. From Ref. [8]

3. Injuries to the Brain

In addition to the HIC described above, another injury criterion for the brain involving the angular motion of the head has been proposed. As an extension of studies involving rhesus monkeys, squirrel monkeys, and chimpanzees, Ref. [19] has developed a preliminary tolerance threshold for the onset of cerebral concussion based on the head angular velocity and angular acceleration. *Taber's Cyclopedic Medical Dictionary* [Ref. 11] associates the following symptoms with cerebral concussion: transient dizziness, paralyses, or unconsciousness; unequal pupils; shock; vomiting; rapid pulse; headache; and cerebral irritation.

It is presumed that the crucial injury mechanism leading to the onset of cerebral concussion is severe shear strain imposed by brain rotation. The thresholds proposed to predict a 50 percent probability of the onset of cerebral concussion in terms of angular velocity is 50 rad/sec, and in terms of angular acceleration is 1800 rad/sec^2. These

preliminary thresholds may be applied for not only rotational motions imparted by impact, but for those imparted during a whiplash type event. [Ref. 19]

4. Injuries to the Bones of the Face and Skull

In addition to the HIC, several tolerance levels relating impact force to fractures of the bones of the face and skull have been proposed. Reference [20] reports on a variety of experiments concerning the relationship between impact force and fracture of the bones of the face and skull. In most of these studies, impactors of various shapes and sizes were struck against various portions of cadaver skulls and faces. The force of impact was measured and the resulting fracture (if any) recorded. For any particular bone, the force required to cause fracture has significant variability from cadaver to cadaver, but a tolerance limit, below which fracture is not likely, can be proposed. It was noted that the rate of onset of the force, the force pulse duration, and the impactor curvature did not appear to have an effect on the fracture force. It was also noted that female skulls, in general, have lower fracture forces than do male skulls. The suggested threshold forces reported in Ref. [20] are summarized in Table 5. The particular bones that are in question can be seen in Figure 43. [Ref. 20]

Table 5. Fracture Forces for Skull and Facial Bones. After Ref. [20]

	Region	Threshold Fracture Force
Skull	Frontal	4000 N (900 lbf)
	Temporoparietal	2000 N (450 lbf)
Face	Zygomatic	1000 N (225 lbf)
	Maxilla	670 N (150 lbf)
	Anterior-Posterior mandible	1780 N (400 lbf)
	Lateral mandible	890 N (200 lbf)

5. Injuries to the Cervical Spine Due to Axial Loading

The nature of axial loading of the cervical spine can be broken up into the broad categories of compression and tension, although due to the complexity of the cervical structure, the loading will rarely be purely compressive or tensile [Ref. 22]. It is rather

more likely that the loading will be in compression-extension, compression-flexion, tension-extension, or tension-flexion. The mechanisms of injury associated with each of these loading types are summarized in Table 6.

Figure 44 illustrates some of the flexion-compression injury mechanisms, including wedge and burst fractures and anterior dislocation of cervical vertebrae. Jefferson fractures, occurring in compression, are a particular case of multipart fractures of the atlas with the specific fracture locations as shown in Figure 45. Facet dislocations refer to injuries in which the superior vertebral body is displaced anteriorly over its subjacent vertebra with a subsequent locking of the vertebrae in a tooth-to-tooth fashion. If the facet dislocation is bilateral, the facets on both sides of the vertebral body are displaced, resulting in a significant reduction in the neural canal anterior-posterior diameter, an effect usually associated with spinal cord damage. If the facet dislocation is unilateral, only one of the facets is displaced and the likelihood of spinal cord injury is low. [Ref. 22]

Figure 46 illustrates some typical tension-extension injury mechanisms. Occipitoatlantal dislocation is a displacement, either unilateral or bilateral, of the occipital condyles with respect to the atlas typically resulting in ligamentous damage without bony fractures. Unfortunately, the occipitoatlantal dislocation frequently results in damage to the spinal cord near the brain stem and is often fatal. Hangman's fractures are fractures of the axis, separating the anterior and posterior portions, and typically result in a subsequent transection of the spinal cord. Hangman's fracture can occur as a result of a forceful blow to the face or chin, or as a result of properly performed judicial hanging. [Ref. 22]

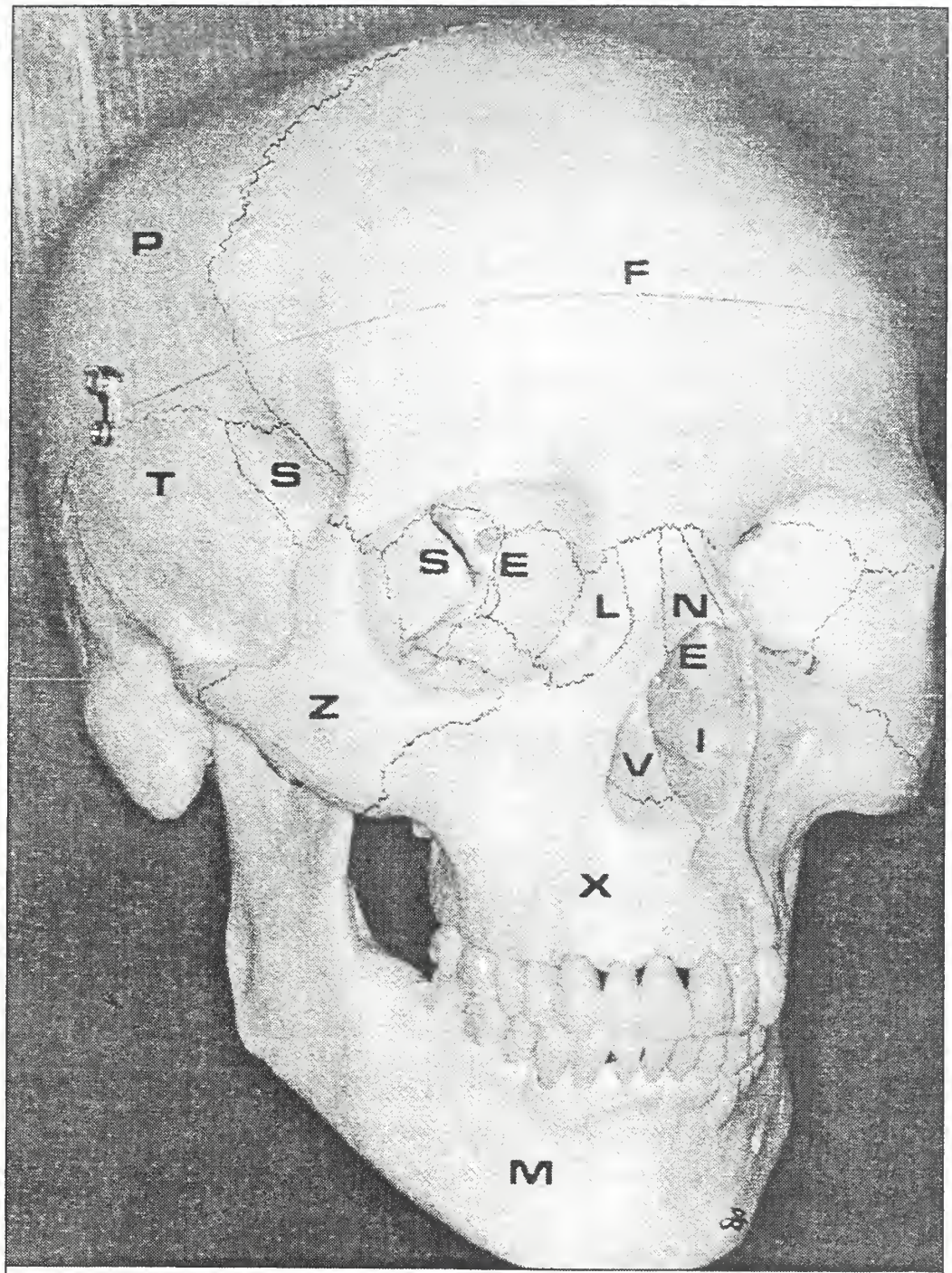

E = Ethmoid, F = Frontal, I = Inferior Nasal Concha, L = Lacrimal,
M = Mandible, N = Nasal, P = Parietal, S = Sphenoid, T = Temporal,
V = Vomer, X = Maxilla, Z = Zygomatic.

Figure 43. Bones of the Skull. From Ref. [21]

Table 6. Cervical Spine Injury Mechanisms. After Ref. [22]

Loading	Mechanism of Injury
Compression	Jefferson fracture Multipart atlas fracture Vertebral body compression fracture Burst fracture
Compression-flexion	Vertebral body wedge compression fracture Hyperflexion sprain Unilateral facet dislocation Bilateral facet dislocation Teardrop fracture
Compression-extension	Posterior element fractures
Tension	Occipitoatlantal dislocation
Tension-flexion	Bilateral facet dislocation
Tension-extension	Whiplash Anterior longitudinal ligament tears Disk rupture Horizontal vertebral body fractures Hangman's fracture Teardrop fracture

The tolerance levels associated with each of the described loading directions are extremely difficult to define. This is partially a result of the sensitivity of fracture forces to the initial position of the cervical spine, the manner and direction of loading, and the end constraints imposed upon the cervical spine [Ref. 22]. Table 7 summarizes some of the fracture force tolerance levels used in this research to estimate the injuries associated with predicted loading of the cervical spine. The duration of loading tolerances used for estimating neck injuries in axial compressive or tensile loading as provided in Ref. [8] and as shown in Figure 47 and Figure 48, respectively, were used in conjunction with the values listed in Table 7.

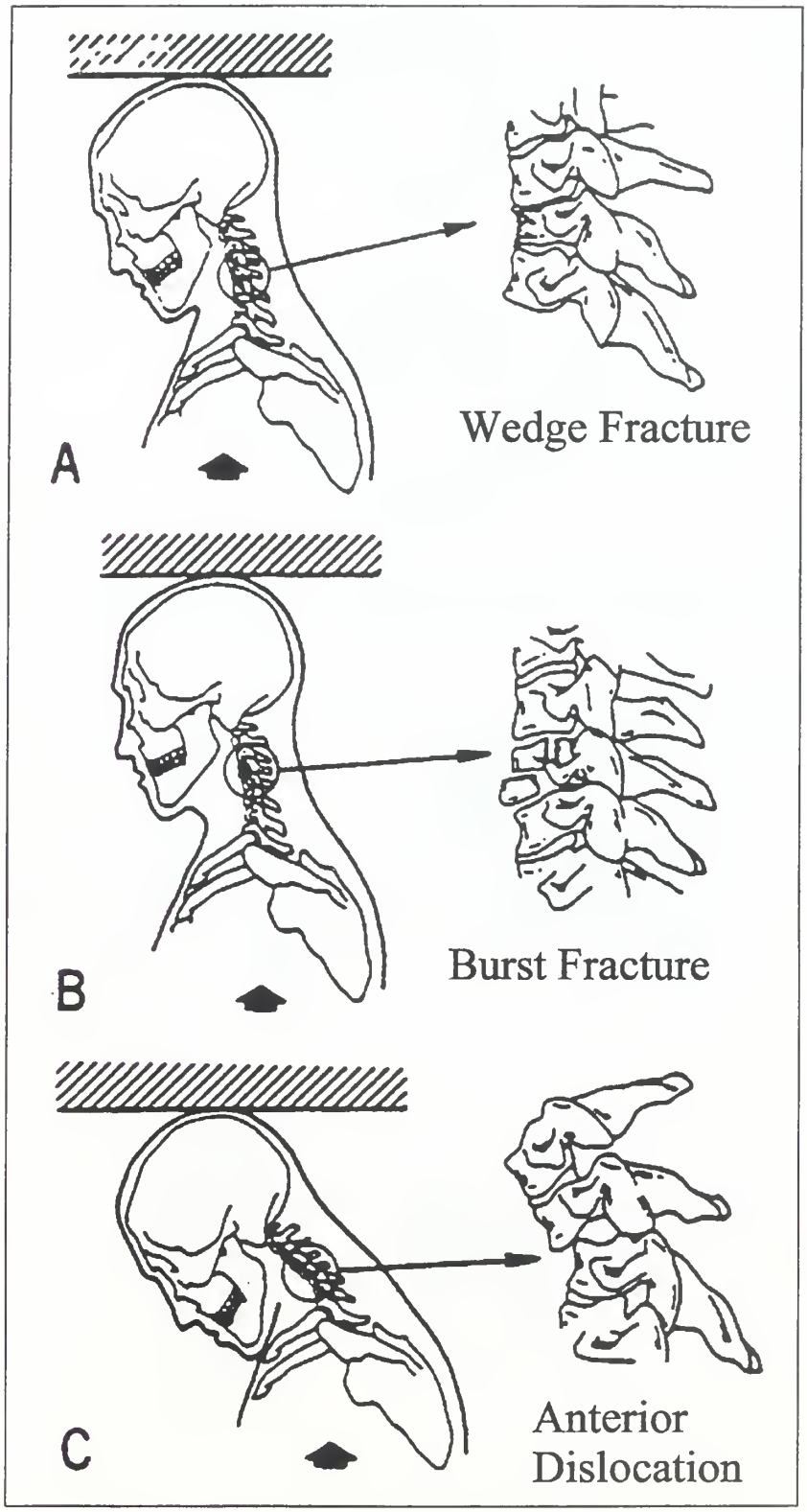

Figure 44. Compression-Flexion. After Ref. [22]

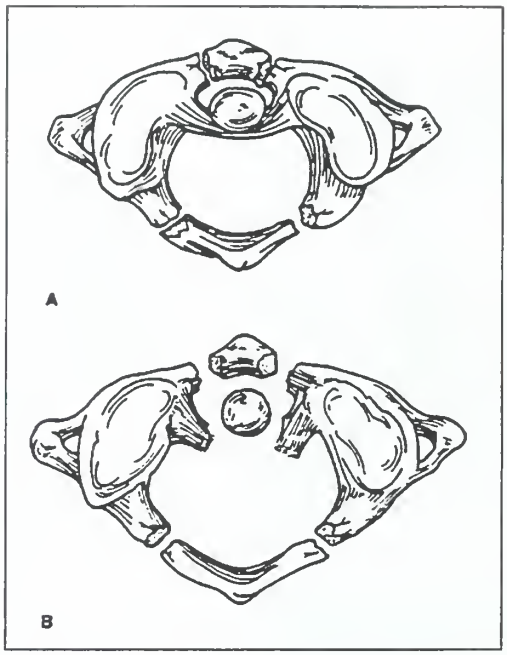

Figure 45. Jefferson Fracture. From Ref. [22]

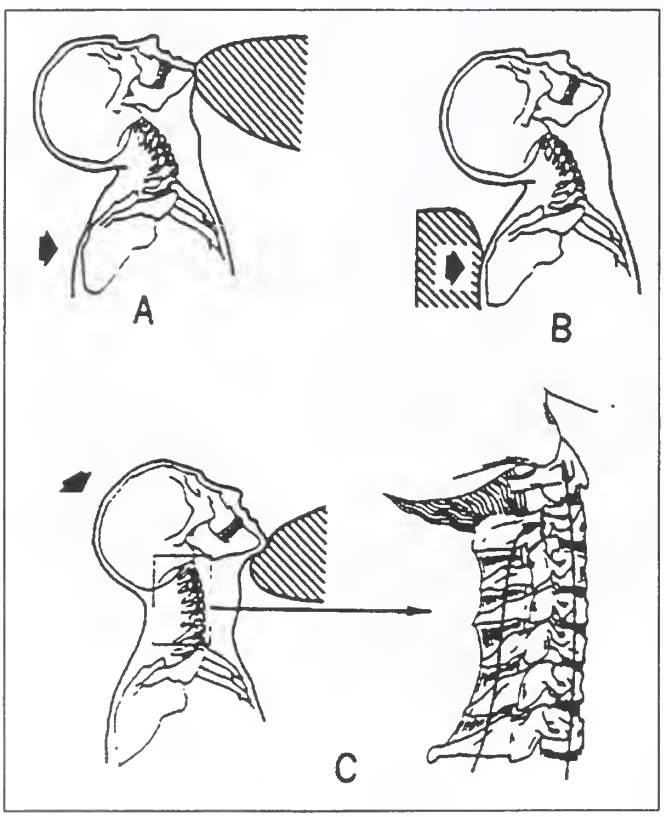

Figure 46. Tension-Extension. From Ref. [22]

Table 7. Tolerance Levels for Axial Loading of the Cervical Spine

Loading	Threshold Force	Source
Compression	6000 N (1350 lbf)	Ref. 23
Compression-flexion	2000 N (450 lbf)	Ref. 23
Compression-extension	2200 N (495 lbf)	Ref. 23
Tension	1450 N (325 lbf)	Ref. 22
Tension-flexion	None found	
Tension-extension	1160 N (260 lbf)	Ref. 22

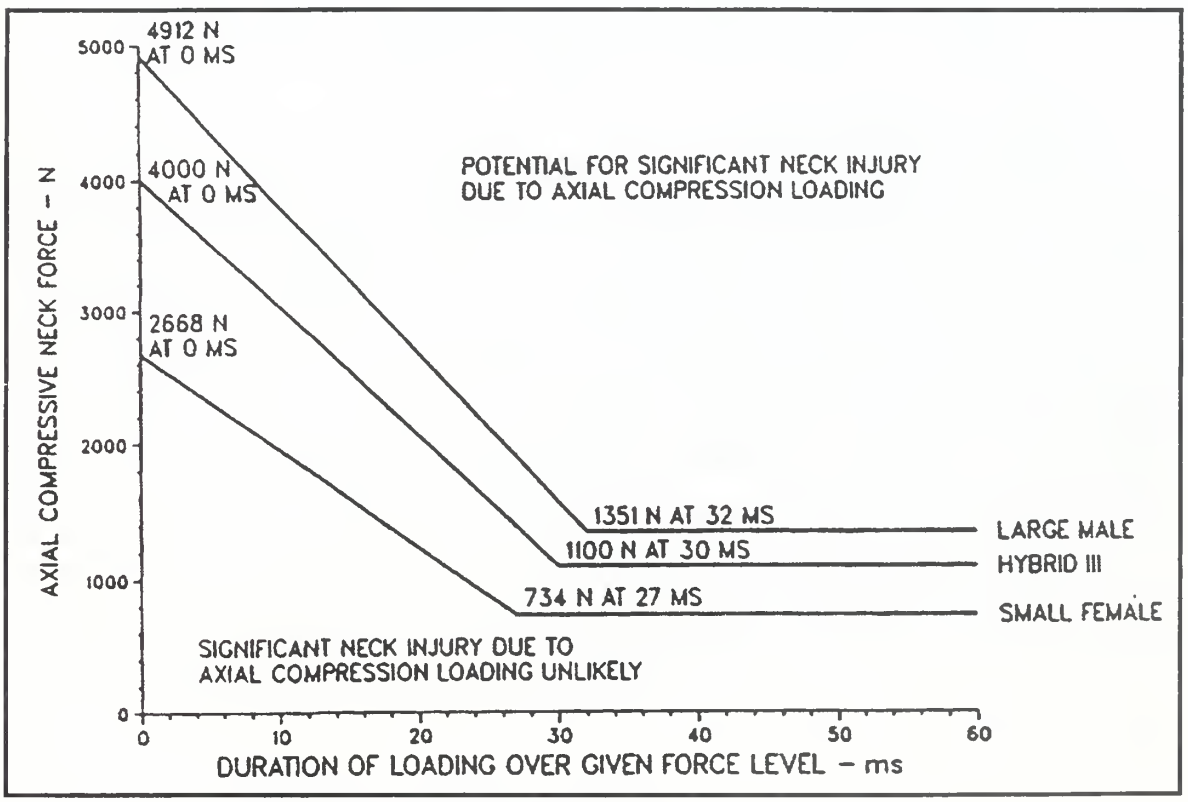

Figure 47. Axial Compressive Neck Force Threshold. From Ref. [8]

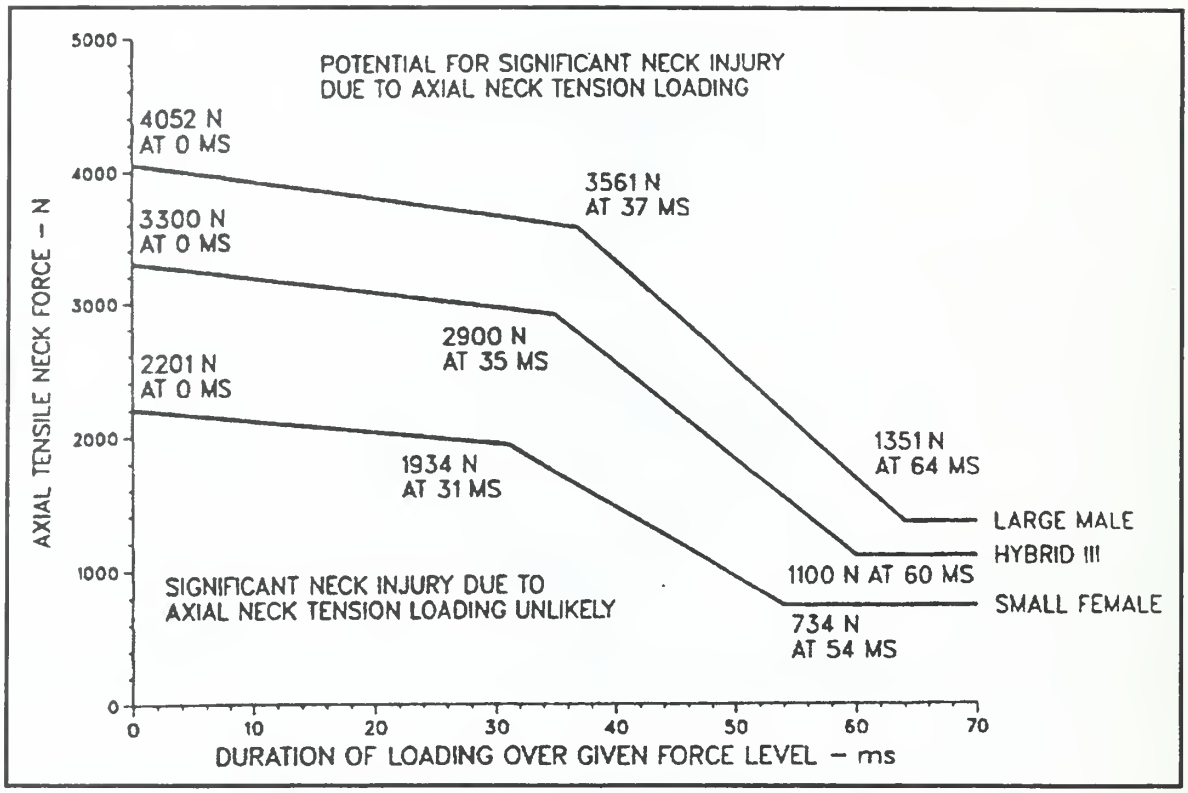

Figure 48. Axial Tensile Neck Force Threshold. From Ref. [8]

6. Injuries to the Femur

Since much of the research concerning the ability of the human body to tolerate various loads is performed with automotive safety in mind, the majority of the femur loading research used knee impacts as the loading mechanism. Some criteria, however, do refer directly to the axial compressive force experienced by the femur. The FMVSS 208 specifies the femur load criteria as 1700 lbf (7.6 kN) [Ref. 8]. However, due to the fracture tolerance strain rate sensitivity of the femur (ultimate strength increases as loading duration decreases), is has been suggested that this limit is too conservative for short pulse loadings [Ref. 24]. As a result, the injury tolerance values for compressive loading of the femur selected for use in this research are those provided in Ref. 8 for evaluating the femur loads measured using Hybrid III ATD's. These tolerances are shown in Figure 49.

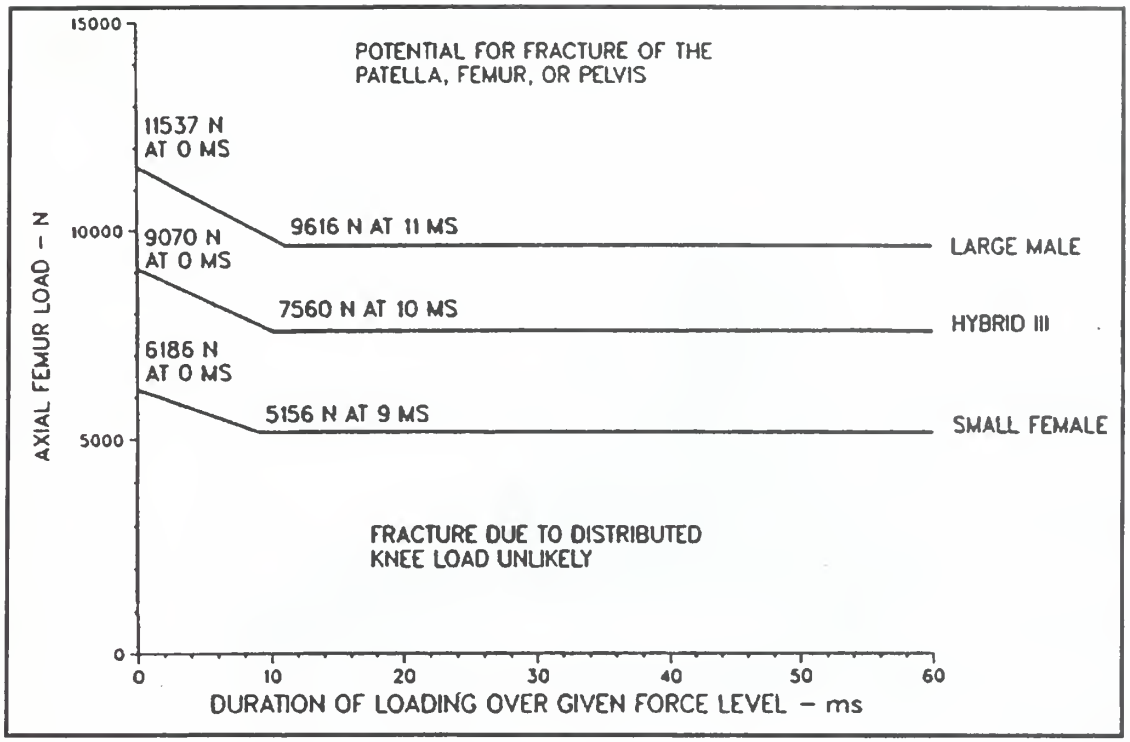

Figure 49. Axial Femur Force Threshold. From Ref. [8]

7. Injuries to the Foot/Ankle Complex

As was the case with femur injury research, much of the research concerning foot/ankle injuries is associated with automotive safety. The predominant loading paths are through the car's foot controls and foot pan. However, since the likelihood of death or paralysis is low for an injury to the foot/ankle complex, the quantity of available information is much less than for injuries to the head/neck complex. In a study where intact adult lower legs (cadaveric) were subjected to an impact to the bottom of the foot, the fracture force, as measured at the superior end of the tibia, ranged from 4.3 to 11.4 kN [Ref. 25]. The predominant injury mechanism was axial compression, with the force passing through the calcaneus, talus, and tibia, and rotational injury modes were less predominant [Ref. 25]. Figure 50 shows the bones that make up the foot/ankle complex, as well as the bones of the lower leg. The tolerance curve is shown as Figure 51. This curve is derived from statistical analysis of the fracture force data. The heavy black line represents the probability distribution for a foot/ankle injury based only upon the applied force, and the thinner lines show the associated plus/minus one standard deviation

boundaries. The black circles are the actual fracture/non-fracture data points. Reference [25] does not make any distinction as to which bone or bones are fractured for a given force level, only that there is a fracture to the bones of the foot/ankle complex.

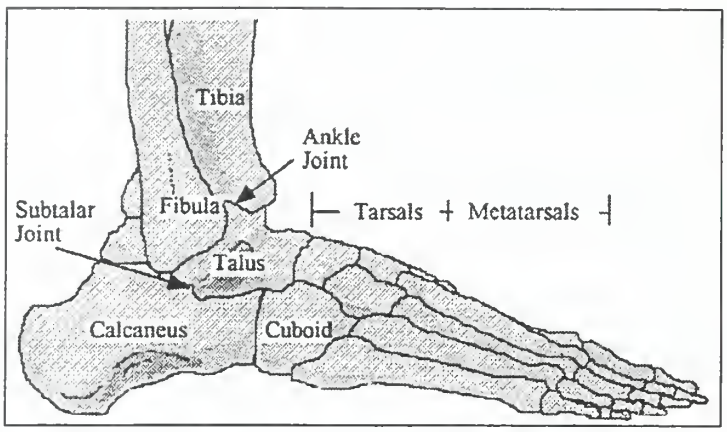

Figure 50. Bones of the Foot and Ankle. After Ref. [26]

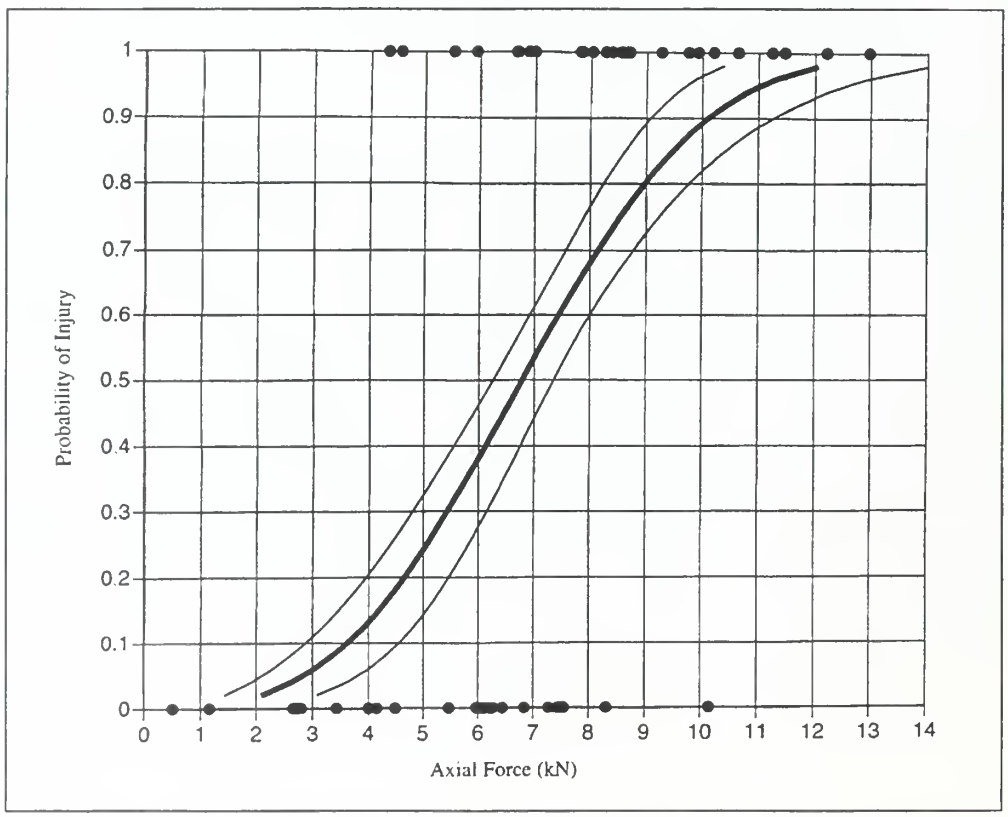

Figure 51. Foot/Ankle Injury Probability Curve. From Ref. [25]

C. SUMMARY OF INJURY CRITERIA

The various injury criteria presented in the previous sections are summarized in Table 8. These are the values used in this research for the estimation of injury potentials associated with predicted bodily responses to underwater explosion induced loading.

Table 8. Summary of Injury Criteria

Body Region	Injury	Criteria	Source
Head	AIS ≥4	Small Female – HIC ≥ 1113 Mid-size Male – HIC ≥ 1000 Large Male – HIC ≥ 957 Figure 42	Ref. [8]
	Cerebral concussion	$\omega \geq 50$ rad/sec $\alpha \geq 1800$ rad/sec^2	Ref. [19]
	Skull bone fracture	Table 5	Ref. [20]
	Facial bone fracture	Table 5	Ref. [20]
Head/Neck Interface	Whiplash	Neck extension ≥ 80 deg	Ref. [13]
		Neck flexion ≥ 58 deg	Ref. [13]
		Occipital condyle torque in flexion - Figure 40	Ref. [16]
		Occipital condyle torque in extension - Figure 41	Ref. [16]
Cervical spine	Fracture force in compression loading	Table 7	Ref. [23]
		Figure 47	Ref. [8]
	Fracture force in tension loading	Table 7	Ref. [23]
		Figure 48	Ref. [8]
Femur	Fracture force in compression loading	Figure 49	Ref. [8]
Foot/Ankle Complex	Fracture force in compression loading	Figure 51	Ref. [25]

VI. EXTENSIONS OF MODELS TO HUMAN SUBJECTS

Once the models of the shipboard environment and shock induced excitation for both the seated (Shot 9991) and standing (Shot 9993) Hybrid III dummies was validated through comparisons of predicted and recorded gross body motions and head, thorax, and pelvis triaxial linear accelerations, these models were extended in order to estimate injuries to both male and female human subjects. In each case, the subjects were modeled in different positions and subjected to the shock excitation. The predicted responses of the subject were compared against the injury criteria described in Chapter V to obtain estimates of the degree of injury expected.

A. METHODS OF EXTENSION

The extensions of the validated model of the shipboard environment and shock induced deck excitation all involved removing the model of the 50^{th} percentile male Hybrid III dummy and substituting in a model of a human subject. For this research, each extension was performed for a 50^{th} percentile adult male and again for a 5^{th} percentile adult female. The basic dimensions for these subjects are shown in Table 9. These models of the human subjects were then positioned as desired, either within the chair for the seated model or upon the deck for the standing model. The simulations were performed and the predicted responses of the human subjects were compared against the specific injury criteria previously discussed. For more information concerning the manner in which extensions were made to the validated models, see Ref. [1].

Three separate situations were modeled as extensions of the seated simulation. First, no changes were made except to the initial position of the subject. The original position of the Hybrid III dummy for the actual test as seen in Figure 6 was not considered particularly natural. Rather, it was desired to have the subject seated upright with both hands resting on the upper legs as seen in Figure 52 and Figure 53 for the male and female, respectively. The male and female human subjects were thus positioned in this manner and equilibrium reestablished prior to performing the simulations.

Table 9. Basic Dimensions of Male and Female Human Subjects

	50th Percentile Male	5th Percentile Female
Weight	173.5 lb	99.98 lb
Standing Height	69.82 in	59.94 in
Seated Height	36.69 in	31.99 in

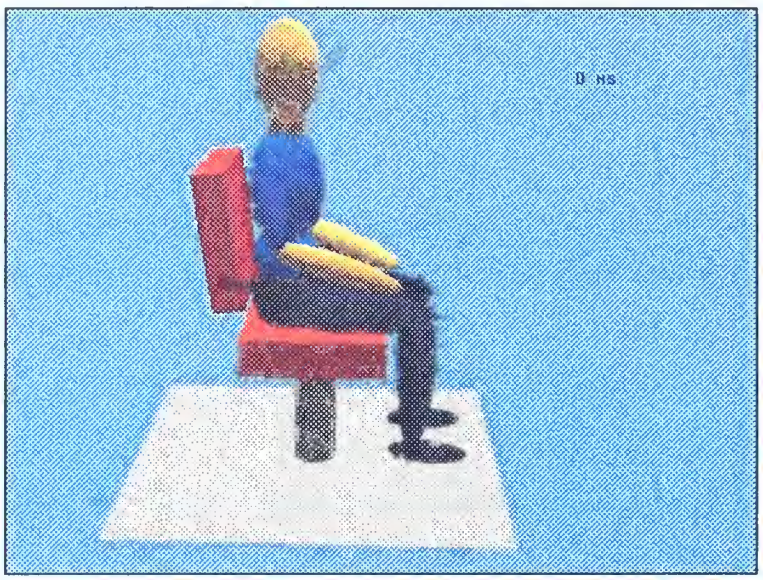

Figure 52. Belted Male Initial Position

Figure 53. Belted Female Initial Position

The second extension of the seated model was the removal of the lap belt and the addition of a desk. The lap belt was simply deleted from the model with no repositioning of the models of the test subjects required. The desk shown in Figure 6 was considered to be unrealistically far forward of the chair, so the model of the desk was placed closer to the subject. For more information concerning the modeling of the desk, consult Ref. [1]. The initial positioning of the male and female subjects, and the position of the desk surface, can be seen in Figure 54 and Figure 55, respectively. Note that the edge of modeled desk is above the subjects knees, where as the original desk, as shown in Figure 6, is well forward of the ATD's knees.

The third and final extension of the seated simulation was based upon the second extension. The lap belt was still removed and the desk was modeled exactly as before, but a computer keyboard and terminal were added. The keyboard was modeled as a single plane, and the terminal was modeled with a single plane for the screen, and another for the top. The male and female subjects, as shown in Figure 56 and Figure 57, respectively, were positioned the same as in the previous simulation. The sides of the keyboard and computer are shown for aesthetic purposes alone and are incapable of generating contact forces.

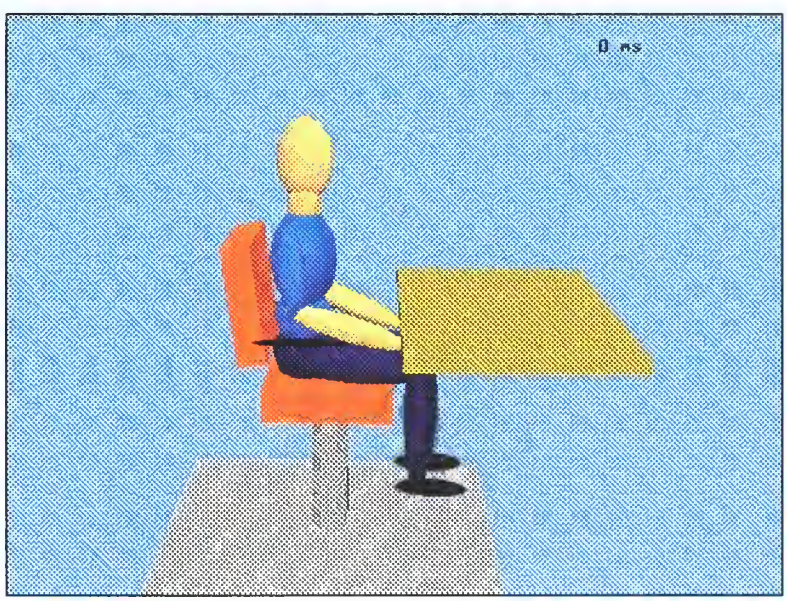

Figure 54. Unbelted Male Initial Position

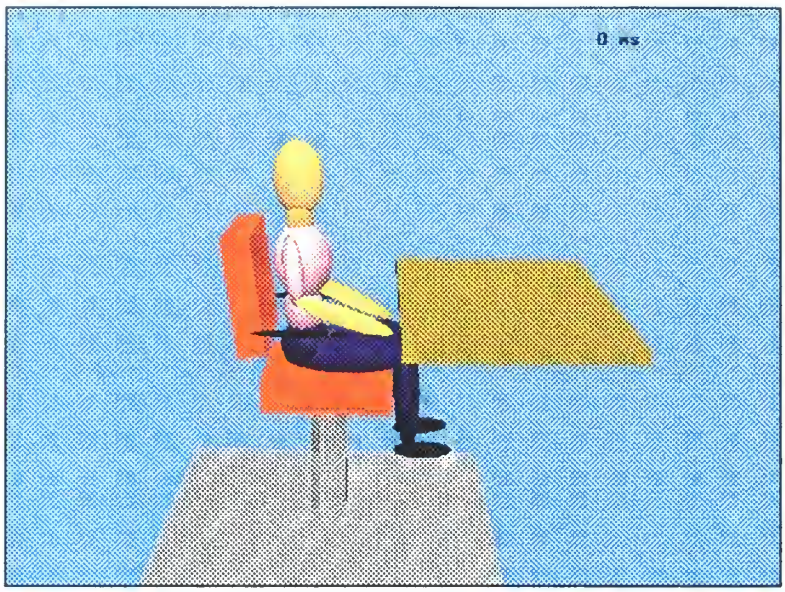

Figure 55. Unbelted Female Initial Position

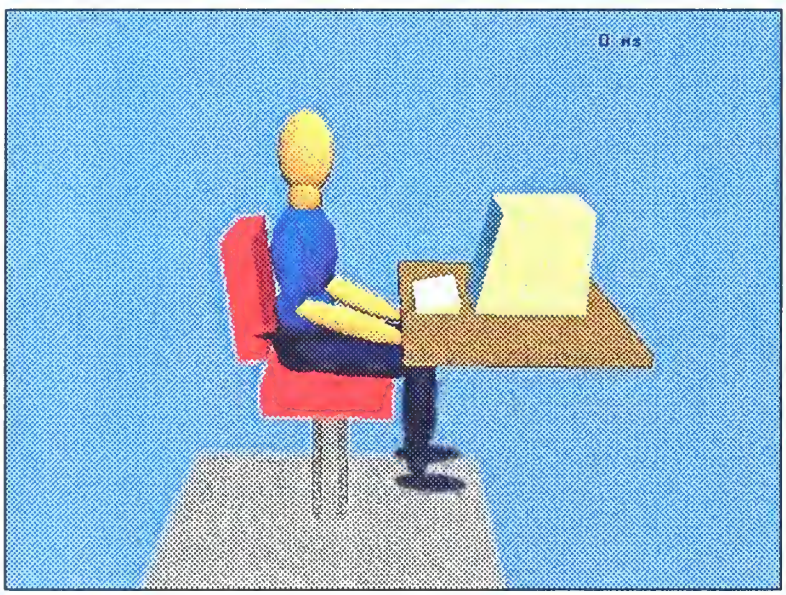

Figure 56. Male at Computer Initial Position

Two separate situations were modeled as extensions of the standing simulation. As was the case for the seated simulations, each situation was simulated for both a 50th percentile adult male and a 5th percentile adult female. In both of the situations modeled, the elastic cords supporting the Hybrid III dummy were deleted. The first extension of the standing simulation was for subjects standing erect with legs straight (knees locked).

The setup for the male and female subjects can be seen in Figure 58 and Figure 59, respectively. The second extension of the standing simulation was to position the subjects with their knees bent as shown in Figure 60 and Figure 61 for the male and female, respectively.

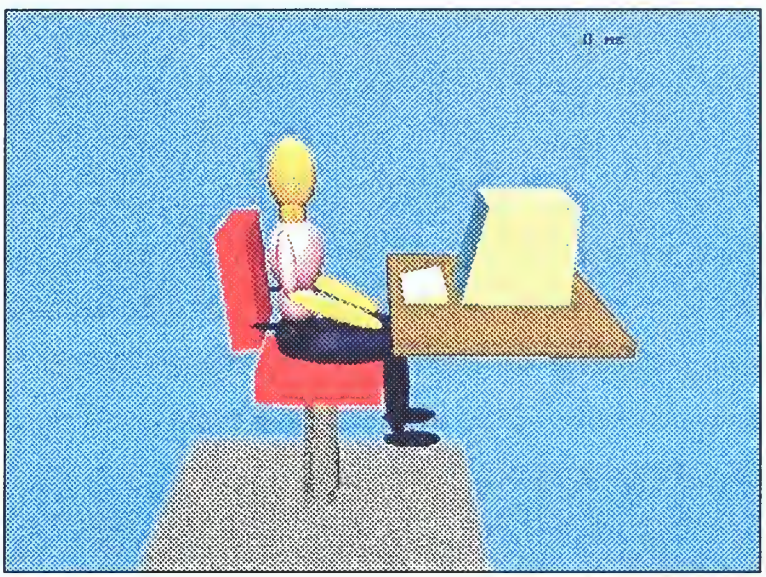

Figure 57. Female at Computer Initial Position

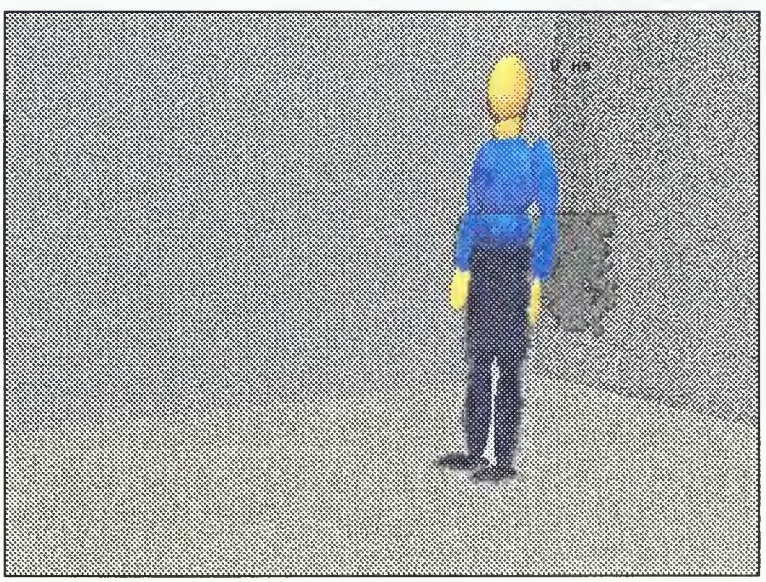

Figure 58. Male with Locked Knees Initial Position

For both of these extensions, the subjects were kept in their initial positions from the start of the simulation until the first significant deck acceleration (approximately 15 msec) by locking the hips, knees, and ankles. These joints remained locked until the specified torque was exceeded then were free to move within the constraints of their joint parameters. The torque values were chosen such that the joints became unlocked when the initial deck acceleration occurred. The locking of these joints served a similar purpose as did the elastic cords that supported the Hybrid III dummy during the actual test. They kept the subject in the desired position until the shock excitation could be applied. Unlike the cords, however, the locking of the joints had no effect upon the simulation once the specified torque levels were exceed and the joints became unlocked.

The walls shown in each of the figures help provide a visual frame of reference when viewing the motion of the standing subjects. As was the case for the sides of the keyboard and computer terminal in the third extension of the seated simulation, these walls are incapable of generating contact forces.

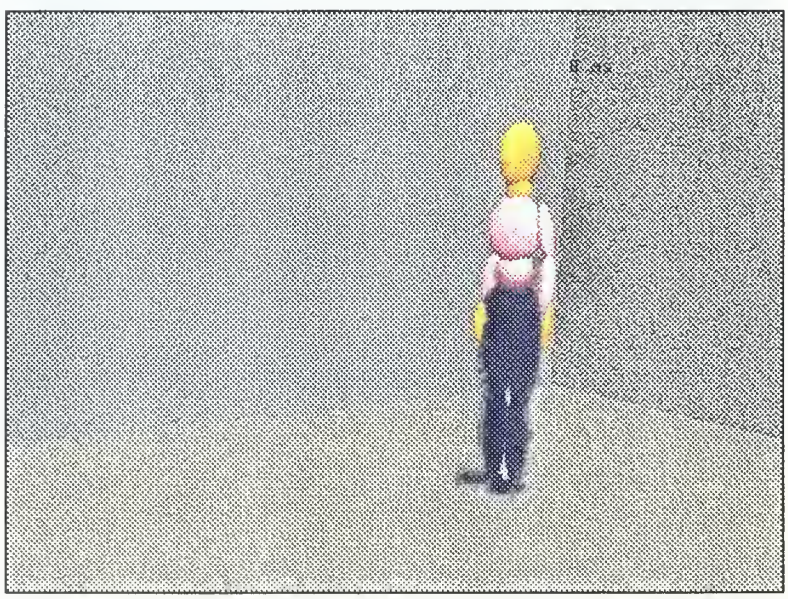

Figure 59. Female with Locked Knees Initial Position

Figure 60. Male with Bent Knees Initial Position

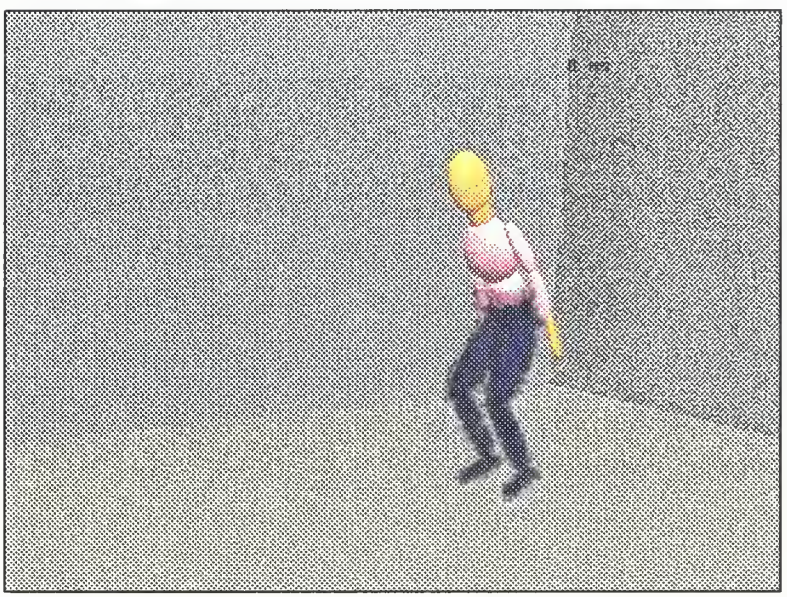

Figure 61. Female with Bent Knees Initial Position

B. COMPUTATION OF PARAMETERS

All of the data that is needed to perform estimates of the injury potentials described in Chapter V was generated using the ATB program. Some of the data

required further manipulation, such as for the computation of segment axial forces, but most simply required unit conversions to agree with the units used in the injury criteria.

The HIC was computed directly using the ATB program in a post-processing run. Unfortunately, the ATB program does not limit the time period to 15 msec as does the ISO. Rather, any two time points that maximize the expression for HIC (Equation 1) serve to form the HIC interval. As will be seen in the discussion of the results, the larger values of HIC tended to have short time intervals near 15 msec in length, and none of the HIC values exceeded the specified criteria.

The head angular acceleration and velocity values used for estimating the likelihood of cerebral concussion were generated directly using the ATB program. The resultant values of the head's angular acceleration and velocity, predicted at the center of gravity of the head, were simply converted from revolutions/sec^2 to radians/sec^2, in the case of acceleration, and from revolutions/sec to radians/sec, in the case of velocity.

The impact forces used for estimating the likelihood of fractures to the bones of the face and skull were also generated directly using the ATB program. The resultant (normal and friction) head-desk, head-computer, or head-deck forces generated through contact between the head segment and the environmental contact surface modeling the desk, computer, or deck, as appropriate, were taken from the individual output files. To estimate the specific region of the face or skull subjected to this force, and thus the potential fracture site, the motion simulation generated using the IMAGE program was studied closely and the area of the ellipsoid representing the head coming in contact with the appropriate surface was correlated to the corresponding region of the face or skull. Thus, the skull and facial bone fracture estimates are estimates both of the force applied and of the location of the application of this force.

The angle of the head with respect to the upper torso used in estimating whiplash injuries and for determining flexion or extension of the neck for spinal fracture estimates was also generated directly using the ATB program. The angle of the head segment was generated with respect to the upper torso segment. The pitch component of this relative angle was used as the angle of flexion or extension. No unit conversion was necessary. The torque at the occipital condyles, used for estimates of whiplash injury, was taken to

be the resultant (spring and viscous) torque generated at the head pivot joint. The units were converted from in-lb to ft-lb to be consistent with the injury criteria.

The remaining three injury criteria, cervical spine injury due to tension or compression loading, femur fracture due to compression loading, or fracture in the foot-ankle complex due to compression loading, were all estimated in a similar manner. First, the axial force in the segment of interest (neck, upper leg, or lower leg) had to be estimated. This estimate was based on the positions of the joints at either end of the segment and the associated joint forces. Figure 62 provides some insight into the procedure used to determine the axial force on an arbitrary segment, Segment A, based on the forces and positions of the joints at either end of the segment, Joints 1 and 2.

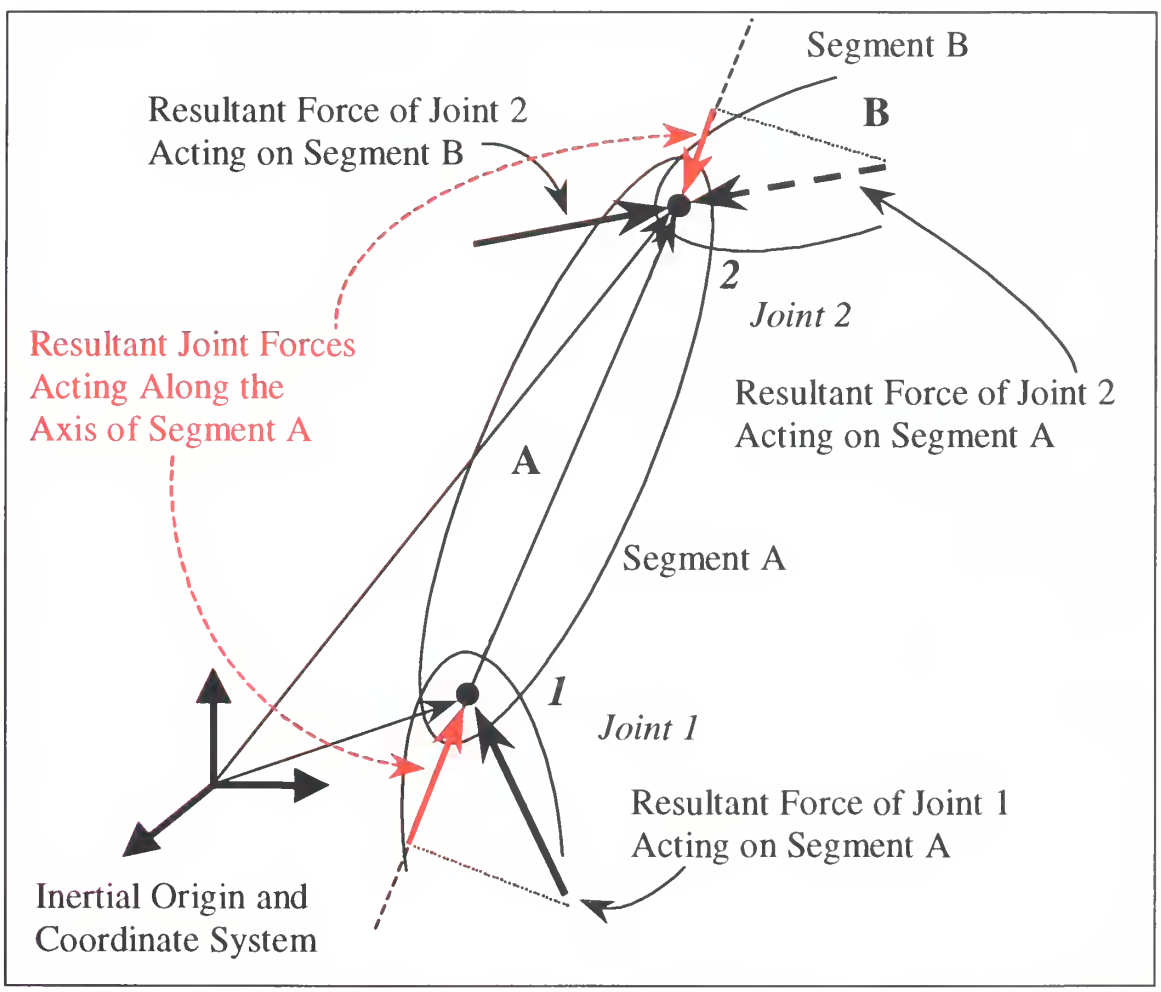

Figure 62. Method of Axial Force Determination

Joint positions, in inertial coordinates, were generated using the ATB program. These points were taken as the terminal points of position vectors from the origin to location of the joints. The vector difference between these two position vectors is a vector from Joint 1 to Joint 2 as seen in Figure 62. This vector was taken to be the axis of the joint and was converted to a unit vector by dividing it by its Euclidean length.

The joint forces generated using the ATB program are output in X, Y, and Z (inertial) component form as forces applied by the joint to the attached segment. Thus, the forces at Joint 1 are applied to Segment A and the forces at Joint 2 are applied to Segment B. The forces at Joint 2 applied to Segment A are then equal and opposite to those applied to Segment B. The scalar products of these resultant joint force vectors with the unit vector in the axial direction of the segment determined the component of each of the joint forces that acted axially. These axial components are shown as red arrows in Figure 62. The net axial force, with compression defined to be negative, was determined by subtracting the axial component at Joint 1 from the axial component at Joint 2. The final step was unit conversion from lbf to Newtons to be consistent with the injury tolerances.

C. EXTENSION OF SEATED SIMULATION

As previously described, the validated model of the operator's chair and deck excitation for Shot 9991 was extended to three separate situations. The first situation was identical to the original model, but the human subjects were positioned more naturally. The second situation involved removing the lap belt and placing a bare desk in front of the subjects. The third simulation was the same as the second, but with a computer terminal and keyboard placed on the desk. For each situation, the simulation was performed for a 50^{th} percentile male subject and for a 5^{th} percentile female subject. Thus, six separate simulations were performed as extensions of the validated model of the chair and deck excitation for Shot 9991. No examination was made of the femur or of the foot-ankle complex for the seated simulations since there were no significant forces expected. In addition, the potential head impact injuries (HIC and fracture to skull or facial bones) were only estimated for the second and third simulations where heat impact occurred.

1. Wearing Lap Belt

a. Results for the male subject

The gross bodily motion experienced by the seated male subject wearing a lap belt is illustrated in Figure 63 by a series of frames taken from the motion visualization generated using the IMAGE program from the response predicted using the ATB program. As expected, this motion is quite similar to that of the Hybrid III dummy, shown in Figure 19 and Figure 20. The subject's upper body moves forward, bending over the lap belt, while the lower legs extend. At around 350 msec, the upper torso strikes the upper legs and the entire upper body rebounds with an associated flexion of the neck. This rebound is not as severe as the one experienced by the Hybrid III dummy in that the upper body does not fully contact the seat back and cause a significant extension of the neck. This effect is likely a result of the differences in initial positions of the arms. For the Hybrid III dummy, the arms were initially folded across the chest. When the torso folded forwards, the elbows struck the upper legs and arrested the forward motion, keeping the torso in a more erect posture. By repositioning the arms, this arresting action was eliminated as the elbows went to either side of the upper legs and the torso was free to continue in forward motion until it struck the upper legs.

The male subject underwent three additional cycles of the torso rebounding off the upper legs, but none as violent as the first. These rebounds occurred at approximately 1050 msec, 1350 msec, and 1850 msec. The final position of the subject was with the torso bent forward, neck in flexion, and both arms dangling between the legs.

No head impact criteria, such as the HIC or fracture of the bones of the skull or face, were evaluated for the seated male subject wearing the lap belt since there was no head impact. However, to allow comparison to the results of the other simulations, the resultant linear acceleration of the center of gravity of the head is shown in Figure 64. The peak head linear acceleration was 14.3 g's and occurred at 354 msec during the first rebound of the torso off the upper legs.

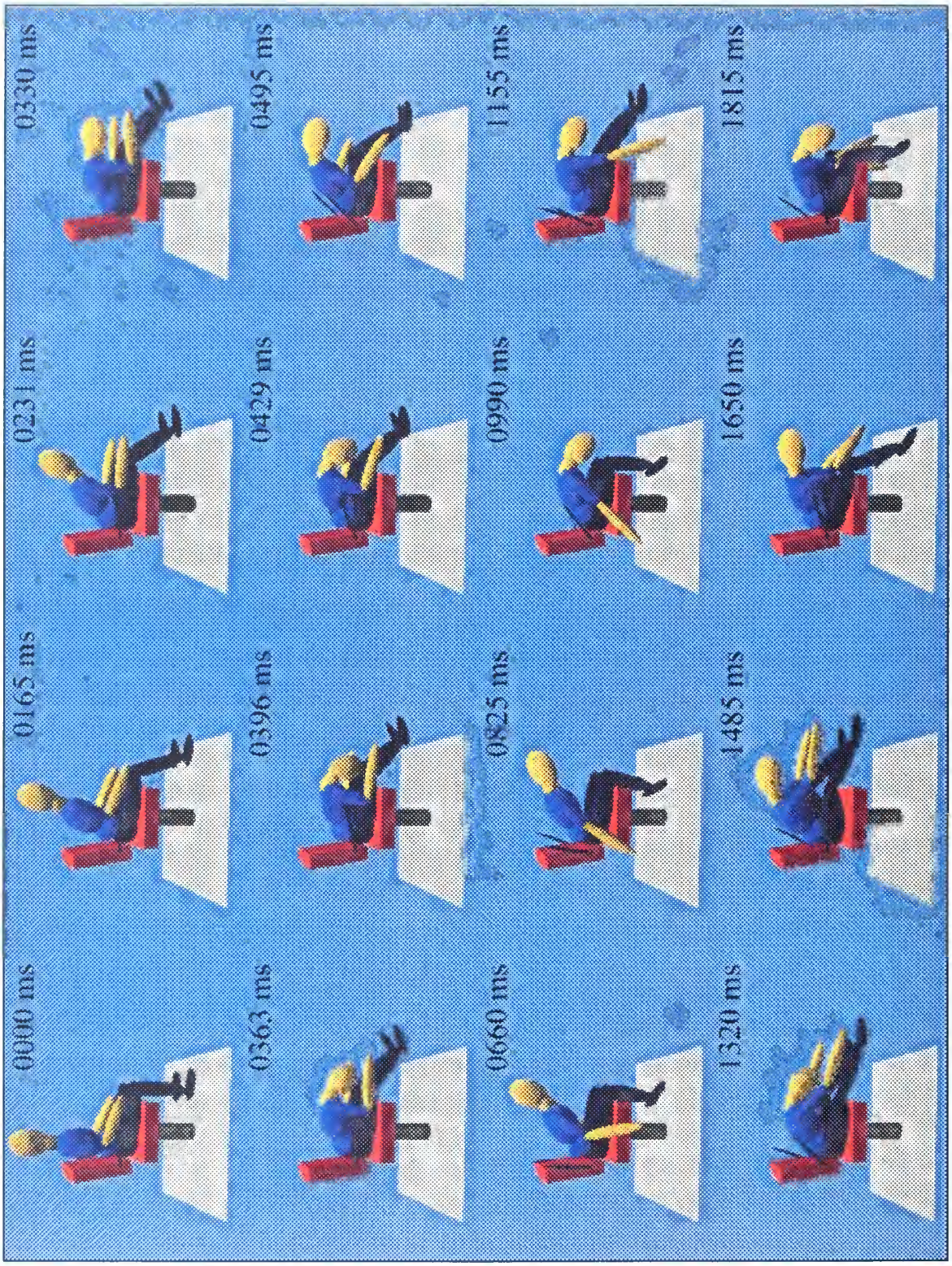

Figure 63. Predicted Motion of the Male Subject Wearing a Lap Belt

The head resultant angular accelerations and velocities, shown in Figure 65 and Figure 66, respectively, were examined and compared against the criteria for cerebral concussion. The peak head angular acceleration was 2242 rad/sec^2, occurring at 388 msec, and the peak head angular velocity was 29.3 rad/sec, occurring at 368 msec. Both of these peaks are results of the inertial loading of the head as the upper torso rebounds off the upper legs for the first time. The peak angular acceleration exceeds the tolerance value of 1800 rad/sec^2, but the peak angular velocity falls below the tolerance value of 50 rad/sec. Based on the angular acceleration, the subject would possibly receive a cerebral concussion during the first torso rebound.

In order to estimate the likelihood of whiplash injuries, both the head position with respect to the torso, shown in Figure 67, and the torque at the occipital condyles (head pivot), shown in Figure 68, were examined. Looking first at the head position, the angle in flexion was found to exceed the 58 degree tolerance limit four separate times, once for each of the torso rebounds. The first occurrence was at 398 msec where the head reached an angle of 91.8 degrees. During this rebound cycle, the peak torque at the occipital condyles was 44.1 ft-lb, occurring at 389 msec. This is slightly above the 44 ft-lb pain threshold for flexion. Finally, since whiplash is a tension-extension or tension-flexion injury, the neck axial force, shown in Figure 69, was consulted to verify that neck was actually in tension during this period. Since the neck was found to be in tension, with an angle of flexion well in excess of the limit, and with a head pivot torque value at the pain threshold, it is probable that the subject would experience a whiplash injury during the first rebound of the torso off the upper legs.

The second occurrence of the neck flexion angle exceeding the 58 degree limit was at 1020 msec where the angle reached 63.0 degrees during the second torso rebound. While the neck was in tension during this period, the head pivot torque was low. Thus, a whiplash injury during this rebound was deemed possible, but not likely. The third occurrence of excessive neck flexion angle was during the third torso rebound where the angle reached 82.8 degrees at 1344 msec. The head pivot torque during this rebound peaked at 12 ft-lb, occurring at 1327 msec. The neck was lightly loaded in compression during this period, so a whiplash injury was not expected to occur during the

third rebound. The fourth rebound resulted in the final occurrence of excessive neck flexion angle. The peak angle was 79.1 degrees and occurred at 1851 msec. The associated head pivot torque was only 5.5 ft-lb, occurring at 1832 msec, and the neck was loaded in tension. Thus, similar to the second rebound, the fourth rebound resulted in a possible, but not likely, whiplash injury.

Examination of the axial loads experienced by the cervical spine, shown in Figure 69, indicated that all forces were well below the limits for both compression and tension. The peak compressive load was 714 N and occurred at 86 msec and the peak tensile load was 519 N and occurred at 341 msec. The peak compressive load was a result of the initial upwards acceleration of the chair, while the peak tensile load occurred as a result of inertial loading of the neck during the first bounce of the torso off the upper legs.

The injury estimates for the seated male wearing the lap belt are summarized, along with the estimates for the female, in Table 10.

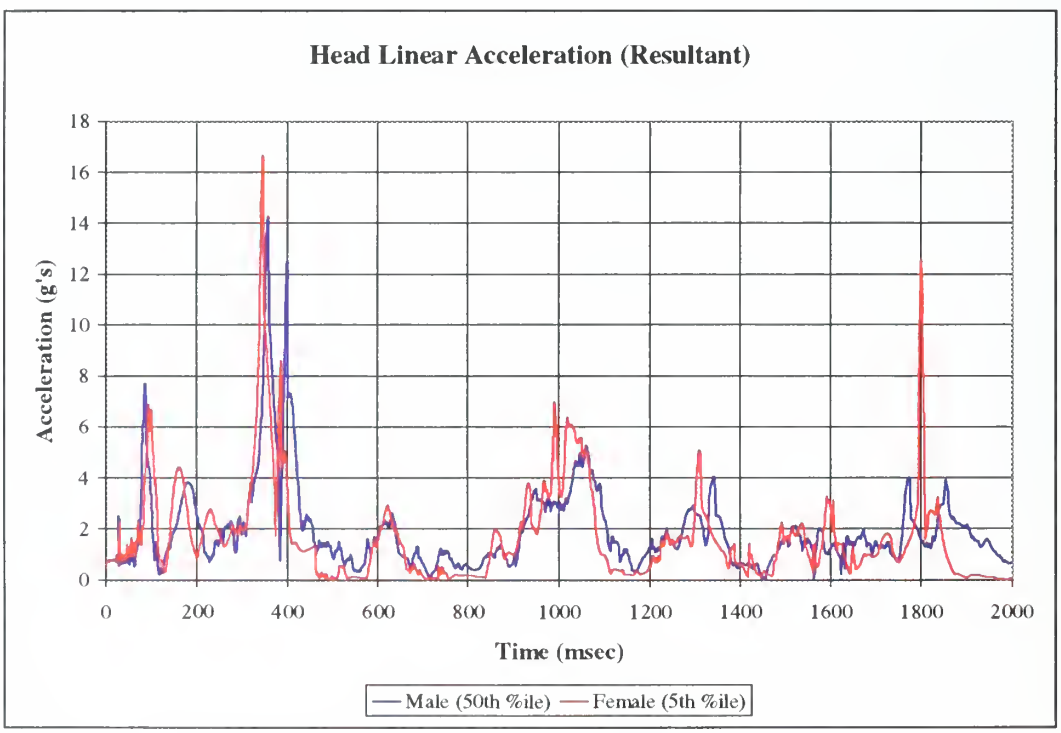

Figure 64. Head Linear Accelerations for Belted Subjects

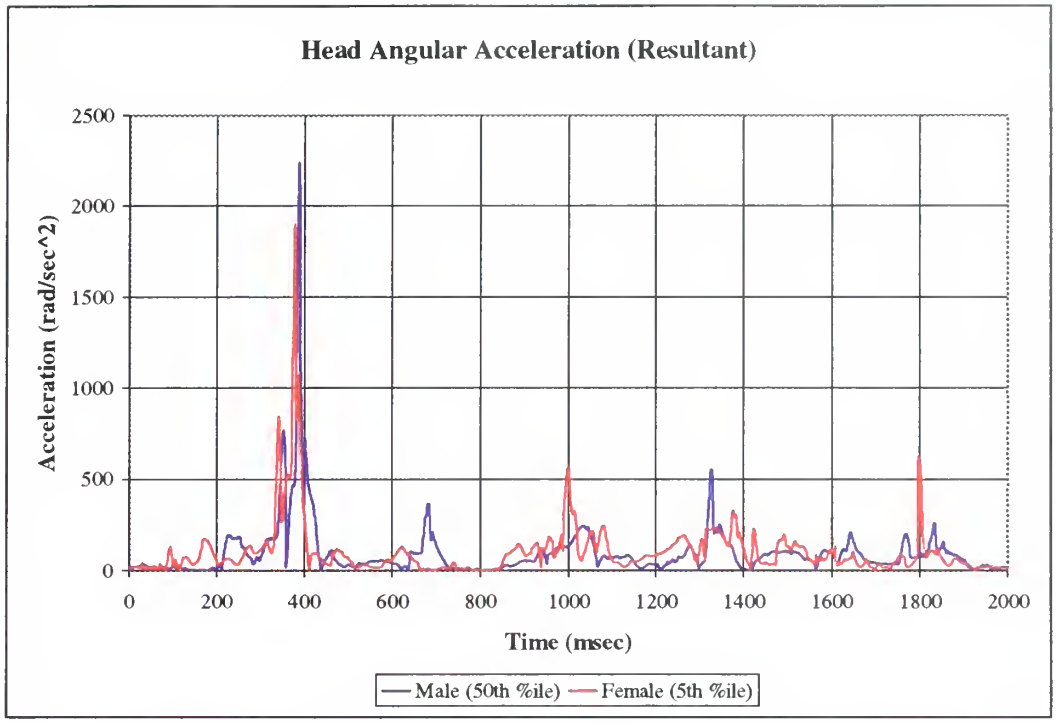

Figure 65. Head Angular Accelerations for Belted Subjects

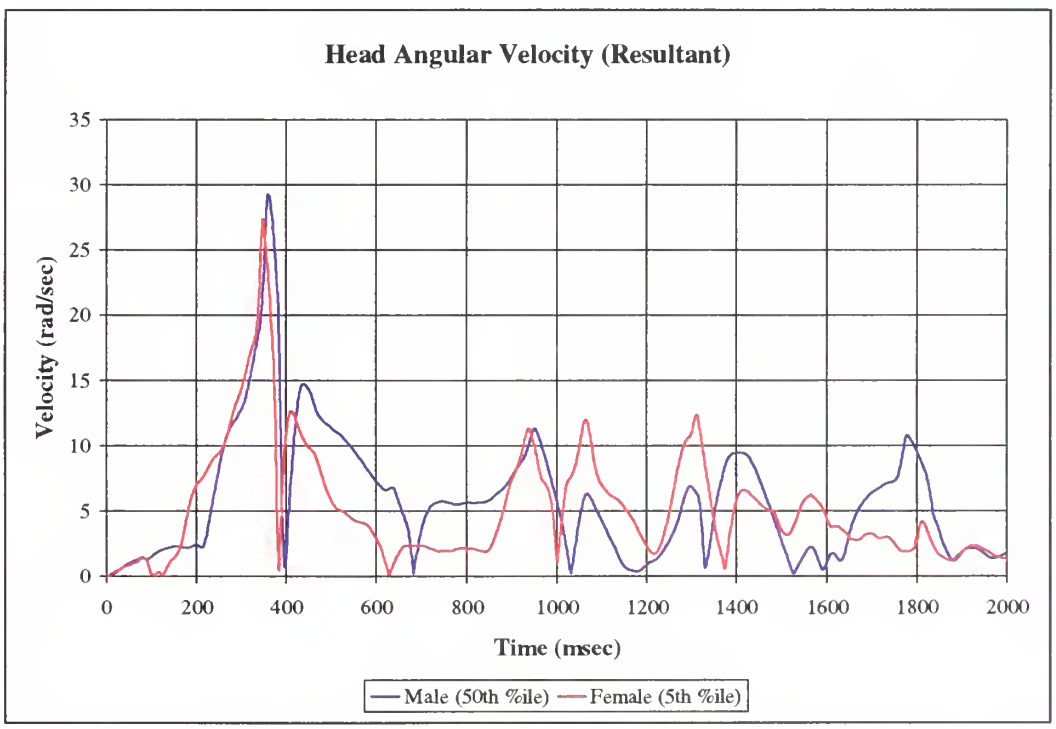

Figure 66. Head Angular Velocities for Belted Subjects

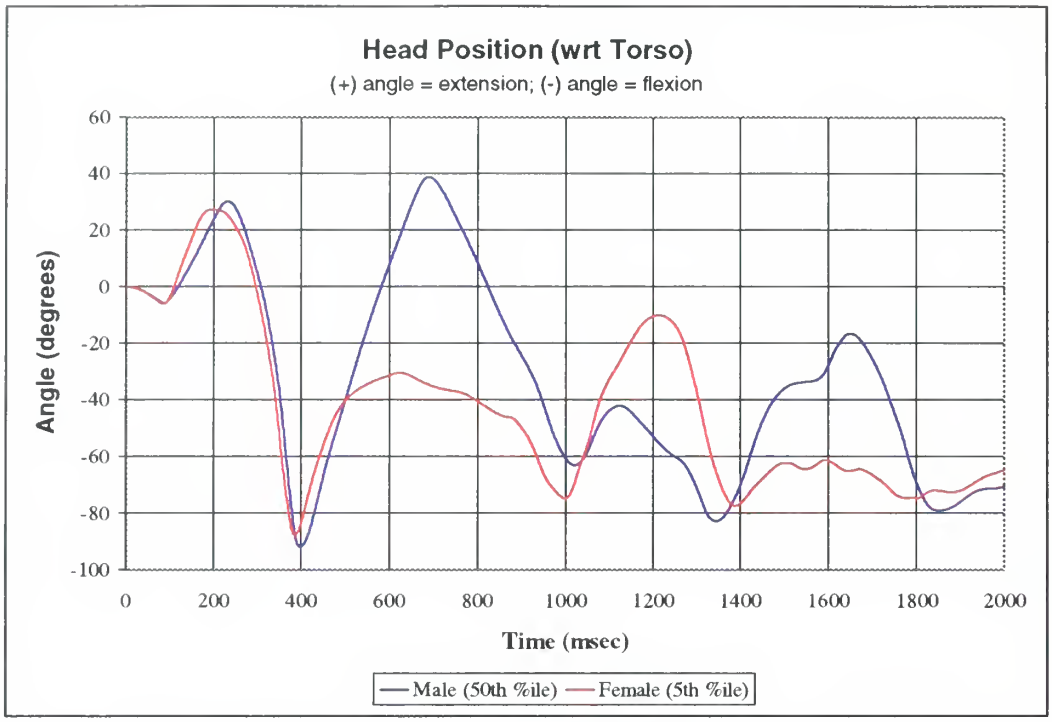

Figure 67. Head Angular Positions for Belted Subjects

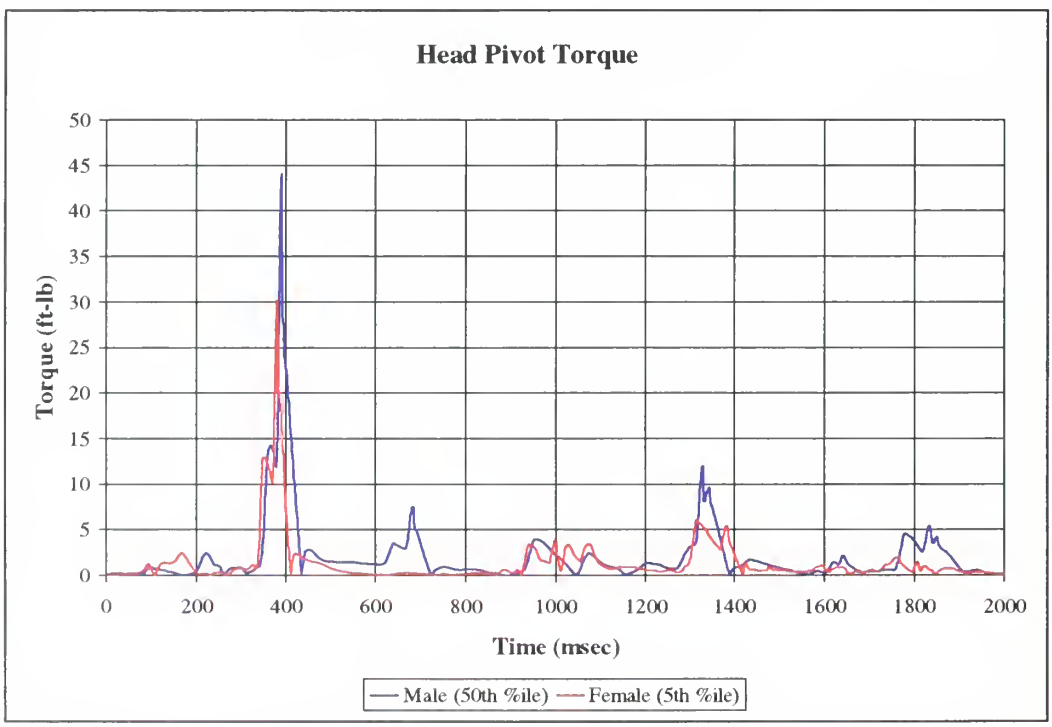

Figure 68. Head Pivot Torque's for Belted Subjects

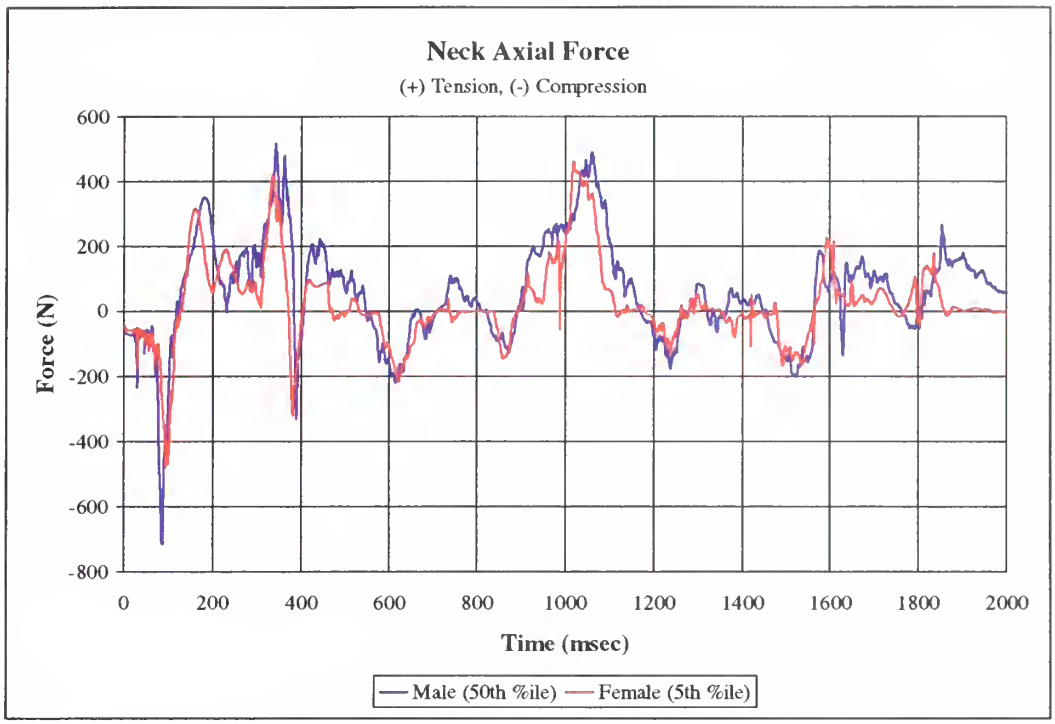

Figure 69. Neck Axial Forces for Belted Subjects

b. Results for the female subject

The gross bodily motion of the female subject wearing the lap belt, shown in Figure 70, was quite similar to that of the male subject. The female subject also underwent four cycles of rebound of the torso off the upper legs, but these cycles were in general less severe. In addition, the timing of the rebounds for the female subject is quite similar to that of the male subject. The first rebound of the female subject resulted in angles of flexion similar to those experience by the male, but the subsequent upwards motion of the female's torso did not induce any extension of the neck at all. This is in contrast to the male subject where significant extension angles were developed during upwards motion following the first rebound.

The final position of the female subject also differed from that of the male subject. Like the male, the female was bent forwards over the lap belt with neck in flexion and arms dangling. However, the female's upper torso was rotated to the right, causing the subjects head to be positioned above the knee, the left arm dangling between the legs, and the right arm dangling to the right of the operator's chair.

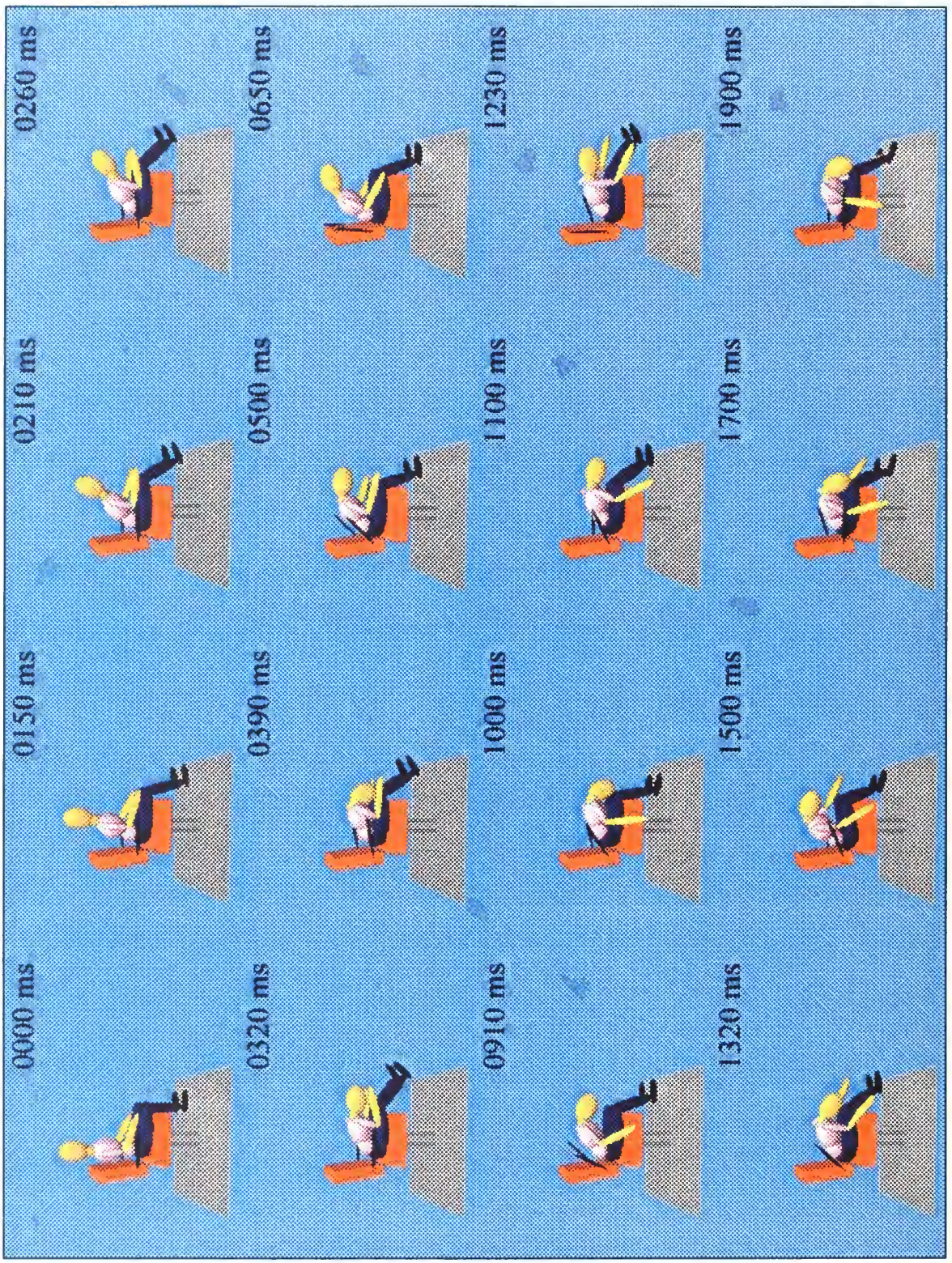

Figure 70. Predicted Motion of the Female Subject Wearing a Lap Belt

As was the case for the male subject wearing the lap belt, the potential injuries related to head impact were not examined since there was no head impact. The resultant linear acceleration of the head center of gravity, however, is shown in Figure 64 for comparison purposes. The peak linear acceleration was 16.7 g's and occurred at 354 msec during the first rebound of the torso off the lower legs. The peak linear acceleration of the female's head exceeds that of the male's head by 2.4 g's.

The resultant angular accelerations, as shown in Figure 65, and angular velocities, as shown in Figure 66, for the center of gravity of the female subject's head were examined and compared against the injury criteria for cerebral concussion. As was the case for the male subject, the peak values of angular acceleration and velocity occurred during the first rebound. For the female, the peak angular acceleration of the head was 1903 rad/sec^2, occurring at 379 msec, and the peak angular velocity was 27.5 rad/sec, occurring at 347 msec. Based on the angular acceleration, which exceeds the tolerance of 1800 rad/sec^2, it is possible that the female subject would receive a cerebral concussion during the first rebound.

Head angle with respect to the upper torso, shown in Figure 67, and torque at the occipital condyles, shown in Figure 68, were examined to estimate the likelihood that the female subject wearing the lap belt would receive a whiplash injury. During the first rebound, the female subject's head reached a peak flexion angle of 87.8 degrees at 386 msec, with associated peak head pivot torque of 30.2 ft-lb at 380 msec. The female subject's axial neck loading, shown in Figure 69, was examined and did confirm that the neck was in tension during this period. The 87.8 degree angle of flexion exceeds the 58 degree limit, but the torque at the head pivot is below the 44 ft-lb pain threshold. However, the torque values provided in Ref. [16], and used as whiplash injury criteria for this research, are specified tolerances for a 50th percentile male and the values for a small female subject are expected to be lower. Thus, considering that the neck was in hyperflexion and tension, and that the torque at the occipital condyles was greater than two-thirds the pain threshold for a 50th percentile male, the 5th percentile female subject is likely to receive a whiplash injury during the first rebound.

The female subject's neck angle reaches peak values in excess of the 58 degree limit during both the second and third rebounds. During the second rebound, the peak flexion angle of the neck was 74.8 degrees and it occurred at 999 msec. The neck was in tension during this period, but the associated torque at the occipital condyles was low so it is possible, but not likely, that the female subject would receive a whiplash injury during the second rebound. During the third rebound, the peak flexion angle of the neck was 77.4 degrees and it occurred at 1387 msec. The neck was slightly loaded in compression during this period, and the head pivot torque was again low, thus it is not expected that the female subject would receive a whiplash injury during the third rebound.

The axial forces experienced by the female subject's neck, shown in Figure 69, were similar in magnitude and phasing to those experienced by the male subject. The values were all well below the specified limits. The peak compressive force was 479 N and it occurred at 94 msec. The peak tensile force was 464 N and it occurred at 1018 msec.

c. Summary of results for belted subjects

The estimated injury potentials for the 50^{th} percentile male and 5^{th} percentile female subjects wearing the lap belt are summarized in Table 10. The two subjects are expected to receive comparable injuries. It is possible that each subject would receive a cerebral concussion, resulting from excessive head angular acceleration, during the first rebound of the subject's torso off the lower legs. It is also probable that each subject would receive a whiplash injury (acceleration induced trauma to the cervical spine), resulting from inertial loading of the cervical spine by the head, during the first rebound. It is also possible, but not likely, that each subject would receive an additional whiplash injury during the second rebound of the torso off the upper legs. Finally, it is again possible, but not likely, that the male subject would receive another whiplash injury during the fourth rebound.

Table 10. Summary of Results for Subjects Wearing Lap Belt

	Time (msec)	Parameter	Value	Limit	Source (Ref. #)	Outcome
50th Percentile Male	388	Head Ang. Accel.	2242 r/s^2	1800 r/s^2	19	Possible cerebral concussion
	398	Head Pos.	91.8 deg	58 deg	13	Probable whiplash injury
	389	Torque	44.1 ft-lb	44 ft-lb	16	
	1020	Head Pos.	63.0 deg	58 deg	13	Possible whiplash injury (not likely)
	1851	Head Pos.	79.1 deg	58 deg	13	Possible whiplash injury (not likely)
5th Percentile Female	379	Head Ang. Accel.	1903 r/s^2	1800 r/s^2	19	Possible cerebral concussion
	386	Head Pos.	87.8 deg	58 deg	13	Probable whiplash injury
	389	Torque	30.2 ft-lb	44 ft-lb	16	
	999	Head Pos.	74.8 deg	58 deg	13	Possible whiplash injury (not likely)

2. Not Wearing Lap Belt, Seated at Desk

a. Results for the male subject

The motion of the male subject that is not restrained by the lap belt, but is seated at a desk, is shown in Figure 71. As a result of the initial shock excitation, the male subject's entire body is propelled forward until motion was arrested by the contact of the lower arms and upper legs against the edge of the desk. At that point, the inertia of the subject's torso caused rotation about the pelvis until the upper torso struck the desk surface. The inertia of the subject's head caused it to rotate forward rapidly and contact the desk surface at approximately 430 msec. The subject rebounded and continued moving backwards until motion was arrested by the lower torso contacting the seat back. At that time, the upper body of the subject was well above the seat bottom. The subject then dropped downward in to the seat and went through another cycle of forward motion beginning at approximately 1000 msec. That second cycle was significantly more violent than the first. The subject experienced a more severe head strike against the desk (at approximately 1250 msec) and rebounded higher in the air. The subject was still in motion at the end of the simulation with the lower torso raised above the seat bottom.

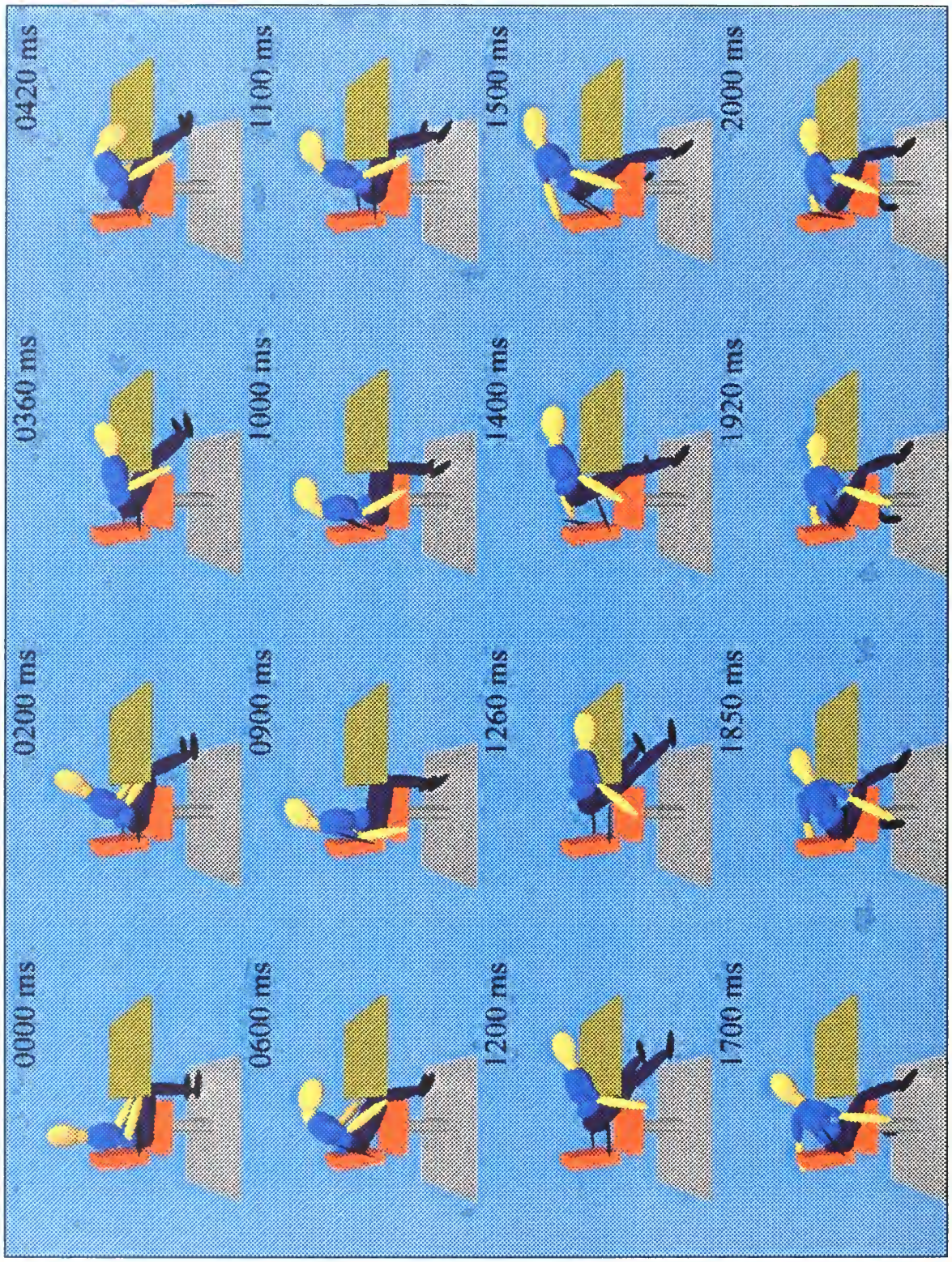

Figure 71. Predicted Motion of the Unbelted Male Subject

Since multiple head impacts occurred during the simulations of the unbelted subjects seated at a desk, the head impact injury estimates were performed. The first such estimate was the HIC. For the male subject, the HIC was computed, using the ATB program, to be 18.35. This is well below the limit of 1000, so no severe head injury (AIS $\geq$ 4) is expected. The time interval found to maximize the HIC value was 351 to 416 msec, with an average acceleration of 9.6 g's. This interval occurred during the first striking of the head against the desk. The peak linear acceleration of the of the head was 43.4 g's, as seen in Figure 72, and it occurred during the second head strike at 1257 msec.

The head angular accelerations, as seen in Figure 73, and angular velocities, as seen in Figure 74, were examined and compared against the injury criteria for cerebral concussion. The peak angular acceleration of the head, 2109 rad/sec^2, occurred during the first head strike at 431 rad/sec. The peak angular velocity, 28.1 rad/sec, also occurred during the first head strike, but at an earlier time of 381 msec. Since the angular acceleration is in excess of the 1800 rad/sec^2 limit, the male subject would possibly receive a cerebral concussion during the first head strike. Although the linear acceleration experience by the head was significantly larger during the second head strike than during the first, the angular acceleration only reached a peak of 1219 rad/sec^2 during the second strike.

The head-desk contact forces, shown in Figure 75, were examined in order to make estimates of possible fractures of the bones of the skull or face. The first head strike involves a contact of the frontal region of the skull (see Figure 43 for the bones of the face and skull) with the desk. The peak force during this contact was 53.6 lb, well below the 900 lb tolerance level for the frontal region of the skull. The second head-desk contact was essentially a full-face strike against the desk. The peak force developed during this period was 465 lb and it occurred at 1257 msec. This force is in excess of the 150 lb tolerance level for the maxilla bone, thus a possible fracture of this bone could have resulted from this contact. The third head-desk contact was an impact of the right cheek on the desk surface and developed a peak force of 309 lb at 1917 msec. This force is in excess of the 225 lb tolerance level for the zygomatic bone, thus a possible fracture of this bone could have resulted from this final head-desk contact.

Examination of the head angular position with respect to the torso, as shown in Figure 76, revealed a peak angle in flexion of 87.5 degrees occurring at 436 msec. A torque at the occipital condyles of 38.4 ft-lb, as seen in Figure 77, occurred at 431 msec and is below the 44 ft-lb pain threshold in flexion. The predicted neck axial forces, shown in Figure 77, revealed that the neck was loaded in compression during this period. As such, it is not expected that a whiplash injury would result during this period. Since no other head angles or torque values were in excess of the appropriate tolerances, no whiplash injury is expected for the unbelted male subject.

The peak tensile load in the neck, 1048 N, occurred at 364 msec as seen in Figure 78 and was a result of inertial loading when the forward motion of the upper torso was arrested by the desk. The peak compressive load, 1934 N, occurred at 908 msec and was again a result of inertial loading. The compressive load occurred when the subject dropped down into the seat after striking the seat back. Both of these forces are below the appropriate limits.

The injury estimates for the unbelted subjects are summarized in Table 11.

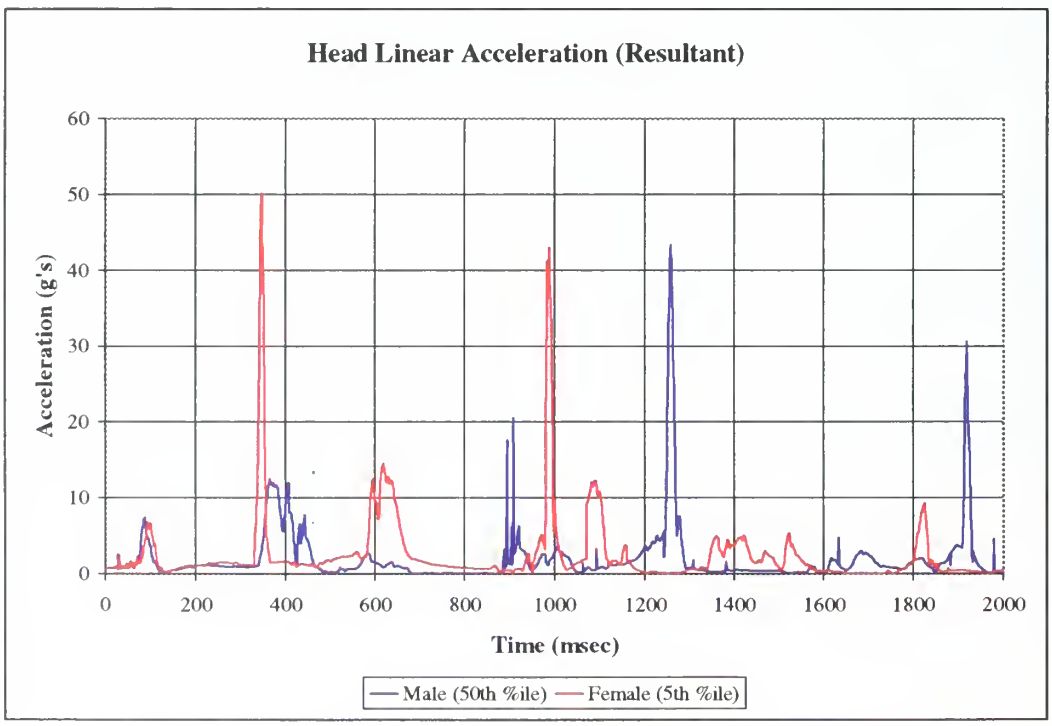

Figure 72. Head Linear Accelerations for Unbelted Subjects

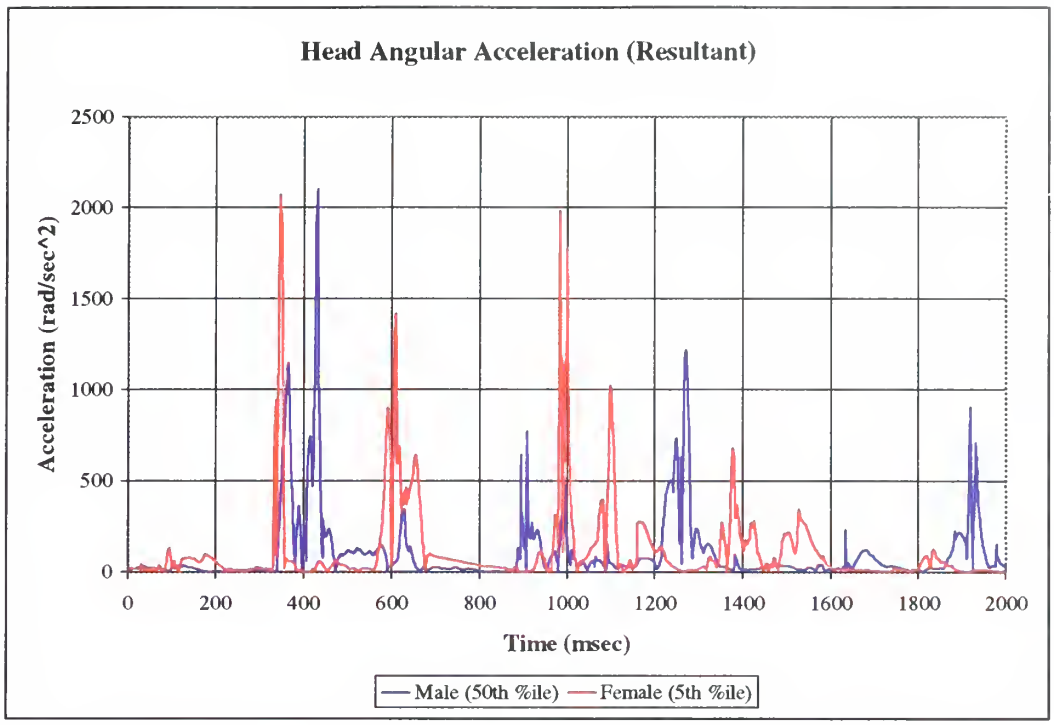

Figure 73. Head Angular Accelerations for Unbelted Subjects

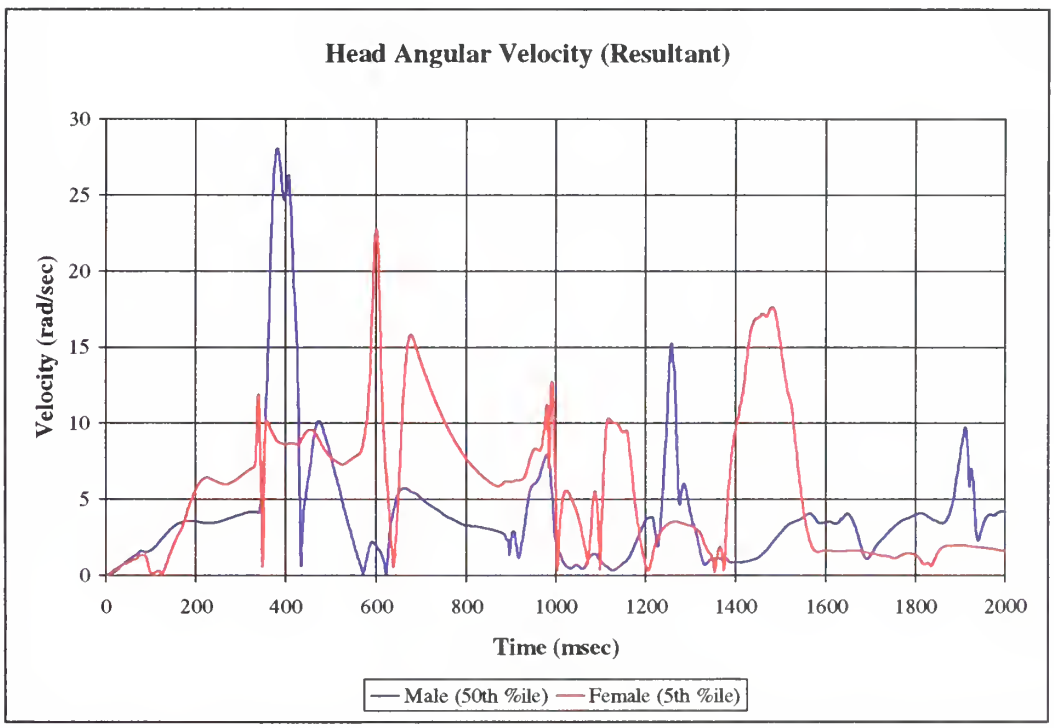

Figure 74. Head Angular Velocities for Unbelted Subjects

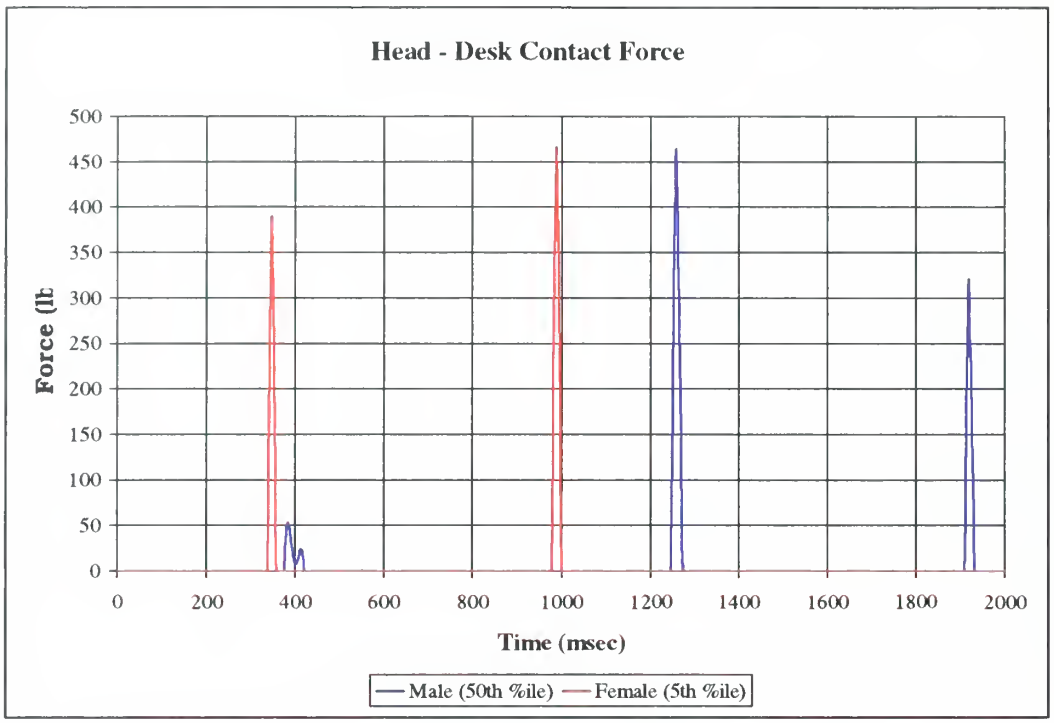

Figure 75. Head-Desk Contact Forces for Unbelted Subjects

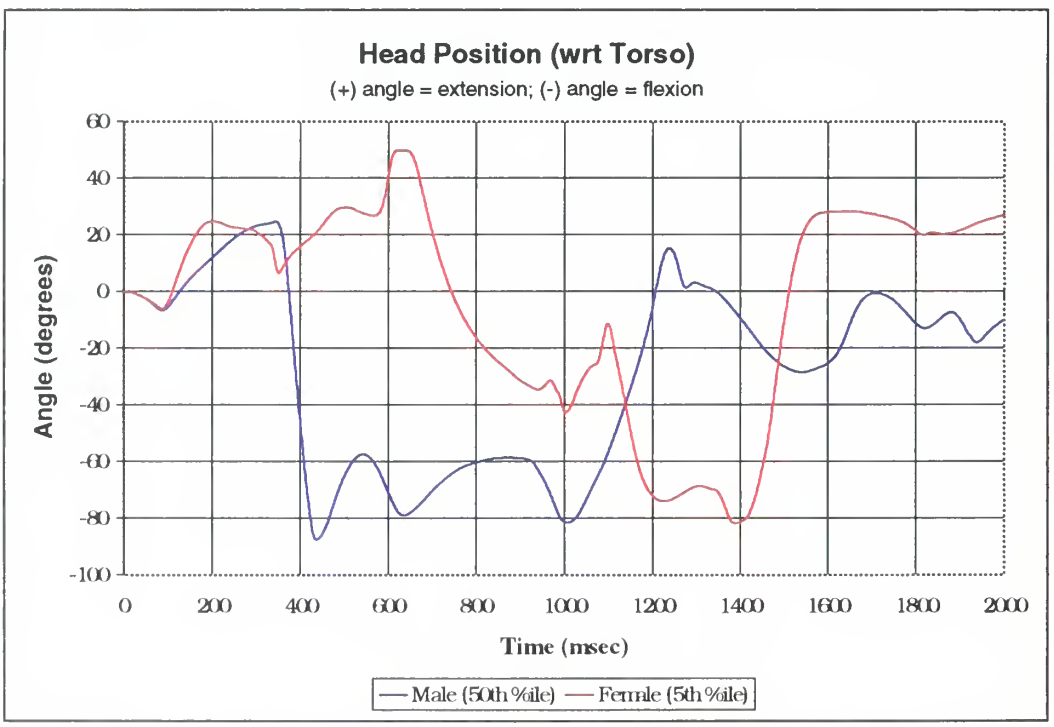

Figure 76. Head Angular Positions for Unbelted Subjects

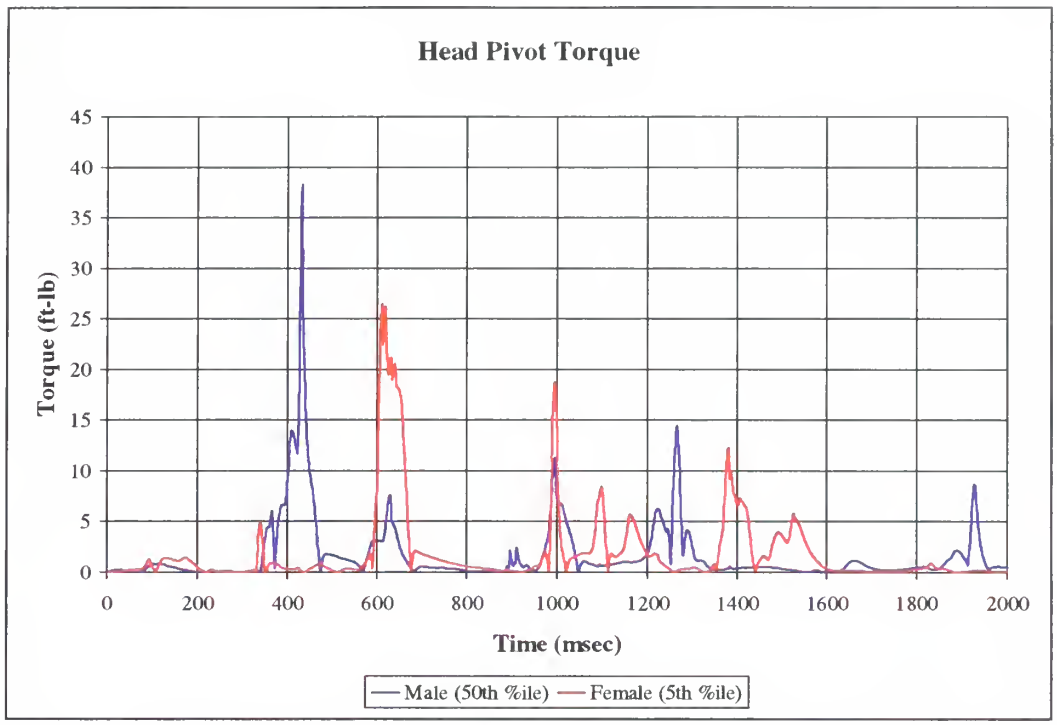

Figure 77. Head Pivot Torque's for Unbelted Subjects

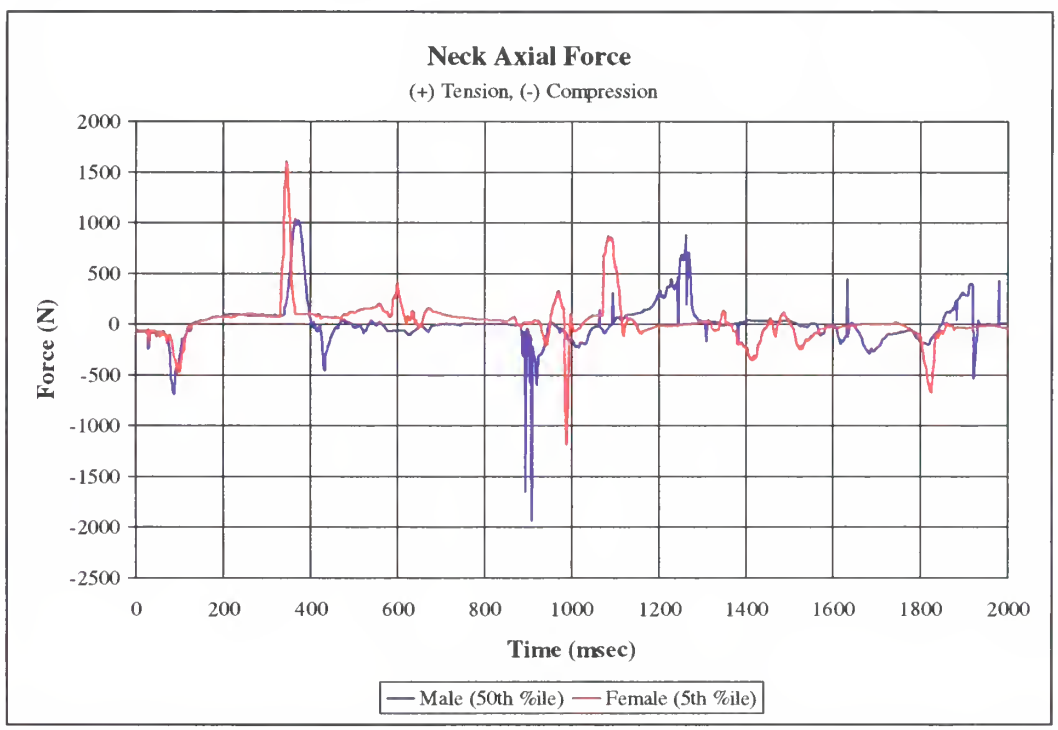

Figure 78. Neck Axial Forces for the Unbelted Subjects

b. Results for the female subject

The motion of the unbelted female subject, shown in Figure 79, began in much the same way as did the motion of the unbelted male subject. The first strike of the head against the desk was more violent and the associated rebound of the body into the seat back resulted in significant extension of the neck as the backward motion of the upper body was arrested. The second cycle of motion resulted in another head strike against the desk, but at an earlier time than for the male subject. Only two head strikes were experienced by the female subject, compared to three for the male subject. The final position of the female subject is very similar to the initial position.

For the female subject, a HIC of 122.31 was computed using the ATB program. This value is well below the limit of 1113 for the small (5^{th} percentile) female, so no AIS ≥ 4 head injury is expected for the female subject. The time interval found to maximize the HIC value was 339 to 352 msec, with an average acceleration of 38.9 g's. This interval occurred during the first striking of the head against the desk. The peak linear acceleration of the center of gravity of the head, 50.2 g's as seen in Figure 72, also occurred during the first head strike at time 346 msec.

The head angular accelerations, as seen in Figure 73, and angular velocities, as seen in Figure 74, were examined and compared against the injury criteria for cerebral concussion. The peak angular acceleration of the head, 2074 rad/sec^2, occurred during the first head strike at 346 msec. The angular velocity peak associated with the first head strike was 11.9 rad/sec and it occurred at 339 msec. During the second head strike, the angular acceleration of the head reached a peak value of 1984 rad/sec^2 at 983 msec with associated peak angular velocity of 12.8 rad/sec occurring at 991 msec. For both of these head strikes, the peak angular acceleration exceeds the 1800 rad/sec^2 tolerance level and the peak angular velocity is below the 50 rad/sec tolerance level. Thus, based on the angular accelerations, the unbelted female would possibly receive a cerebral concussion during each of the head strikes.

As for the male subject, the head-desk contact forces, shown in Figure 75, were examined in order to make estimates of possible fractures of the bones of the skull or face. For the female subject, the first head strike resulted in a peak force of 390 lb at

346 msec. This contact force was to the subjects chin and exceeds the 200 lb tolerance level for the lateral mandible, and, as such, resulted in a possible fracture of this bone. The second head strike was contact between the frontal portion of the skull and the desk and the peak force developed, 467 lb at 988 msec, is well below the 900 lb tolerance level for the frontal bone.

Examination of the head angular position with respect to the torso, as shown in Figure 76, revealed a peak angle in flexion of 81.8 degrees occurring at 1388 msec. A torque at the occipital condyles of 12.3 ft-lb, well below the 44 ft-lb pain threshold in flexion, occurred at 1379 msec. The predicted neck axial forces, shown in Figure 78, revealed that the neck was lightly loaded in compression during this period. As such, it is not expected that a whiplash injury would result during this period. During the rebound from the first head strike, the neck underwent a period of extension with a peak angle of 49.9 degrees occurring at 618 msec and an associated head pivot torque peak of 26.2 ft-lb occurring at 617 msec. Since both of these values are below the thresholds, no whiplash injury is expected for this motion.

The peak tensile load in the neck was developed as a result of inertial loading when the female subject's upper torso struck the desk during the first cycle. The loading reached 1614 N at 344 msec and the neck was slightly extended. This value exceeds both the 1160 N limit for tension-extension and the 1450 N limit for pure tension given in Table 7, but the time history of the loading does not violate the neck tension threshold shown in Figure 48. As such, it was considered possible, but not probable, that the female subject would receive a significant neck injury resulting from tensile loading during the first cycle of motion. The typical mechanisms of such injuries are summarized in Table 6.

The peak compressive load developed in the neck was 1183 N and occurred during the second head strike at 987 msec with the neck in flexion. This value is well below both the 2000 N tolerance value and the duration of loading tolerance curve. As such, no significant neck injury due to compressive loading is expected.

As previously stated, the injury estimates for both the male and female subjects not wearing a lap belt are summarized in Table 11.

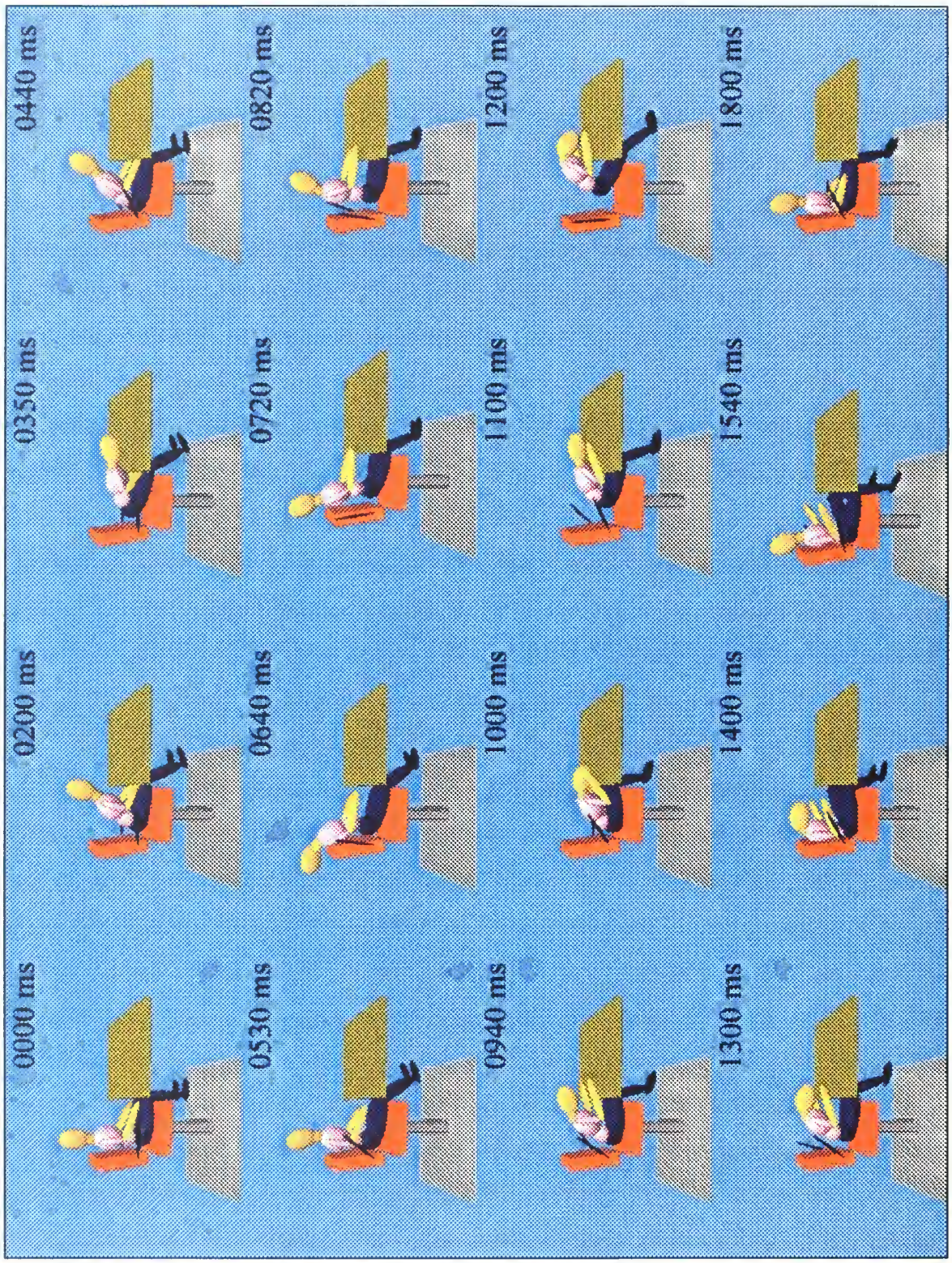

Figure 79. Predicted Motion of the Unbelted Female Subject

c. Summary of results for unbelted subjects

From the summary of estimated injury potentials for the unbelted male and female subjects provided in Table 11, it is apparent that both subjects are likely to receive similar injuries. Both subjects would possibly receive cerebral concussions during the first head impact and the female subject would possibly receive an additional cerebral concussion during the second head impact. During the first head impact cycle, the female subject, in addition to a possible cerebral concussion, would possibly experience a fracture to the lateral mandible and, although not considered likely, a significant neck injury resulting from tensile loading. During the second head impact cycle, the male subject would possibly experience a fracture of the maxilla. Finally, during the third head impact, the male subject would possibly receive another fracture to a facial bone, this time to the zygomatic bone.

Table 11. Summary of Results for Unbelted Subjects

	Time (msec)	Parameter	Value	Limit	Source (Ref. #)	Outcome
50th Percentile Male	431	Head Ang. Accel.	2109 r/s^2	1800 r/s^2	19	Possible cerebral concussion
	1257	Head Cont. Force	465 lb	150 lb	20	Possible fracture of the maxilla bone
	1917	Head Cont. Force	309 lb	225 lb	20	Possible fracture of the zygomatic bone
5th Percentile Female	346	Head Ang. Accel.	2074 r/s^2	1800 r/s^2	19	Possible cerebral concussion
	983	Head Ang. Accel.	1984 r/s^2	1800 r/s^2	19	Possible cerebral concussion
	346	Head Cont. Force	390 lb	200 lb	20	Possible fracture of the lateral mandible
	344	Neck Axial Force	1614 N	1450 N	22	Possible significant neck injury (not likely)

3. Not Wearing Lap Belt, Seated at Desk with Computer Terminal

a. Results for the male subject

The motion of the male subject that is seated at a computer and not restrained by a lap belt is shown in Figure 80. As was the case for the male seated at a deck, the subject's entire body was propelled forward as a result of the initial shock excitation until motion was arrested by the contact of the lower arms and upper legs against the desk edge. This resulted in rotational motion of the upper torso about the pelvis until contact between the head and computer terminal occurred at approximately 300 msec. At that time, the lower torso of the male subject returned to approximately its original position and the upper torso moved backwards. The subject never reached an erect sitting position prior to the second cycle of forward motion. The second cycle was arrested when the top of the head encountered the front surface (screen) of the computer terminal. The entire upper torso of the male subject then rebounded and moved backwards until the seat back was reached, resulting in an extension of the neck. The final position of the male subject was seated upright with arms dangling at the sides and the neck extended and tilted to the subject's left side.

As for the case of the unbelted subjects seated at a bare desk, multiple head impacts necessitated head impact injury estimation. The HIC was computed, using the ATB program, to be 6.64, well below the limit of 1000. Thus, no AIS ≥ 4 head injury is expected based on the HIC computation. The time interval found to maximize the HIC value was 68 to 1112 msec, with an average acceleration of 2.1 g's. The peak linear acceleration of the center of gravity of the head was 18.7 g's, as seen in Figure 81, and it occurred during the second head strike at 1462 msec.

The head angular accelerations, as seen in Figure 82, and angular velocities, as seen in Figure 83, were examined and compared against the injury criteria for cerebral concussion. The peak angular acceleration of the head, 1702 rad/sec^2, occurred during the first head strike at 303 msec. The peak angular velocity, 18.4 rad/sec, occurred shortly after the first head strike at 478 msec. Since both of these values are below their respective tolerances, no cerebral concussion is expected for the male subject seated at a computer.

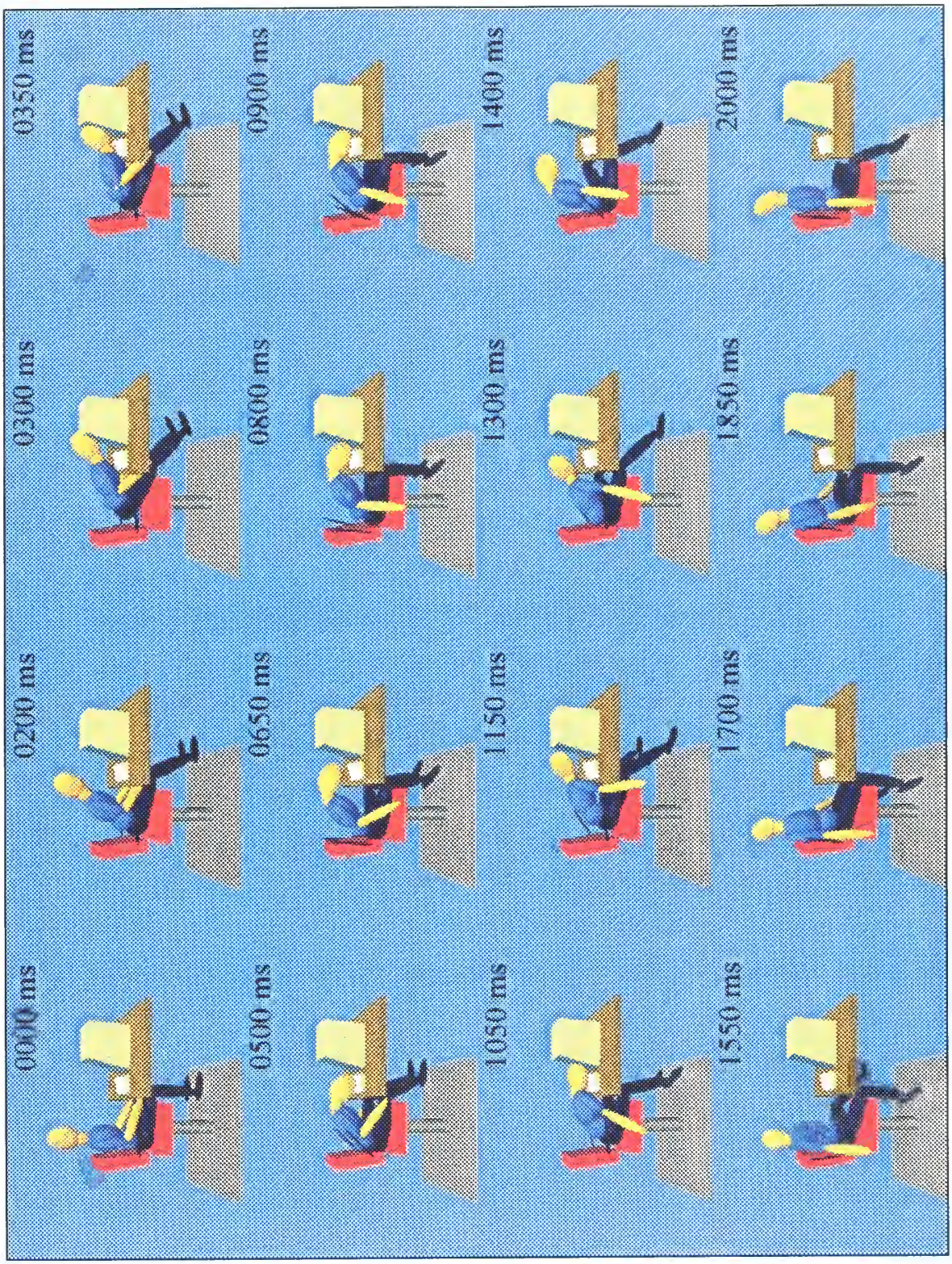

Figure 80. Predicted Motion of the Male Subject at a Computer

The head-computer contact forces, shown in Figure 84, were examined in order to make estimates of possible fractures of the bones of the skull or face. The first head strike involved contact between the upper face (bridge of the nose/forehead area) with the edge formed by the front and top surfaces of the computer terminal. The peak force developed during this contact was 211 lb and it occurred at 304 msec. This force is well below the 900 lb tolerance level for the frontal bone, so no fracture is expected for the first head strike. The second head strike involved contact between the frontal and temporal regions of the skull with the computer screen. The peak force developed during this contact was 237 lb and it occurred at 1044 msec. This force is below both the 900 lb tolerance value for the frontal bone and the 450 lb tolerance value for the temporal bone, thus no fracture is expected during the second head strike either. No provision was made for modeling breakage of the glass of the computer screen, so no estimate can be made of potential lacerations resulting from any such breakage.

Examination of the head angular position with respect to the torso, as shown in Figure 85, revealed a peak angle in flexion of 82.7 degrees occurring at 529 msec. A torque at the occipital condyles of 18.5 ft-lb, shown in Figure 86, occurred at 520 msec and is well below the 44 ft-lb pain threshold in flexion. The predicted neck axial forces, shown in Figure 87, revealed that the neck was lightly loaded in compression during this period. As such, it is not expected that a whiplash injury would result during this period. An occipital condyle torque value of 38.3 ft-lb occurred at 331 msec with the neck in extension. This is above the 35 ft-lb tolerance value for extension, but since the neck is loaded in compression and whiplash is a tension-extension or tension-flexion phenomenon, no injury is expected to occur for this period.

The peak compressive load in the neck, 1821 N, occurred at 1049 msec, as seen in Figure 87, and was a result of the second head contact with the computer terminal. This load is below both the 2000 N tolerance value for compression loading in flexion and the duration of loading curve. Thus, no injury resulting from axial loading of the cervical spine is expected to occur.

The injury estimates for both the male and female subjects seated at the computer are summarized in Table 12.

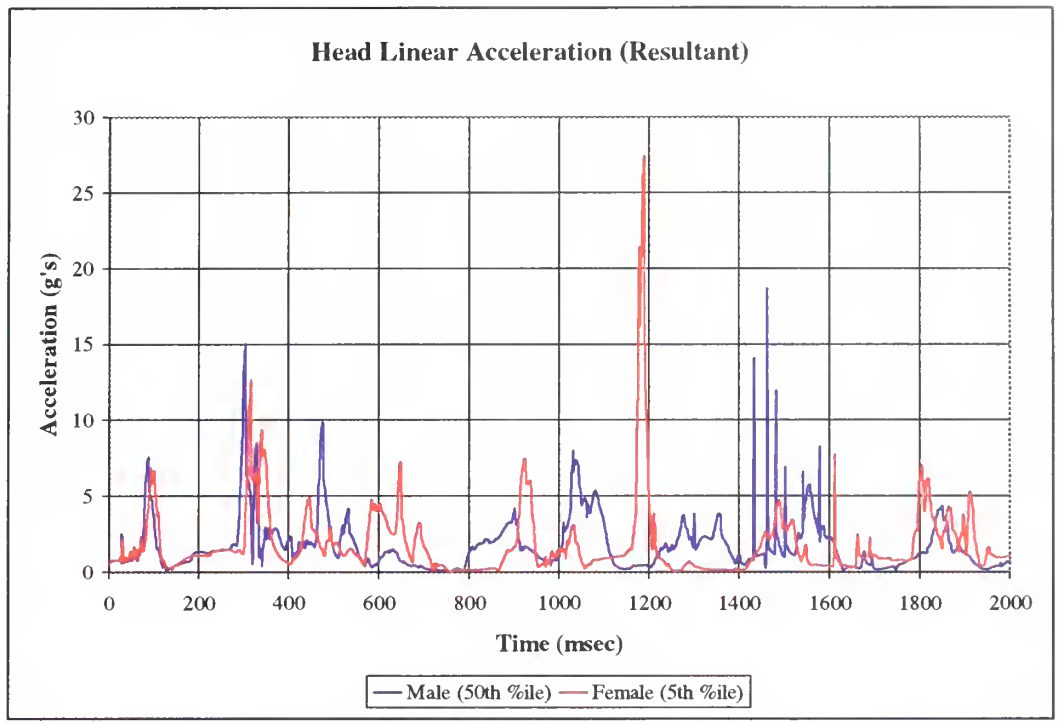

Figure 81. Head Linear Accelerations for Subjects at Computer

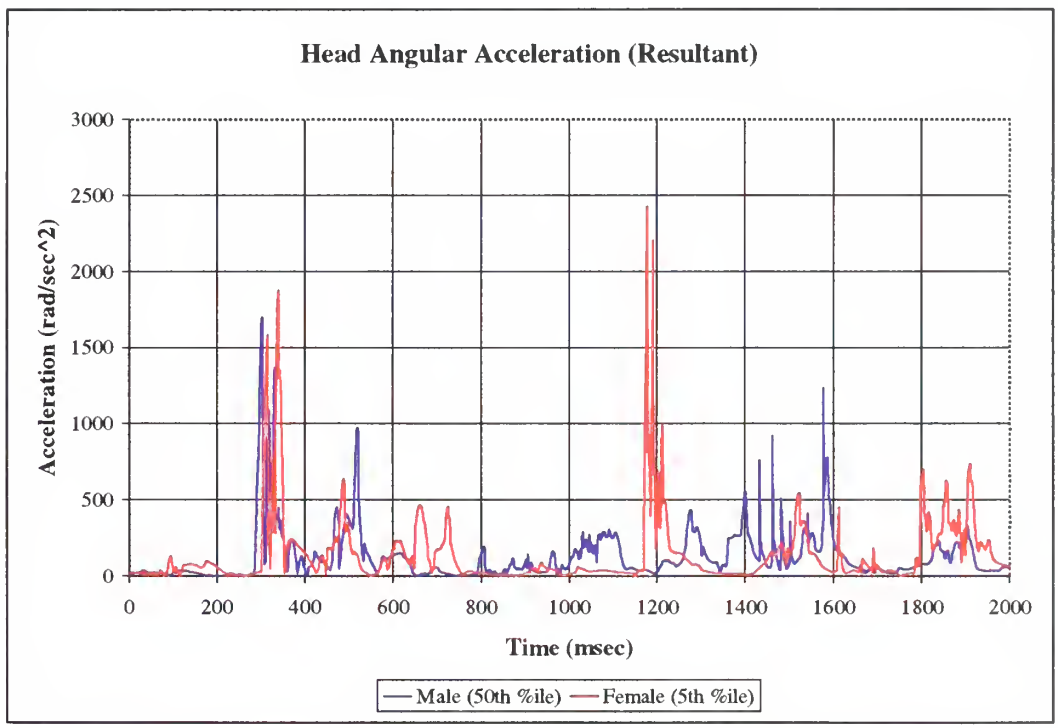

Figure 82. Head Angular Accelerations for Subjects at Computer

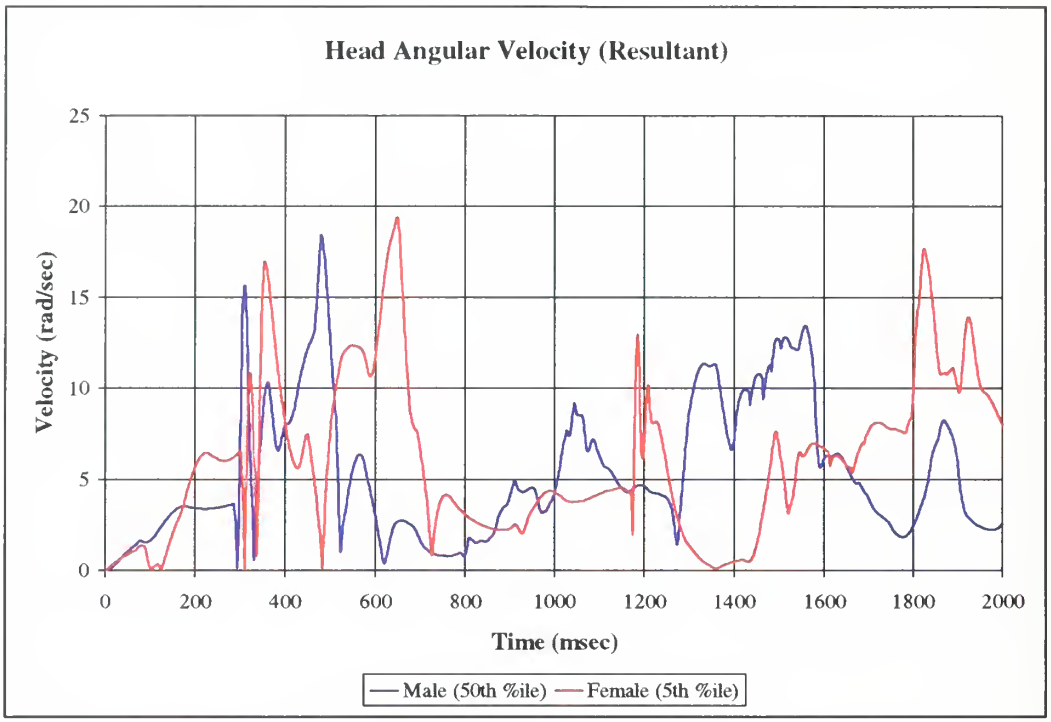

Figure 83. Head Angular Velocities for Subjects at Computer

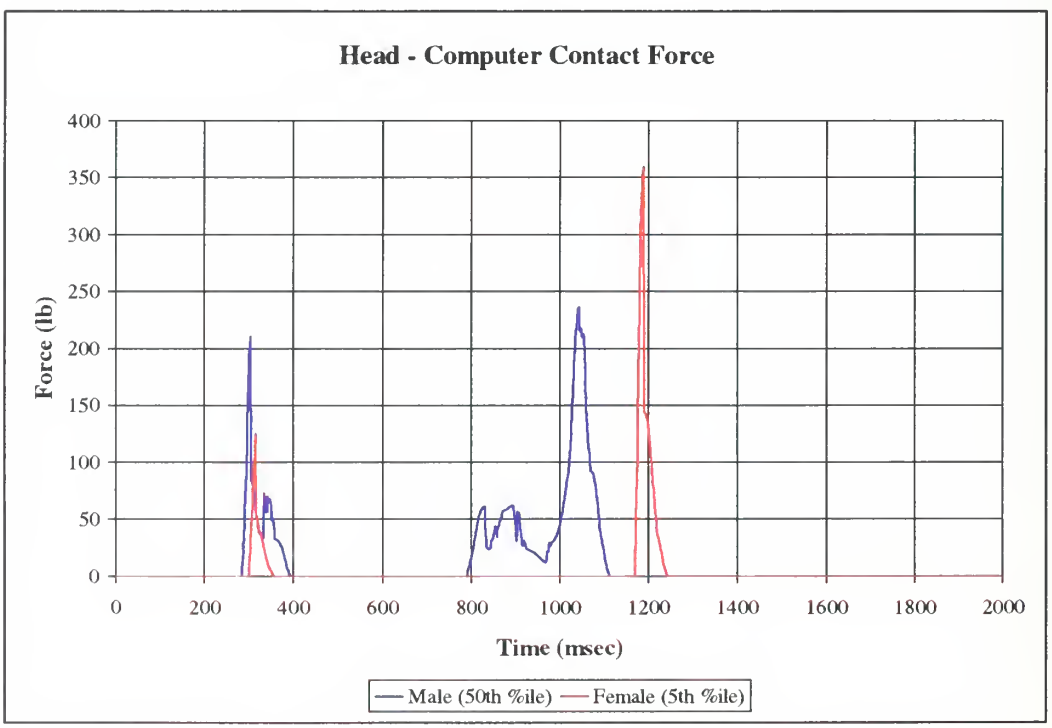

Figure 84. Head-Computer Contact Forces for Subjects at Computer

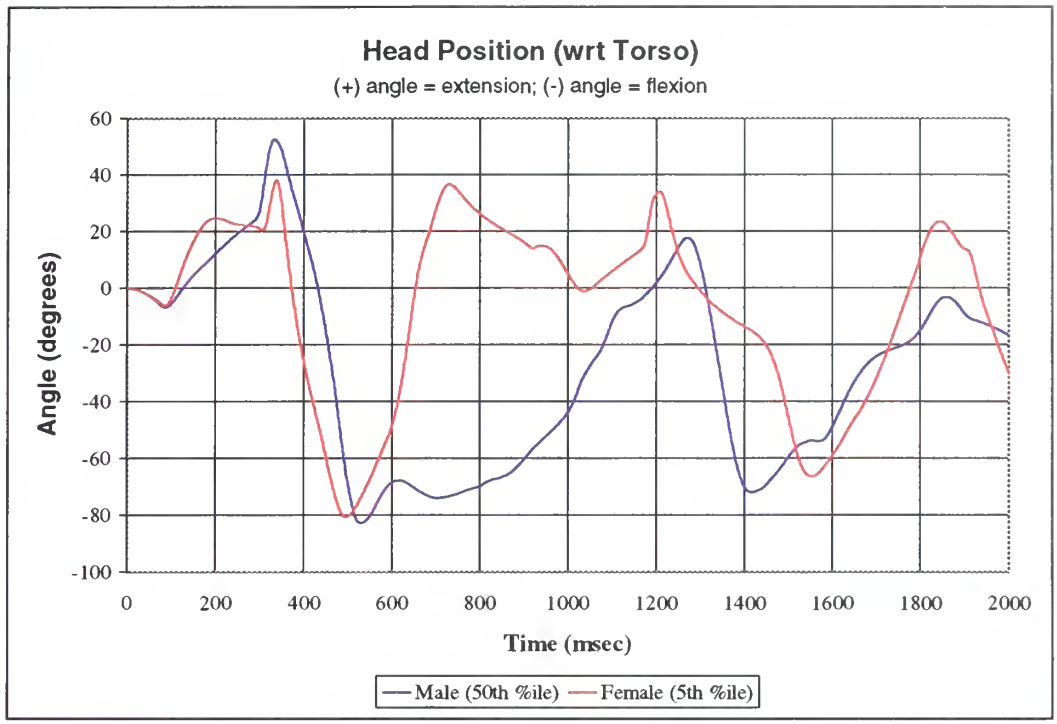

Figure 85. Head Angular Positions for Subjects at Computer

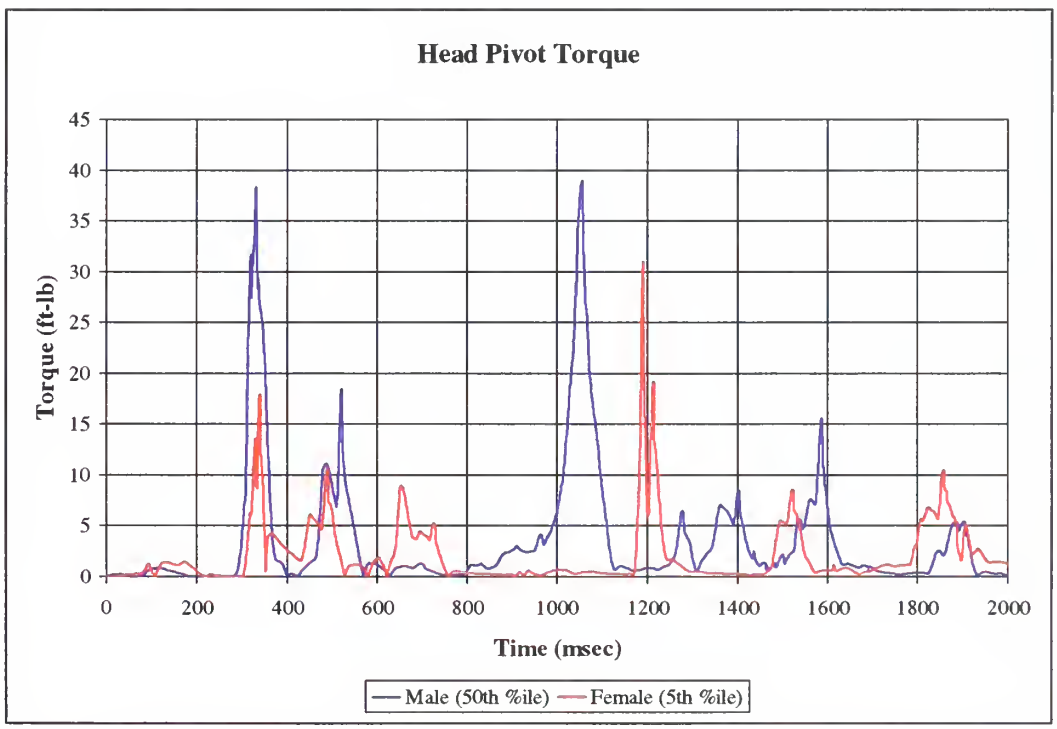

Figure 86. Head Pivot Torque's for Subjects at Computer

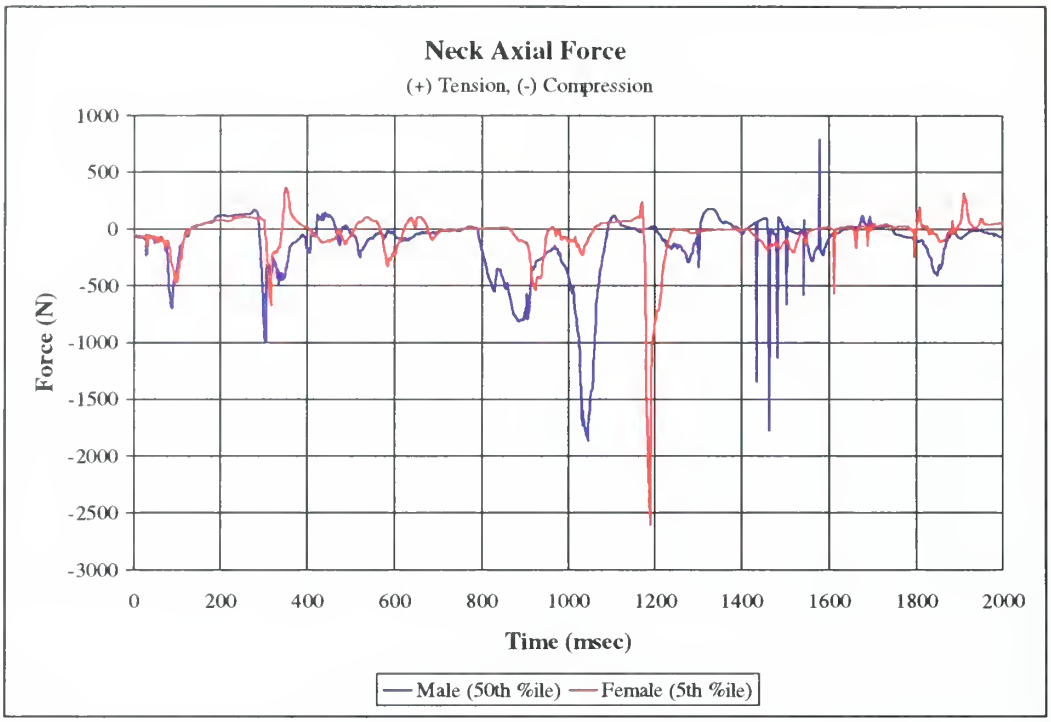

Figure 87. Neck Axial Forces for Subjects at Computer

b. Results for the female subject

The gross bodily motion for the female subject, shown in Figure 88, was similar to that of the male subject seated at a computer. Since the 5th percentile female is significantly shorter than the 50th percentile male, the upper torso rotation during the first forward motion resulted in contact between the frontal region of the subject's skull and the computer screen rather than between the bridge of the nose and the top edge of the computer terminal. The rebound of the female subject's body was more exaggerated than that of the male subject. The female came fully upright in the seat and experienced slight extension of the neck. The second head contact with the computer terminal was more severe and occurred later for the female than for the male subject. The final position of the female subject was with the lower torso in the seat and the upper torso leaning to the right on the armrest.

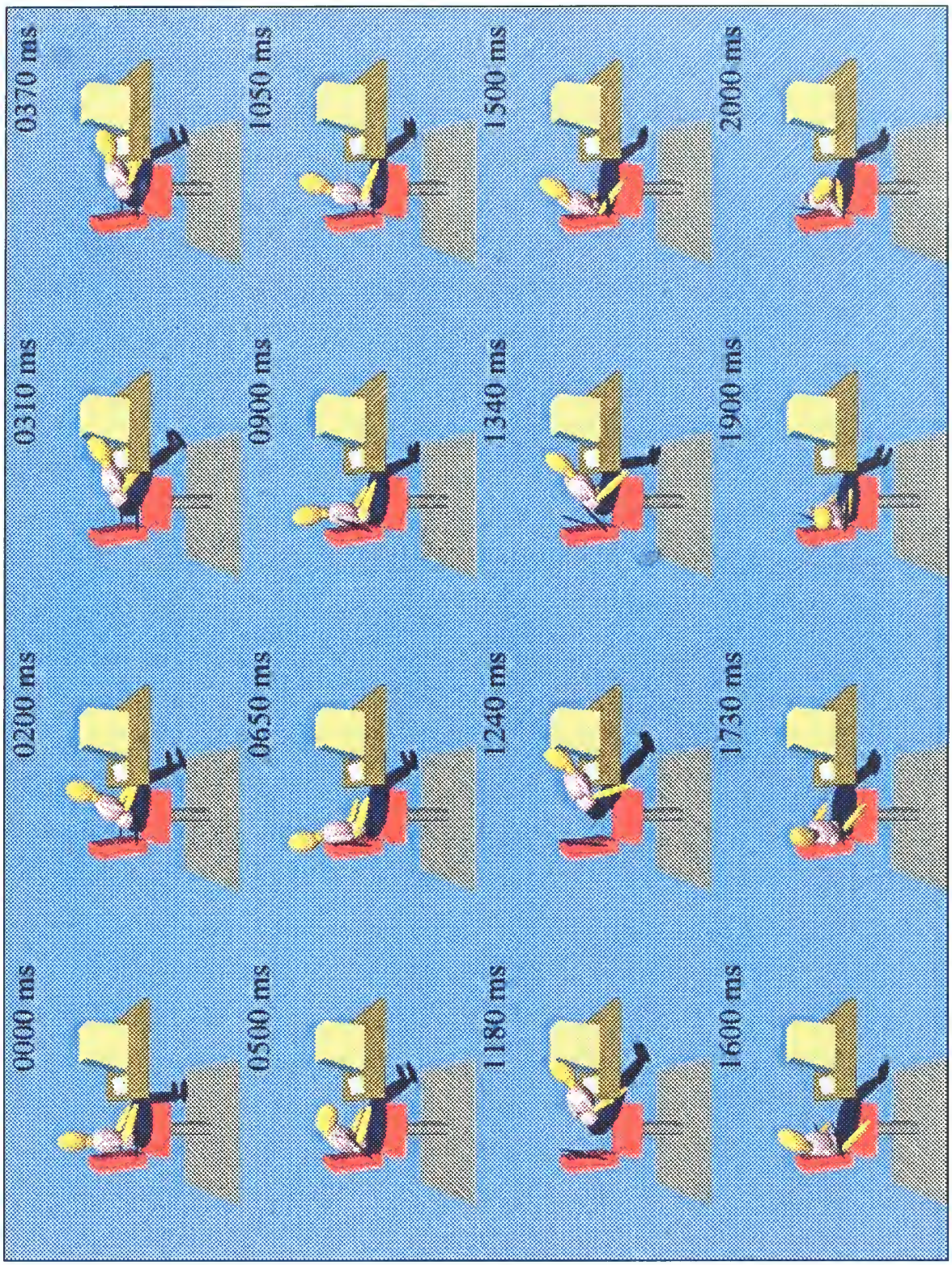

Figure 88. Predicted Motion of the Female Subject at a Computer

For the female subject, a HIC of 31.92 was computed using the ATB program. This value is well below the 1113 limit for the small female, so no AIS ≥ 4 head injury is expected for the female subject. The time interval found to maximize the HIC value was 1175 to 1191 msec, with an average acceleration of 20.9 g's. This interval occurred during the second striking of the head against the computer terminal. The peak linear acceleration of the center of gravity of the head, 27.5 g's as seen in Figure 81, also occurred during the second head strike at time 1189 msec.

The head angular accelerations, as seen in Figure 82, and angular velocities, as seen in Figure 83, were examined and compared against the injury criteria for cerebral concussion. A peak angular acceleration of the head, 1880 rad/sec^2, occurred during the first head strike against the computer at 340 msec. The angular velocity peak associated with the first head strike was 17 rad/sec and it occurred at 354 msec. Although this angular velocity is below the 50 rad/sec tolerance level, the angular acceleration is slightly above the 1800 rad/sec^2 tolerance value. Thus, it is possible that the female subject would receive a cerebral concussion during the first head strike. During the second head strike, the angular acceleration of the head reached a peak value of 2427 rad/sec^2 at 1178 msec with an associated peak angular velocity of 13 rad/sec occurring at 1185 msec. This angular acceleration is well above the tolerance limit, so the female subject would be likely to receive a cerebral concussion during the second head strike.

As for the male subject, the head-computer contact forces for the female subject, shown in Figure 84, were examined in order to make estimates of possible fractures of the bones of the face and skull. The first head strike resulted in a peak force of 126 lb at 316 msec. This contact force was to the frontal region of the subject's skull and is well below the 900 lb tolerance value for that bone. Thus, no fractures were expected to occur during the first head strike. The second head strike resulted in a peak force of 360 lb at 1189 msec. This contact force was to the upper facial region, and, as such, would result in a possible fracture of the zygomatic bone which has a tolerance level of 225 lb.

Examination of the head angular position with respect to the torso, as shown in Figure 85, revealed a peak angles in flexion of 80.6 degrees occurring at 316 msec and 66.4 degrees occurring at 1553 msec. The head pivot torque values associated with these peak angles, as seen in Figure 86, are well below the 44 ft-lb pain threshold in flexion. The predicted neck axial forces, shown in Figure 87, reveal compressive loading during both of these periods, and, as such, no whiplash injury is expected to occur for either period. A peak occipital condyle torque in extension of 31.0 ft-lb, near the 35 ft-lb tolerance value for the 50^{th} percentile male, occurred at 1189 msec, but again compressive loading of the neck indicates that no whiplash injury is to be expected.

The peak compressive load developed in the neck was 2605 N and occurred during the second head strike at 1189 msec with the neck in extension. This value exceeds the 2200 N tolerance value for compression-extension loading of the cervical spine listed in Table 7. The loading duration threshold for axial compression loading shown in Figure 47 is 734 N sustained over 27 msec. By examining the predicted neck forces, which were tabulated every millisecond, a force in excess of 734 N compressive was found to exist from 1177 to 1202 msec, a period of 25 msec. Since the force was significantly in excess of 734 N for a portion of this time interval, the threshold was considered to have been exceeded. Thus, the female subject would likely receive a significant neck injury due to compression-extension loading of the cervical spine during the second head strike. The typical mechanisms for such injuries are summarized in Table 6.

As previously stated, the injury estimates for both the male and female subjects not wearing a lap belt and seated at a computer terminal are summarized in Table 12.

c. Summary of Results for Subjects Seated at Computer

From the summary of estimated injury potentials for the male and female subjects seated at a computer provided in Table 12, it is apparent that the female subject would probably suffer significantly more injuries than the male subject. The male subject's only potential injury would be from lacerations caused by breakage of the

computer screen resulting from the second head strike. The female subject, however, would possibly receive a cerebral concussion during the first head strike. During the second head strike, the female subject would probably receive an additional cerebral concussion, possibly suffer a fractured zygomatic bone, and probably receive a significant neck injury due to compression-extension loading of the cervical spine.

Table 12. Summary of Results for Subjects at a Computer

	Time (msec)	Parameter	Value	Limit	Source (Ref. #)	Outcome
50th Percentile Male	No injury tolerances exceed. Potential exists for lacerations resulting from possible breakage of computer screen during direct head impact.					
5th Percentile Female	340	Head Ang. Accel.	1880 r/s^2	1800 r/s^2	19	Possible cerebral concussion
	1178	Head Ang. Accel.	2427 r/s^2	1800 r/s^2	19	Likely cerebral concussion
	1189	Head Cont. Force	360 lb	225 lb	20	Possible fracture of the zygomatic bone
	1189	Neck Axial Force	2605 N	2200 N	22	Likely significant neck injury

4. Summary of Results for Extensions of the Seated Simulation

From the summary of estimated injury potentials for all of the seated subjects provided in Table 13, several similarities and differences can be noted. The male and female subjects suffer similar injuries in the belted and unbelted cases, but in the computer case, the female suffers quite significant injuries while the male suffers essentially no injuries. The only cases for which whiplash injuries are likely to occur are the two belted cases. Cerebral concussion, however, is a possible, if not probable, occurrence in five of the six cases, with the male seated at the computer the only subject not likely to receive one.

There were no simulations in which the head contact forces developed were sufficient to result in possible skull fractures. However, both of the unbelted subjects and the female subject at a computer experienced head contact forces of sufficient magnitude to possibly fracture various facial bones. The female subjects in the unbelted and computer cases were the only subjects with possible significant neck injuries resulting from axial loading and only in the computer case is the neck injury probable.

Table 13. Summary of Injury Estimates for Seated Subjects

	Subject	Summary of Injury Estimates
Belted	50th %-ile Male	Possible cerebral concussion Probable whiplash injury Possible, but not likely, whiplash injury (two counts)
	5th %-ile Female	Possible cerebral concussion Probable whiplash injury Possible, but not likely, whiplash injury
Unbelted	50th %-ile Male	Possible cerebral concussion Possible fracture of the maxilla bone Possible fracture of the zygomatic bone
	5th %-ile Female	Possible cerebral concussion (two counts) Possible fracture of the lateral mandible bone Possible, but not likely, significant neck injury
Seated at computer	50th %-ile Male	Possible scalp lacerations
	5th %-ile Female	Possible cerebral concussion Probable cerebral concussion Possible fracture of the zygomatic bone Probable significant neck injury

D. EXTENSION OF STANDING SIMULATION

As previously described, the validated model of the deck excitation for Shot 9993 was extended to two separate situations. The first situation was with the subjects standing erect with legs straight. The second situation was with the subjects standing with their knees bent. As for the seated model, the simulation for each situation was

performed once of a 50th percentile adult male and once for a 5th percentile adult female. Thus, four separate situations were performed as extensions of the validated model of the deck excitation for Shot 9993.

1. Knees Initially Locked

a. Results for the male subject

The gross bodily motion experienced by the male subject with initially locked knees is illustrated in Figure 89. Upon the initial shock excitation of the deck, the subject toes pointed upward as the loading traveled through the heel into the torso through the legs. The pelvis was thrust forwards slightly and the inertia of the head caused the neck to move into flexion as the applied loading caused upwards motion of the body. The body remained airborne and experienced slight forward rotation until the feet contacted the deck shortly before 600 msec. At that point, the knees buckled and the downward motion of the body continued until the knees struck the deck. The inertia of the head resulted in hyperflexion of the neck as the downward motion of the body was checked by first foot, and then, at a later time, knee contact with the deck. The body rotated forwards, driving the head into hyperextension, until the upper torso and head contacted the deck at approximately 1250 msec. The upper portion of the body bounced off the deck and the head experienced another impact at approximately 1625 msec.

The multiple head impacts necessitated head impact injury estimation. The HIC was computed, using the ATB program, to be 33.74, well below the limit of 1000. Thus, no AIS ≥ 4 head injury is expected based on the HIC computation. The time interval found to maximize the HIC value was 708 to 862 msec, with an average acceleration of 8.6 g's. The peak linear acceleration of the center of gravity of the head was 98.8 g's, as seen in Figure 90, and it occurred during the first head strike at 1267 msec.

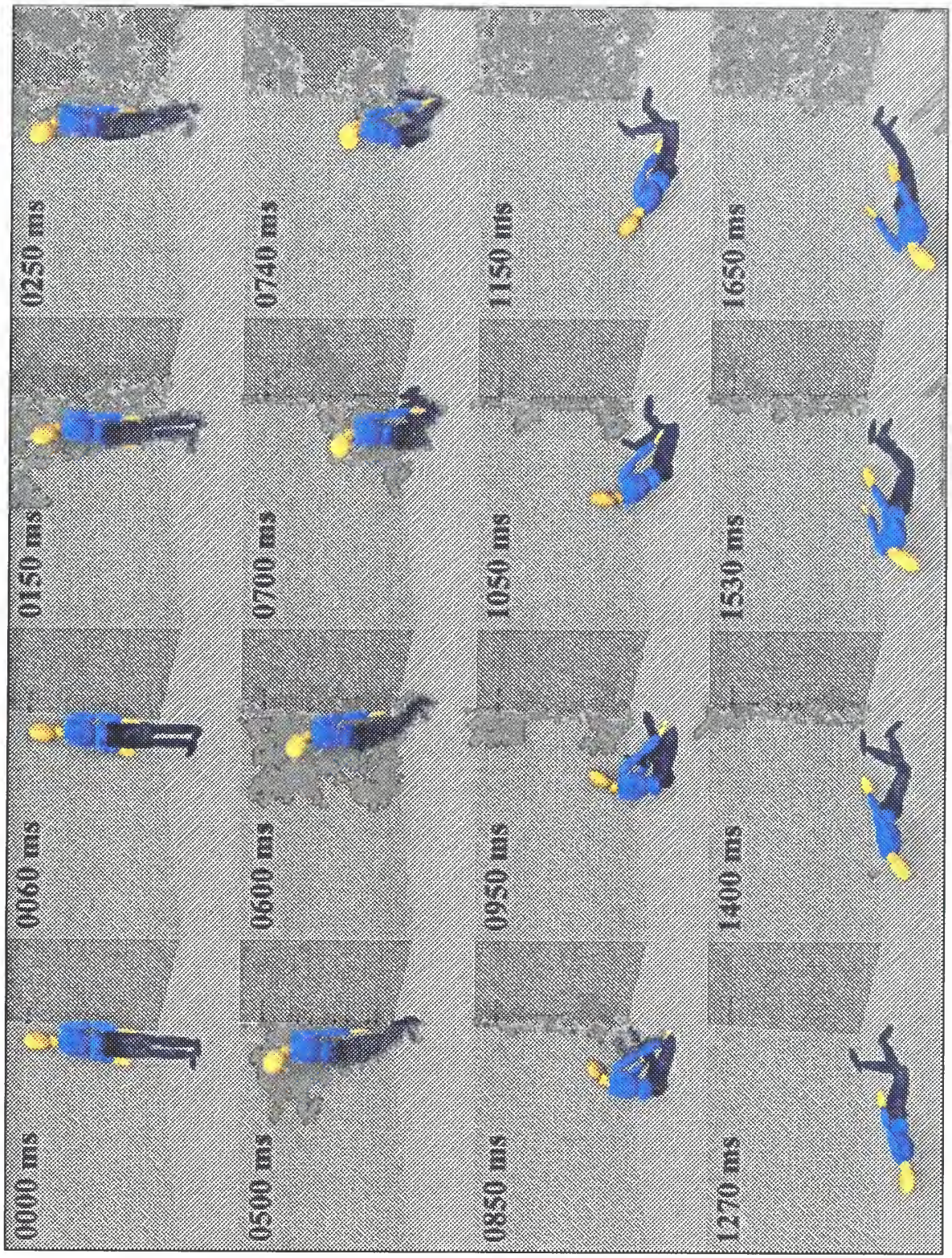

Figure 89. Predicted Motion of the Male Subject with Locked Knees

The head angular acceleration, as seen in Figure 91, and angular velocities, as seen in Figure 92, were examined and compared against the injury criteria for cerebral concussion. There were several angular acceleration peaks, the first of which occurred after the knees struck the deck and the body began to rotate forwards. The peak angular acceleration of the head during this period was 4425 rad/sec^2, occurring at 733 msec, with an associated peak angular velocity of 16.8 rad/sec occurring at 725 msec. The second angular acceleration peak occurred shortly after the first as the head reached the peak angle in extension. This peak value was 3132 rad/sec^2 and it occurred at 831msec. The angular velocity peak associated with this period was 18 rad/sec and it also occurred at 831 msec. The third angular acceleration peak occurred during the first head strike against the deck. The angular acceleration reached a peak value of 6321 rad/sec^2 at 1268 msec and had an associated peak angular velocity of 39.1 rad/sec which occurred at 1274 msec. The final angular acceleration peak occurred during the second head strike against the deck. The peak acceleration during this contact was 4955 rad/sec^2 and it occurred at 1649 msec. The associated angular velocity peak was 18.5 rad/sec and it occurred at the end of the simulation, 1650 msec. All four of these angular acceleration peaks are well above the 1800 rad/sec^2 tolerance value. Even though none of the angular velocity peaks exceeds the 50 rad/sec tolerance value, it is highly probable that each of these periods would result in a cerebral concussion based solely upon the angular acceleration values.

The head-deck contact forces, shown in Figure 93, were examined in order to make estimates of possible fractures of the bones of the skull or face. The first head strike resulted in peak contact force of 992 lb at 1267 msec. This contact was between the right cheek of the male subject and the deck and the force developed exceeds the 225 lb tolerance value for the zygomatic bone. Thus, the first head strike would likely result in a fracture of the subjects zygomatic bone. The second head strike resulted in a peak contact force of 635 lb at 1642 msec. This contact was between the frontal region of the subject's head and the deck and the force developed is below the 900 lb tolerance value for the frontal bone. Thus, the second head strike would not be expected to result in a fracture.

Examination of the head angular position with respect to the torso, as shown in Figure 94, revealed a peak angle in flexion of 101.1 degrees occurring at 736 msec. A torque at the occipital condyles of 94.3 ft-lb, shown in Figure 95, occurred at 733 msec and is well above the 65 ft-lb injury threshold for flexion. However, by examining the neck axial loading, as seen in Figure 96, it was determined that the neck was loaded in compression at this time so a whiplash type injury would not be expected. A peak torque at the occipital condyles of 58.9 ft-lb occurred at 832 msec with the neck reaching a peak extension angle of 51 degrees at 840 msec and lightly loaded. Since the 58.9 ft-lb torque is well above the 35 ft-lb injury threshold in extension, a whiplash injury would likely occur as the subject's head is hyperextended during forward motion of the torso. Another peak torque value occurred at 1649 msec with a magnitude of 81.4 ft-lb. The neck was only slightly extended at the time and loaded in compression, so it is not likely that a whiplash injury would be experience during this period.

The peak tensile load in the neck, 2870 N, occurred at 1266 msec as seen in Figure 96 and was a result of the first head contact with the deck. This value is well above the 1160 N tolerance value for tension-extension given in Table 7, but does not violate the loading duration curve shown in Figure 48. Thus, an injury resulting from tension-extension loading of the cervical spine is possible and a summary of such injuries mechanisms is provided in Table 6. Peak compressive loading occurred at 1270 msec (3490 N) and 1642 msec (3110 N) during the first and second head to deck contacts, respectively. Both of these loads exceed the 2200 N tolerance value for compression-extension loading but do not violate the loading duration curve. Thus, an injury resulting from compression-extension loading of the cervical spine is possible in each instance and a summary of such injury mechanisms is provided in Table 6.

For the standing subjects, substantial loads were expected to be developed throughout the legs, so the axial loading of both the femurs and lower legs were examined and the peak values compared against the associated injury tolerances. The right and left femurs experienced similar loads during the initial shock loading and during the first contact of the knees with the deck. The loads for the left femur are shown in Figure 97 and those for the right femur are shown in Figure 98. The left femur

experiences a peak compressive load of 6122 N at 57 msec and another peak load of 8120 N at 703 msec. The right femur experiences peak loads of 6021 N at 57 msec and 5605 N at 716 msec. Of these loads, only the second peak loading of the left femur exceeds the tolerance value of 7600 N. It remains greater than this value for four msec, but this is less than the 9 msec duration specified for this loading in Figure 49. As such, it was considered possible that the left femur would be fractured when the left knee struck the deck at approximately 700 msec.

Axial forces developed in the left and right lower legs, shown in Figure 99 and Figure 100, respectively, were also examined and the peak values compared against the injury probability curve for fracture of bones in the foot-ankle complex shown in Figure 51. The peak loading for both the left and right lower legs occurred at 57 msec. The left lower leg experienced a peak load of 8046 N and the right lower leg a load of 8168 N. These forces correspond to a probability of injury of approximately 70 percent.

The injury estimates for the male subject with initially locked knees are summarized in Table 14.

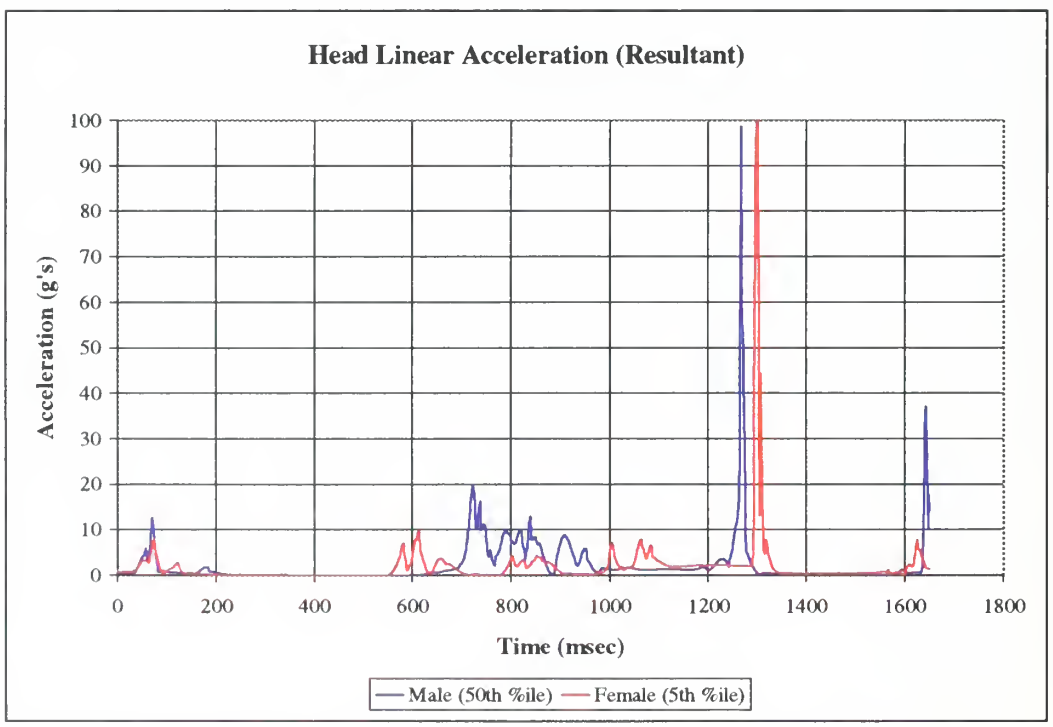

Figure 90. Head Linear Accelerations for Subjects with Locked Knees

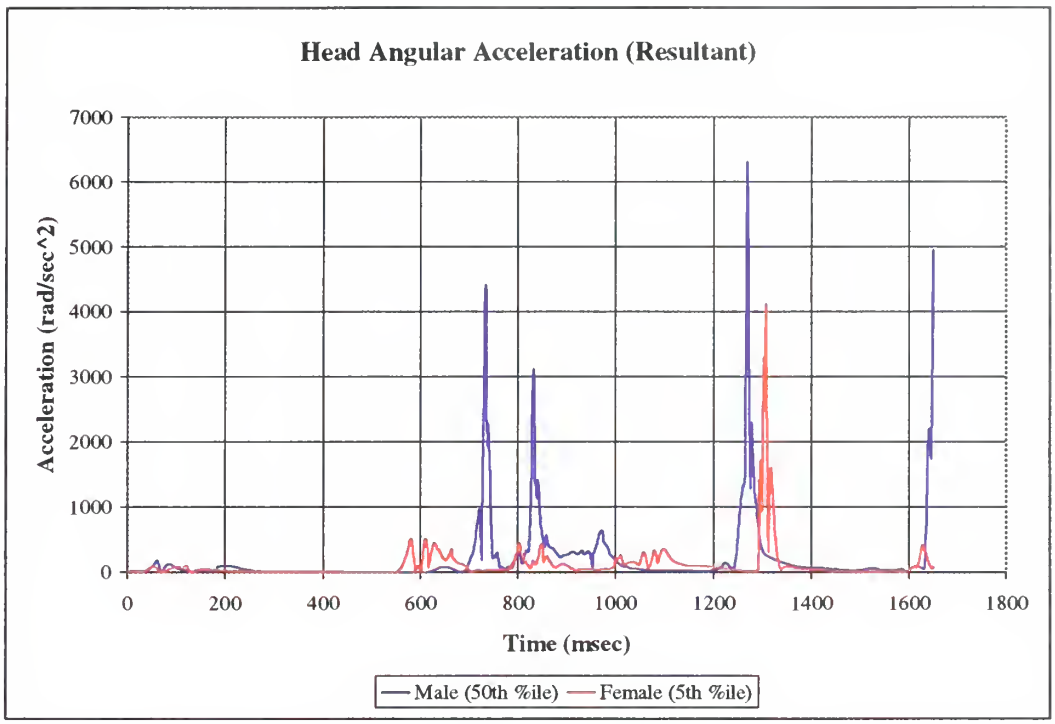

Figure 91. Head Angular Accelerations for Subjects with Locked Knees

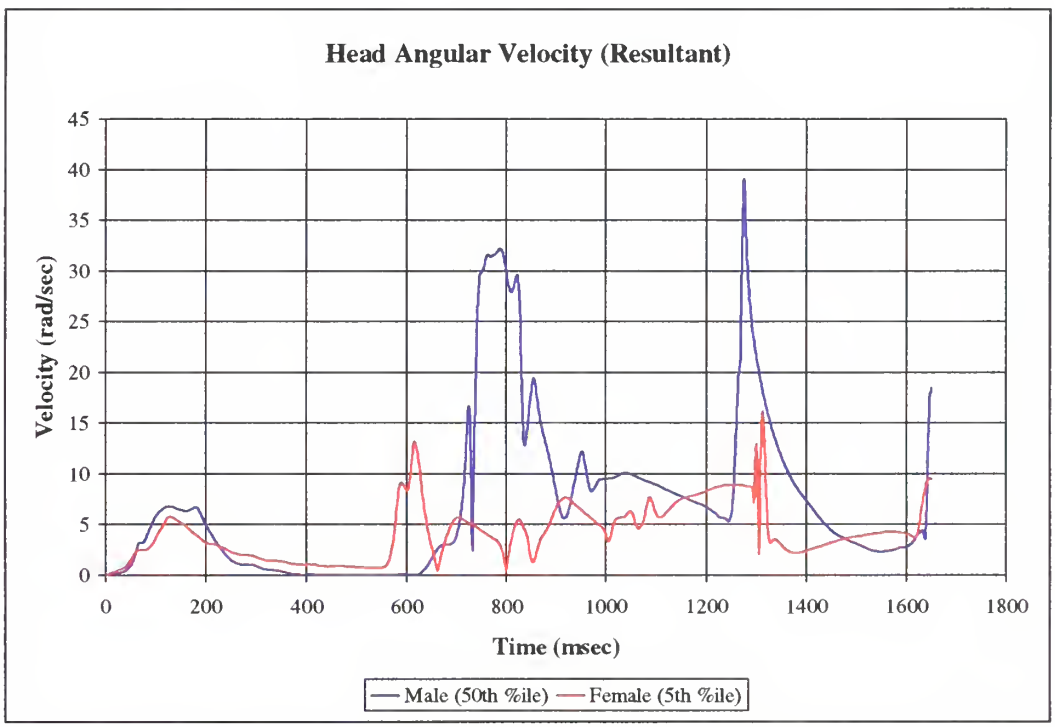

Figure 92. Head Angular Velocities for Subjects with Locked Knees

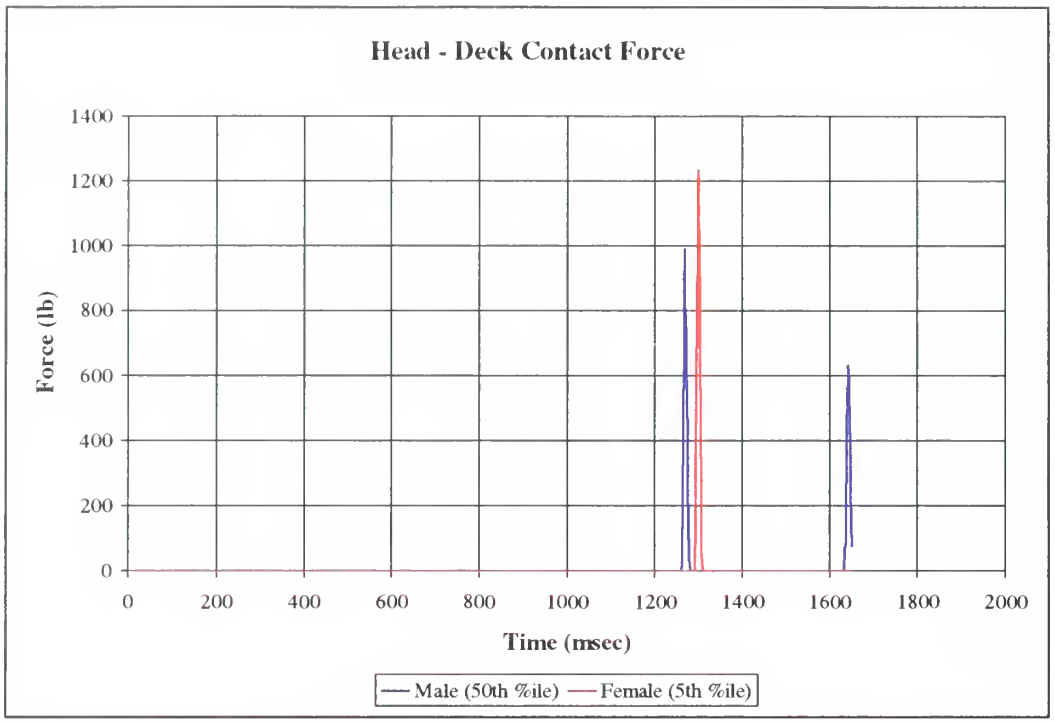

Figure 93. Head-Deck Contact Forces for Subjects with Locked Knees

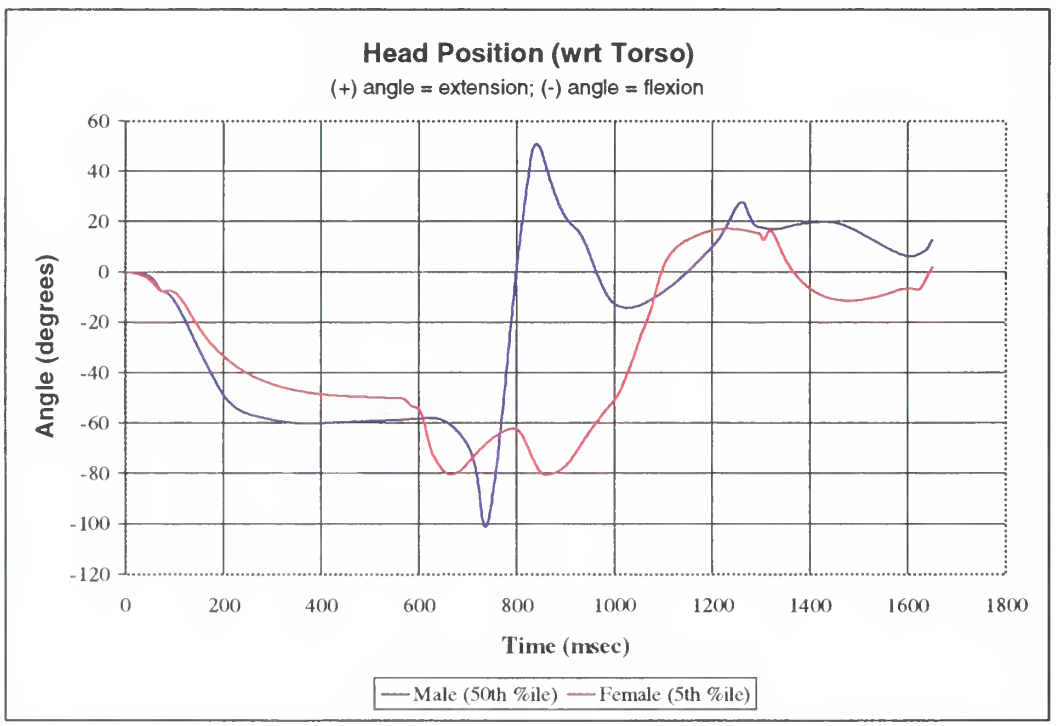

Figure 94. Head Angular Position for Subjects with Locked Knees

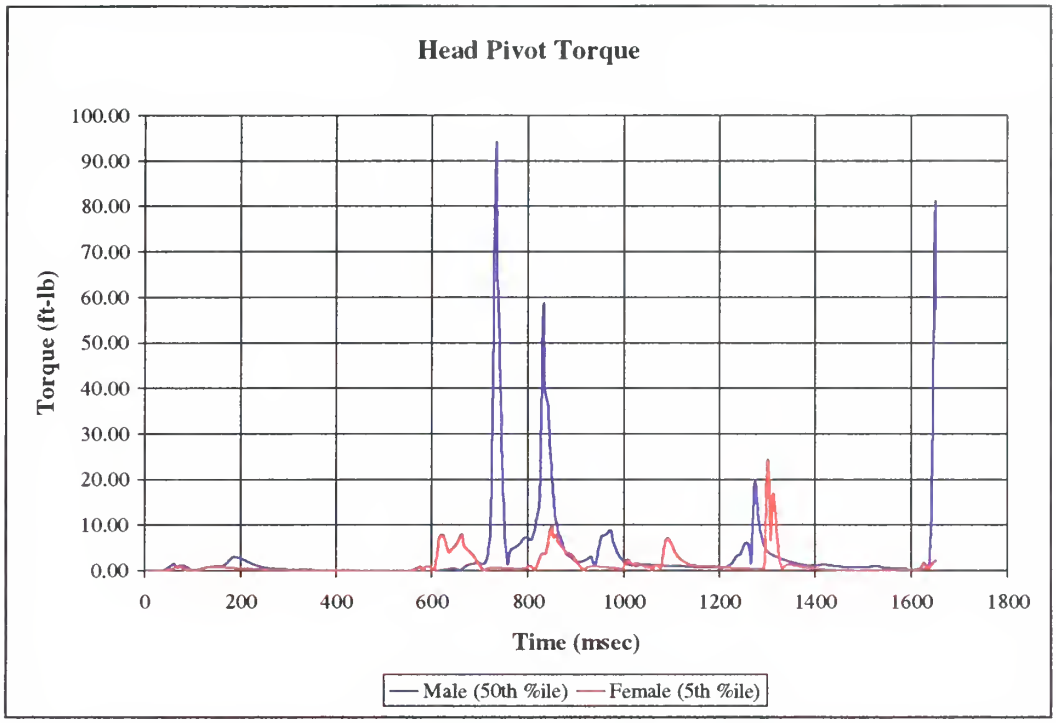

Figure 95. Head Pivot Torque's for Subjects with Locked Knees

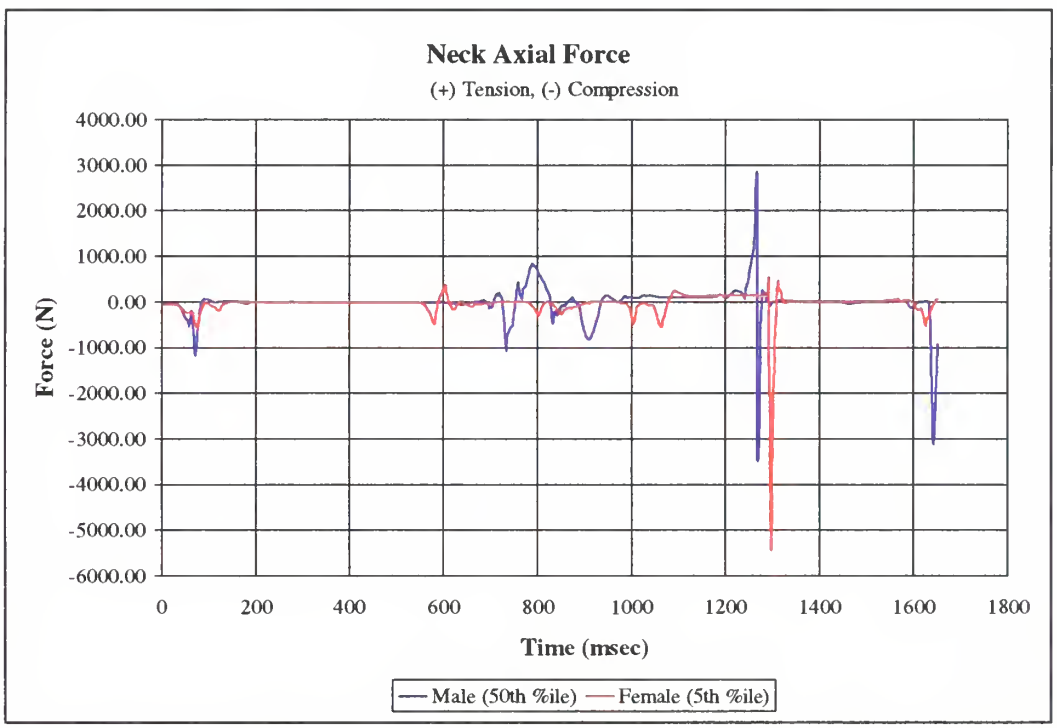

Figure 96. Neck Axial Forces for Subjects with Locked Knees

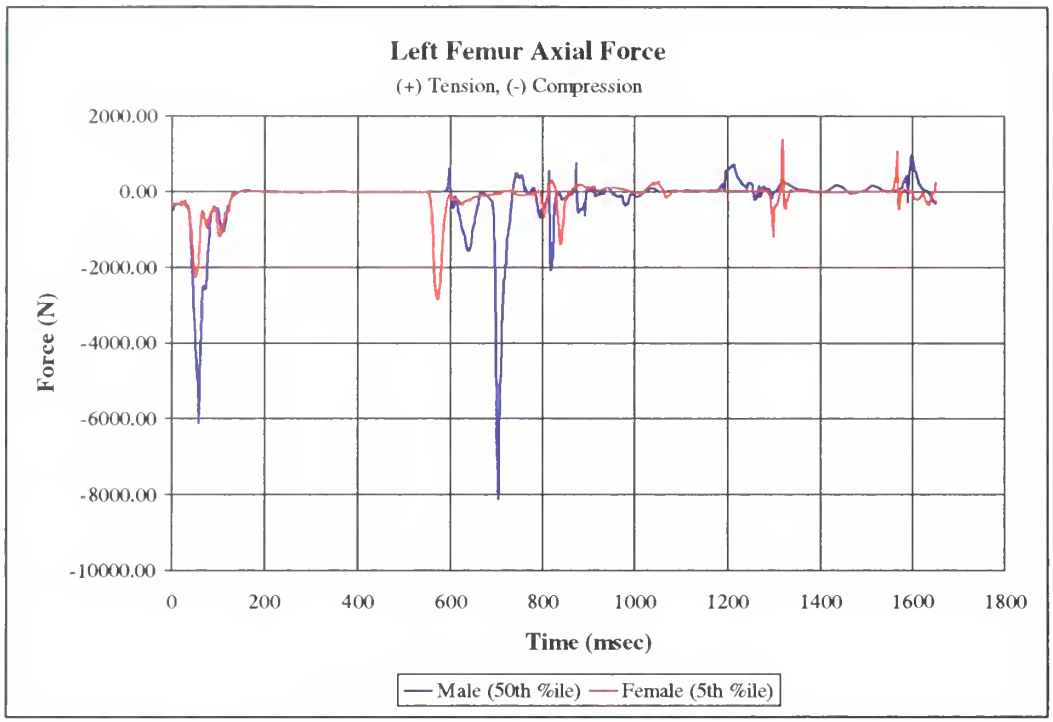

Figure 97. Left Femur Axial Forces for Subjects with Locked Knees

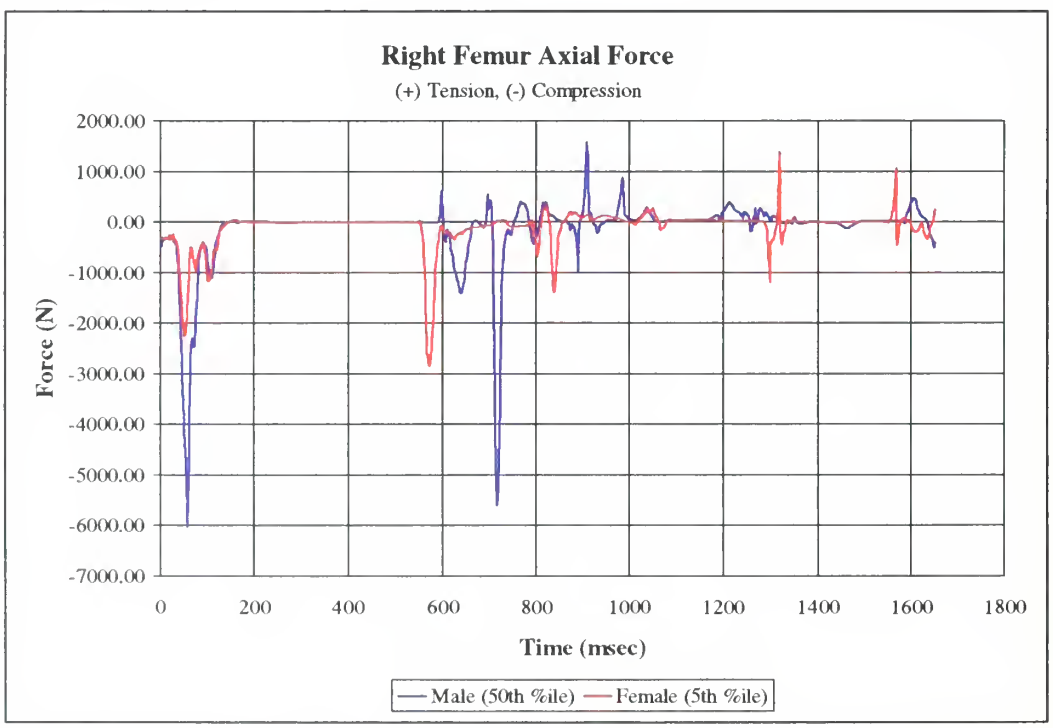

Figure 98. Right Femur Axial Forces for Subjects with Locked Knees

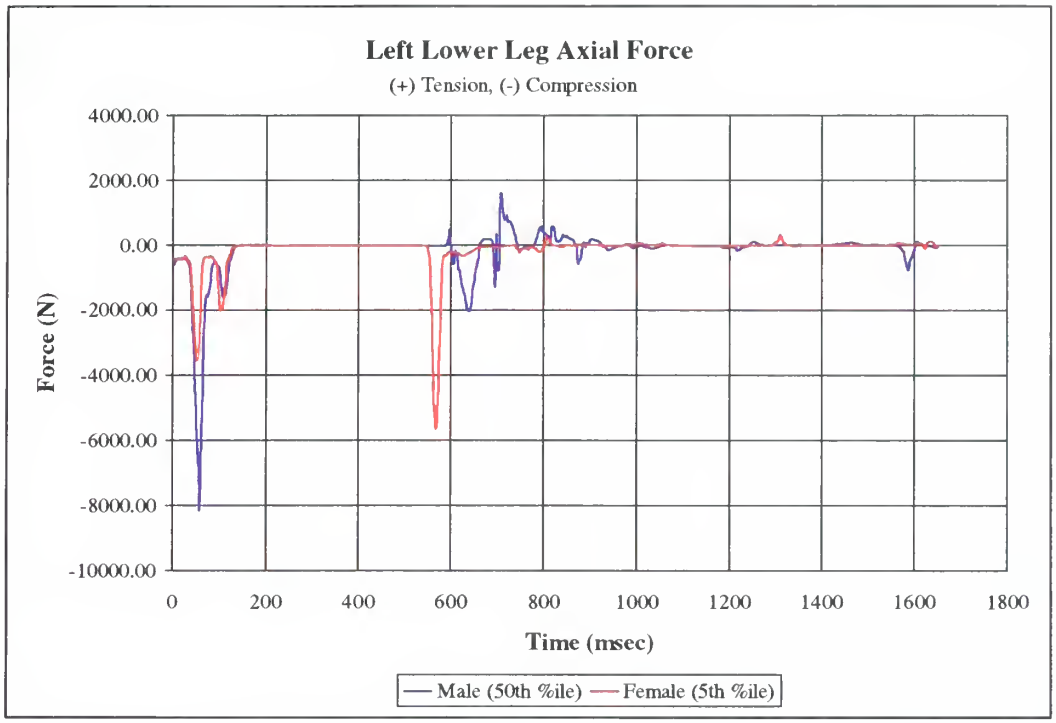

Figure 99. Left Lower Leg Axial Forces for Subjects with Locked Knees

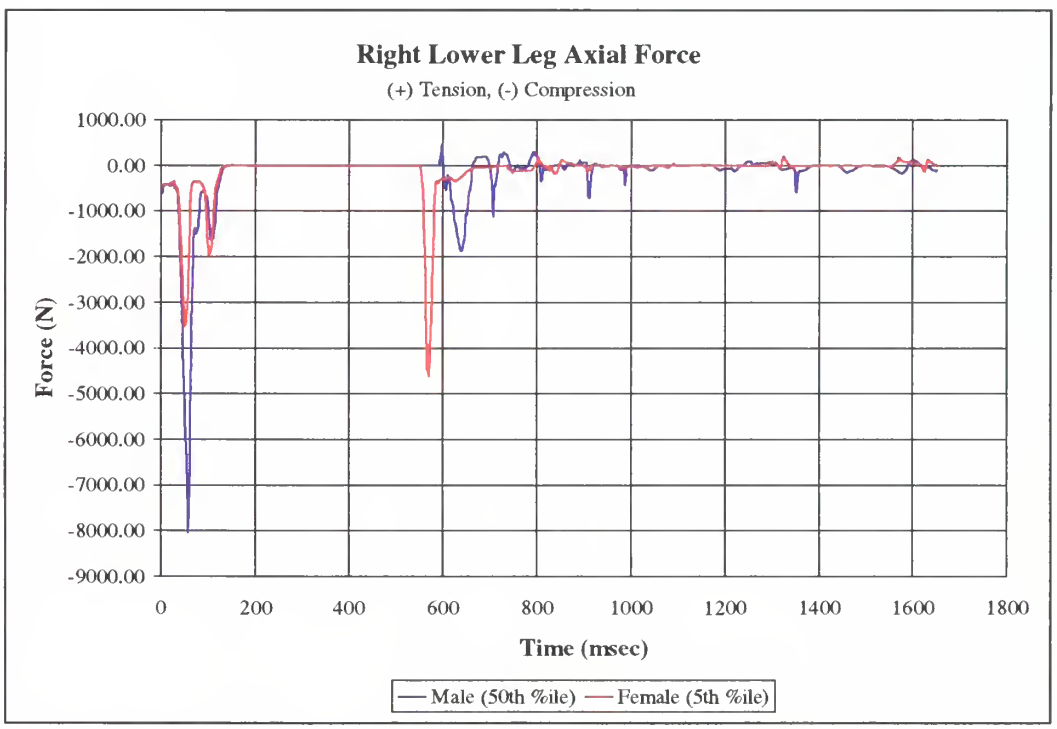

Figure 100. Right Lower Leg Axial Forces for Subjects with Locked Knees

b. Results for the female subject

The gross bodily motion of the female subject was very similar to that of the male subject. The female subject experienced the same motions of the feet, pelvis, and head during the initial shock excitation of the deck. The female subject also rotated slightly forward while airborne and her knees also buckled following foot contact with the deck. The female subject did not experience as much neck extension during the forward motion of the body following knee contact with the deck, but still had similar upper body and head contact with the deck. The female subject's upper body rebounded farther off the deck than did the male subject's and did not strike it a second time prior to the end of the simulation.

As for the male subject, the head impact injury estimates were performed for the female subject. The HIC was computed as 5.0 using the ATB program, well below the 1113 limit for the small female. Thus, no AIS ≥ 4 injury is expected based on the HIC computation. The time interval found to maximize the HIC value was 562 to 1249 msec, with an average acceleration of 2.2 g's. The peak linear acceleration of the center of gravity of the head was 108.4 g's, as seen in Figure 90, and it occurred during the head strike at 1298 msec.

The head angular acceleration, as seen in Figure 91, and angular velocities, as seen in Figure 92, were examined and compared against the injury criteria for cerebral concussion. In contrast to the male subject, the female subject experienced only one angular acceleration peak. This peak, 4125 rad/sec^2, occurred during the head contact with the deck at 1306 msec. The associated angular velocity peak was 16.2 rad/sec and it occurred at 1311 msec. Although the angular velocity is below the 50 rad/sec tolerance value, the angular acceleration is well above the 1800 rad/sec^2 tolerance value. Thus, the female subject is likely to receive a cerebral concussion during the head strike.

The head-deck contact force, shown in Figure 93, reached a peak value of 1237 lb at 1298 msec. This contact occurred between the right cheek of the female subject and the deck, and, since the peak force is well above the 225 lb fracture tolerance for the zygomatic bone, a fracture is likely.

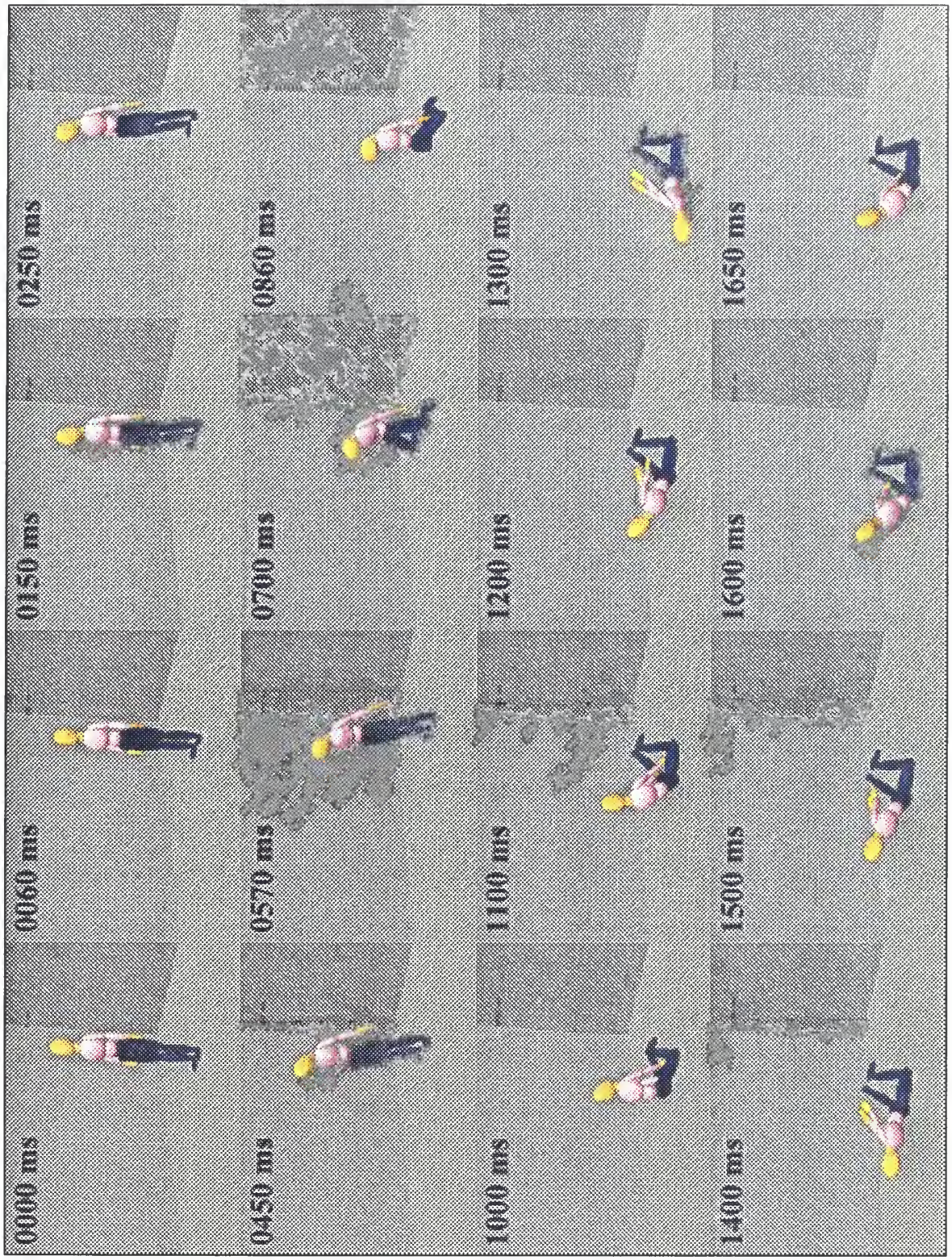

Figure 101. Predicted Motion of the Female Subject with Locked Knees

Examination of the head angular position with respect to the torso, as shown in Figure 94, revealed a peak angle in flexion of 80.4 degrees occurring at 665 msec. The torque at the occipital condyles associated with this peak angle, as seen in Figure 95, is well below the 44 ft-lb pain threshold in flexion. Since the neck is lightly loaded during this period, it is possible, but not likely, that the female subject would experience a whiplash injury during this period. Another peak angle in flexion was reached at 861 msec with an angle of 80.6 degrees. Again, this peak angle was associated with low head pivot torques and light axial loading of the neck. Thus, it was again considered possible, but not likely, that a whiplash injury would be experienced.

The peak compressive load experienced by the neck, 5437 N, occurred at 1298 msec as seen in Figure 96 and was a result of head contact with the desk. This load is well above both the 2200 N limit for compression-extension loading given in Table 7 and the duration of loading curve given in Figure 47. Thus, it is likely that the female subject would experience a significant neck injury due to compression-extension loading. A summary of the associated neck injury mechanisms is given in Table 6.

As for the male subject, the axial loading of both the femur and lower legs were examined. Similar to the male subject, the female subject experienced comparable loading in the left and right femurs during the initial shock excitation. Unlike the male subject, however, the second significant loading of the female subject's femurs occurred when the feet struck the deck at the end of the airborne period rather than when the knees struck the deck. The loads for the left femur are shown in Figure 97 and those for the right femur are shown in Figure 98. The left femur experienced a peak load of 2272 N at 51 msec and another peak load of 3628 N at 568 msec. The right femur experienced peak loads of 2255 N at 50 msec and 2843 N at 571 msec. All four of these peak loads are well below the 7600 N tolerance value as well as the duration of loading curve. Thus, no significant injury to the female subject's femurs is likely to occur.

Axial forces developed in the left and right lower legs, shown in Figure 99 and Figure 100, respectively, were also examined and the peak values compared against the injury probability curve for fracture of bones in the foot-ankle complex shown in Figure 51. A loading peak for the left lower leg occurred at 51 msec with a magnitude of

3542 N. The right lower leg experienced a corresponding peak load of 3524 N at 50 msec. Each of these loads corresponds to a probability of injury of approximately 9 percent. A second peak loading for the left lower leg occurred at 568 msec with a magnitude of 5646 N and an associated probability of injury of approximately 33 percent. A second peak loading of the right lower leg occurred at 569 msec with a magnitude of 4619 N and an associated probability of injury of approximately 18 percent.

The injury estimates for the female subject with initially locked knees are summarized in Table 15.

c. Summary of results for subjects with locked knees

From the summaries of estimated injury potentials for the male and female subjects with initially locked knees provided in Table 14 and Table 15, respectively, it is apparent that both subjects are likely to receive significant injuries. In addition, the male subject appears to suffer more severe injuries on the whole than does the female subject.

The male subject experiences probable cerebral concussion at four separate instances during the simulation. In addition, the male subject will probably sustain a whiplash injury and a fracture of the zygomatic bone. There are three separate instances for which axial loading of the cervical spine would possibly result in significant neck injury. The male subject would also possibly experience a fractured left femur and has a 70 percent likelihood of suffering a fractured bone in both the right and left foot-ankle complexes.

The female subject would probably receive a cerebral concussion, fracture of the zygomatic bone, and significant neck injury due to axial loading. On two separate instances the female subject could possibly receive a whiplash injury, but that occurrence is not likely. In addition, the female subject has 9 and 33 percent chances of experiencing a fracture within the left foot-ankle complex and 9 and 18 percent chances of experiencing a fracture within the right foot-ankle complex.

Table 14. Summary of Results for Male Subject with Locked Knees

	Time (msec)	Parameter	Value	Limit	Source (Ref. #)	Outcome
50th Percentile Male	733	Head Ang. Accel.	4425 r/s^2	1800 r/s^2	19	Probable cerebral concussion
	831	Head Ang. Accel.	3132 r/s^2	1800 r/s^2	19	Probable cerebral concussion
	1268	Head Ang. Accel.	6321 r/s^2	1800 r/s^2	19	Probable cerebral concussion
	1649	Head Ang. Accel.	4955 r/s^2	1800 r/s^2	19	Probable cerebral concussion
	1267	Head Cont. Force	992 lb	225 lb	20	Probable fracture of the zygomatic bone
	832	Head Pivot Torque	58.9 ft-lb	35 ft-lb	16	Probable whiplash injury
	1266	Neck Axial Force	2870 N	1160 N	23	Possible significant neck injury
	1270	Neck Axial Force	3490 N	2200 N	23	Possible significant neck injury
	1642	Neck Axial Force	3110 N	2200 N	23	Possible significant neck injury
	703	Femur Axial Force	8120 N	7560 N	8	Possible fracture of the left femur
	57	Lower Leg Axial Force	8046 N	Figure 51	25	70% likely fracture in left foot-ankle complex
	57	Lower Leg Axial Force	8168 N	Figure 51	25	70% likely fracture in right foot-ankle complex

Table 15. Summary of Results for Female Subject with Locked Knees

	Time (msec)	Parameter	Value	Limit	Source (Ref. #)	Outcome
5th Percentile Female	1306	Head Ang. Accel.	4125 r/s^2	1800 r/s^2	19	Probable cerebral concussion
	1298	Head Cont. Force	1237 lb	225 lb	20	Probable fracture of the zygomatic bone
	665	Head Ang. Position	80.4 deg (flexion)	58 deg.	13	Possible whiplash injury (not likely)
	861	Head Ang. Position	80.6 deg (flexion)	58 deg.	13	Possible whiplash injury (not likely)
	1298	Neck Axial Force	5437 N	2200 N	22	Probable significant neck injury
	51	Lower Leg Axial Force	3542 N	Figure 51	25	9% likely fracture in left foot-ankle complex
	50	Lower Leg Axial Force	3524 N	Figure 51	25	9% likely fracture in right foot-ankle complex
	568	Lower Leg Axial Force	5646 N	Figure 51	25	33% likely fracture in left foot-ankle complex
	569	Lower Leg Axial Force	4619 N	Figure 51	25	18% likely fracture in left foot-ankle complex

2. Knees Initially Bent

a. Results for the male subject

The gross bodily motion experienced by the male subject with initially bent knees is illustrated in Figure 102. This subject's motion was significantly different from that of the subject with locked knees. Upon the initial shock excitation of the deck, the subject's knees buckled and the torso dropped straight down until the subject was in a squatting position. The downward motion of the torso was arrested by contact with the upper legs and this resulted in flexion of the neck due to inertial loading. The next pulse in the deck loading resulted in the subject becoming airborne and rotating forward. When the subject contacted the deck again, it was with both knees and the top of the head. The subject then partially straightened out and bounced off the deck another time.

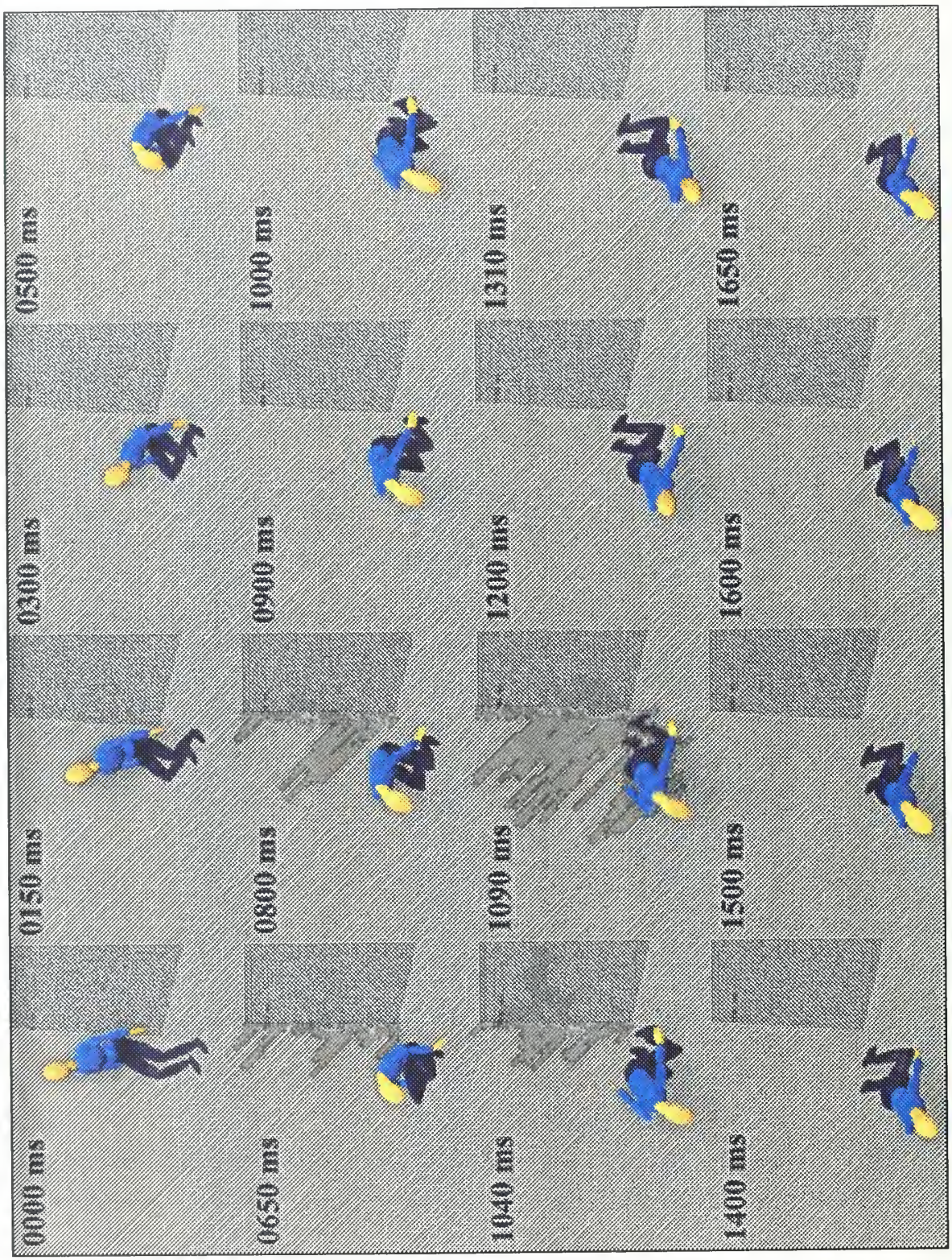

Figure 102. Predicted Motion of the Male Subject with Bent Knees

The HIC was computed using the ATB program to be 425, well below the limit of 1000. Thus, no AIS ≥ 4 head injury is expected based on the HIC computation. The time interval found to maximize the HIC value was 1049 to 107 msec, with an average acceleration of 51.8 g's. The peak linear acceleration of the center of gravity of the head was 86.7 g's, as seen in Figure 103, and it occurred during the initial contact of the head with the deck at 1065 msec.

The head angular accelerations, as seen in Figure 104, and angular velocities, as seen in Figure 105, were examined and compared against the injury criteria for cerebral concussion. There were two significant angular acceleration peaks, the first of which occurred during the initial contact of the head with the deck. The peak angular acceleration of the head during this period was 6863 rad/sec^2, occurring at 1082 msec, with an associated peak angular velocity of 33.9 rad/sec occurring at 1090 msec. The second angular acceleration peak was 4212 rad/sec^2, occurring at 1315 msec, with an associated peak angular velocity of 22.7 rad/sec occurring at 1320 msec. Even though neither of the angular velocity peaks exceeds the 50 rad/sec tolerance value, both angular acceleration peaks are well above the 1800 rad/sec^2 tolerance value and, as such, are likely to each result in cerebral concussion.

The head-deck contact forces, shown in Figure 106, were examined in order to make estimates of possible fractures of the bones of the face or skull. The first head strike resulted in a peak contact force of 1697 lb at 1053 msec. This contact was between the frontal region of the skull and the deck and the force developed exceeds the 900 lb tolerance value for the frontal bone. Thus, the first head strike would possibly result in a fracture of the subject's frontal bone. The second head strike resulted in a peak force of 588 lb at 1320 msec and occurred between the left cheek and the deck. This force exceeds the 225 lb tolerance value of the zygomatic bone and, as such, would possibly result in a fracture of the zygomatic bone. The final head strike developed a peak force of 591 lb at 1614 msec and occurred between the frontal region of the skull and the deck. As this value is well below the 900 lb tolerance value of the frontal bone, no fracture is likely.

Examination of the head angular position with respect to the torso, as shown in Figure 107, revealed a peak angle in flexion of 83.5 degrees occurring at 493 msec. A torque at the occipital condyles of 15.2 ft-lb, shown in Figure 108, occurred at 482 msec and is well below the 65 ft-lb injury threshold in flexion. Examination of the neck axial forces, as seen in Figure 109, revealed that the neck was lightly loaded during this period. Thus, a whiplash injury would be possible for this period, but not likely. A second peak angle in flexion of 86 degrees occurred at 1082 msec with a corresponding head pivot torque of 107 ft-lb, well above the 65 ft-lb injury threshold in flexion, occurring at 1082 msec. However, since the neck was loaded in compression at the time, no whiplash injury is expected to occur.

The peak compressive load in the neck, 10895 N, occurred at 1053 msec as seen in Figure 109 and was a result of the initial contact of the head with the deck. This value is well above all of the limits for compression-flexion loading of the neck and, as such, would probably result in a significant neck injury. A second peak compressive load in the neck, 3837 N, occurred at 1614 msec. This load is also above all of the limits for compression-flexion loading and would also likely result in a significant neck injury. A summary of typical compression-flexion injury mechanisms is provided in Table 6.

The peak loads in the left and right femurs occurred at different times. The left femur experienced a peak load of 2413 N at 1053 msec, as seen in Figure 110, during the initial contact of the knees with the deck. The right femur experienced a peak load of 3071 N at 1314 msec, as seen in Figure 111, during a subsequent contact between the right knee and the deck. Both peak loads are well below the tolerance values for compression loading of the femur and no injuries are expected to result.

The peak loads developed in the left and right lower legs, as seen in Figure 112 and Figure 113, respectively, occurred during the initial shock excitation of the deck. The left lower leg experienced a peak load of 1025 N at 113 msec and the right lower leg experienced a peak load of 1079 N at 111 msec. There is thus an essentially zero percent probability of injury to the foot-ankle complex as can be seen in Figure 51.

The injury estimates for both the male and female subjects with initially bent knees are summarized in Table 16.

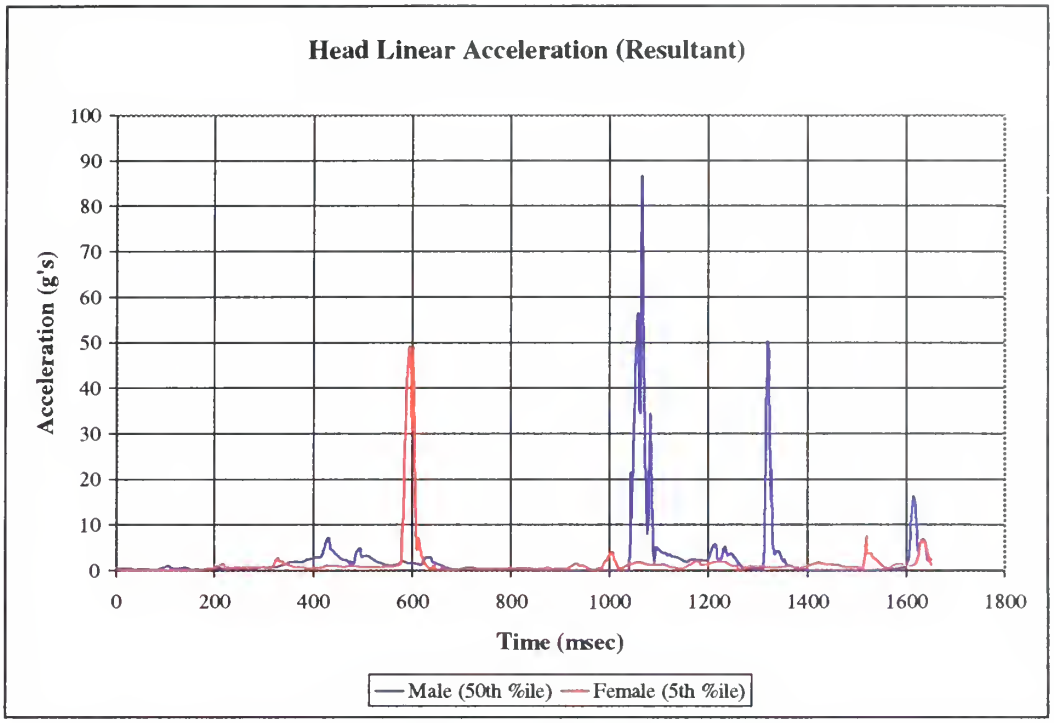

Figure 103. Head Linear Accelerations for Subjects with Bent Knees

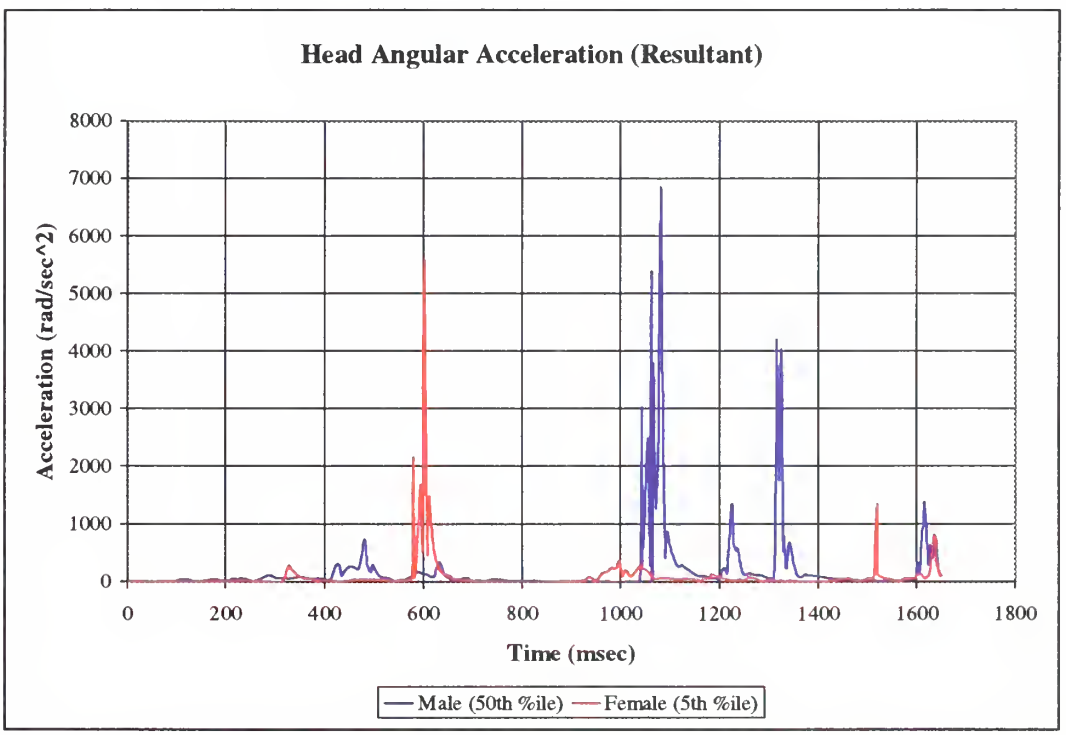

Figure 104. Head Angular Accelerations for Subjects with Bent Knees

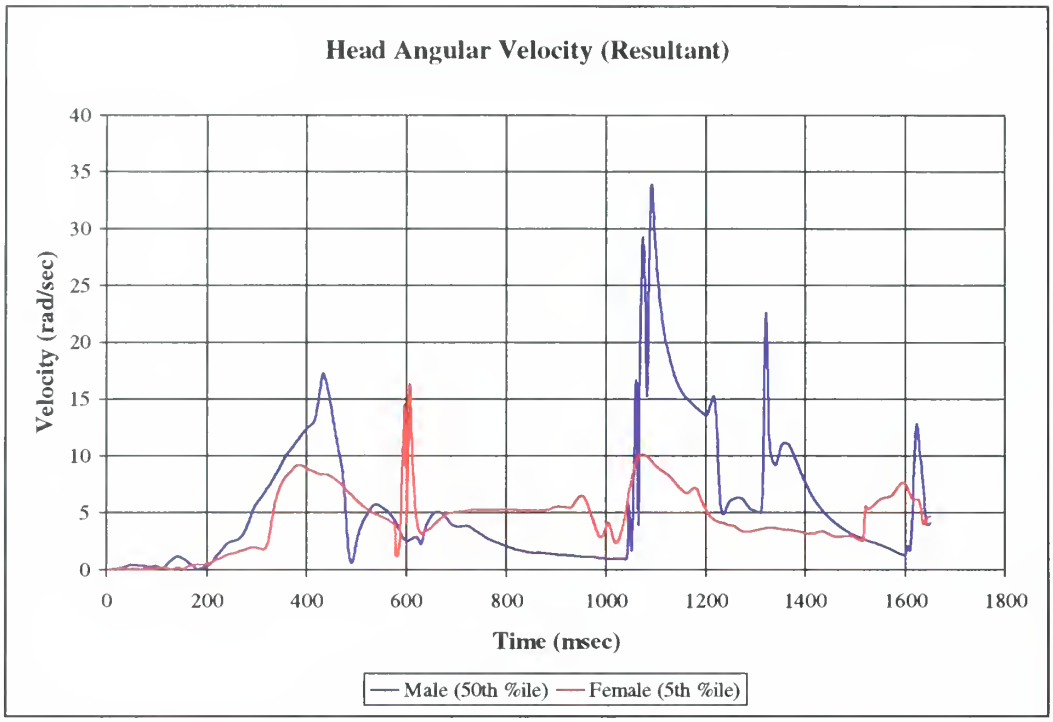

Figure 105. Head Angular Velocities for Subjects with Bent Knees

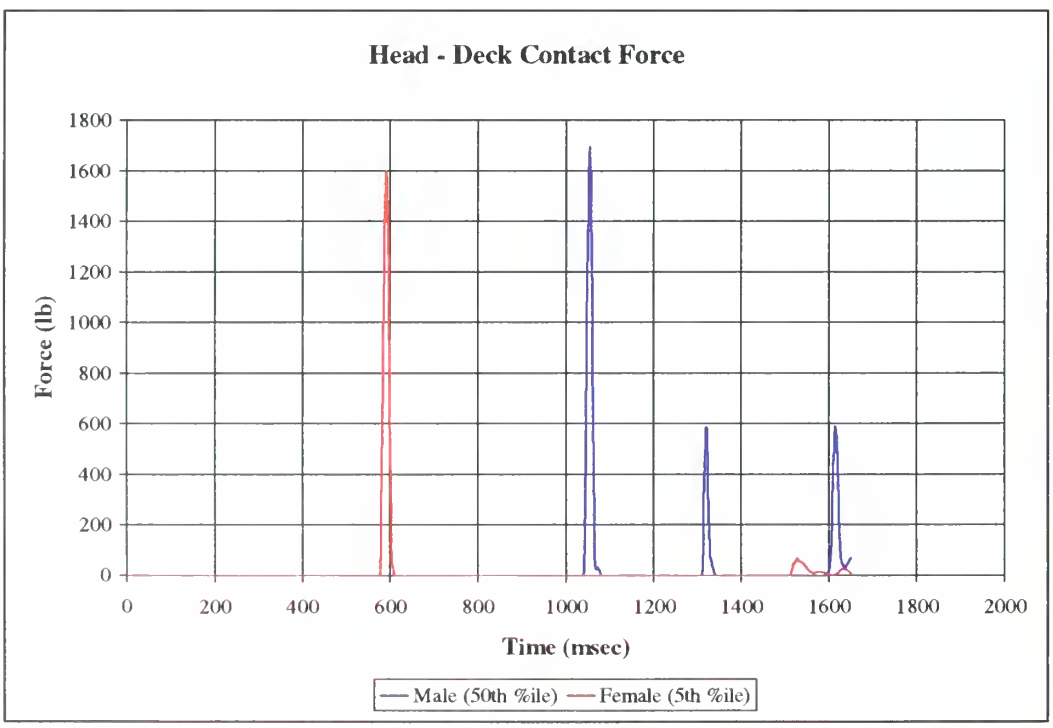

Figure 106. Head-Deck Contact Forces for Subjects with Bent Knees

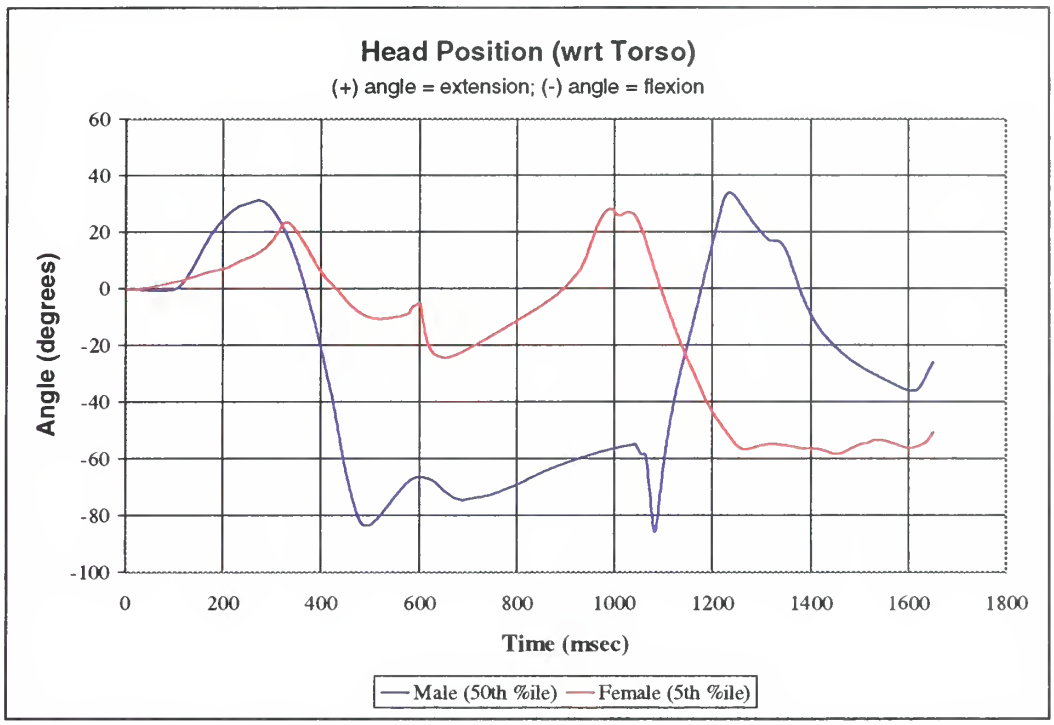

Figure 107. Head Angular Positions for Subjects with Bent Knees

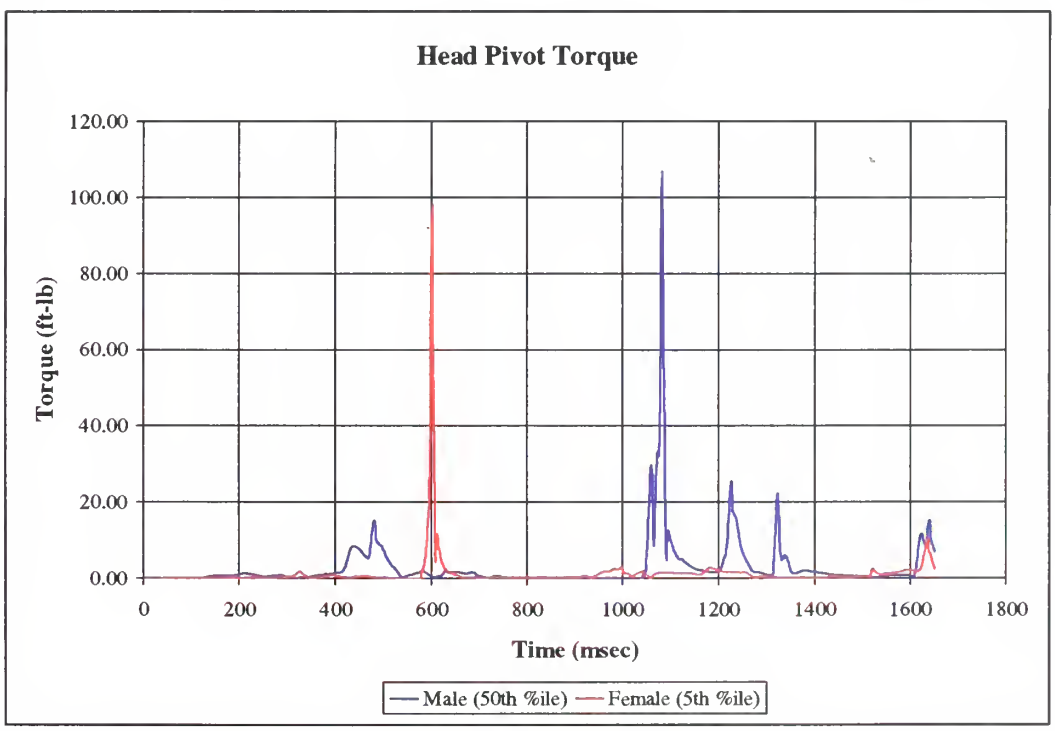

Figure 108. Head Pivot Torque's for Subjects with Bent Knees

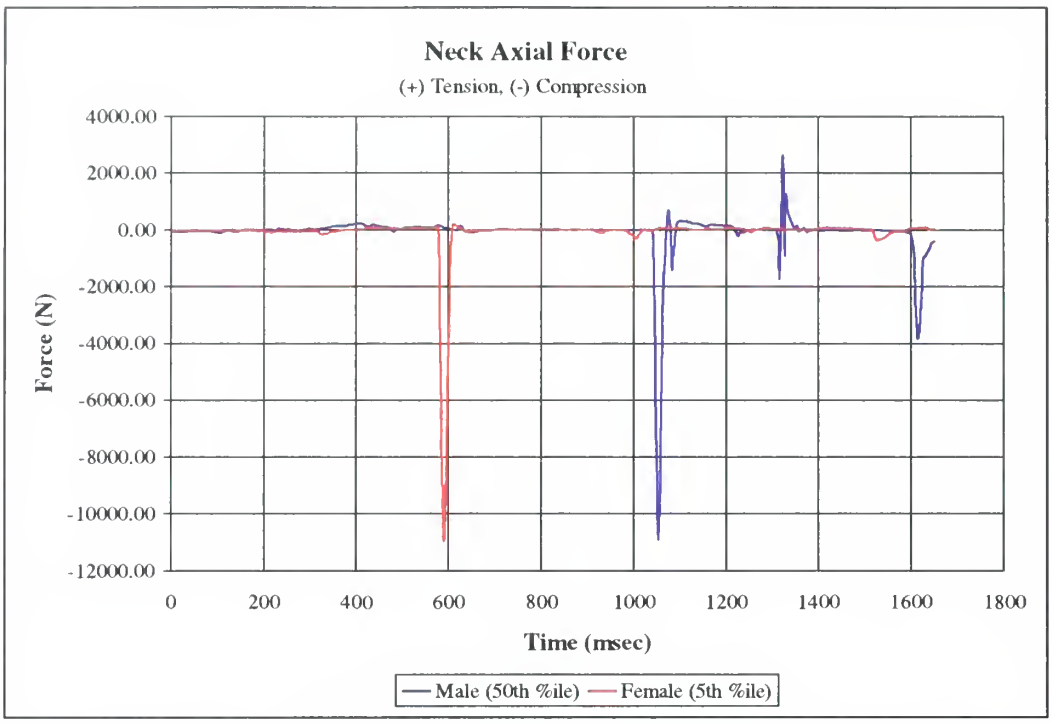

Figure 109. Neck Axial Forces for Subjects with Bent Knees

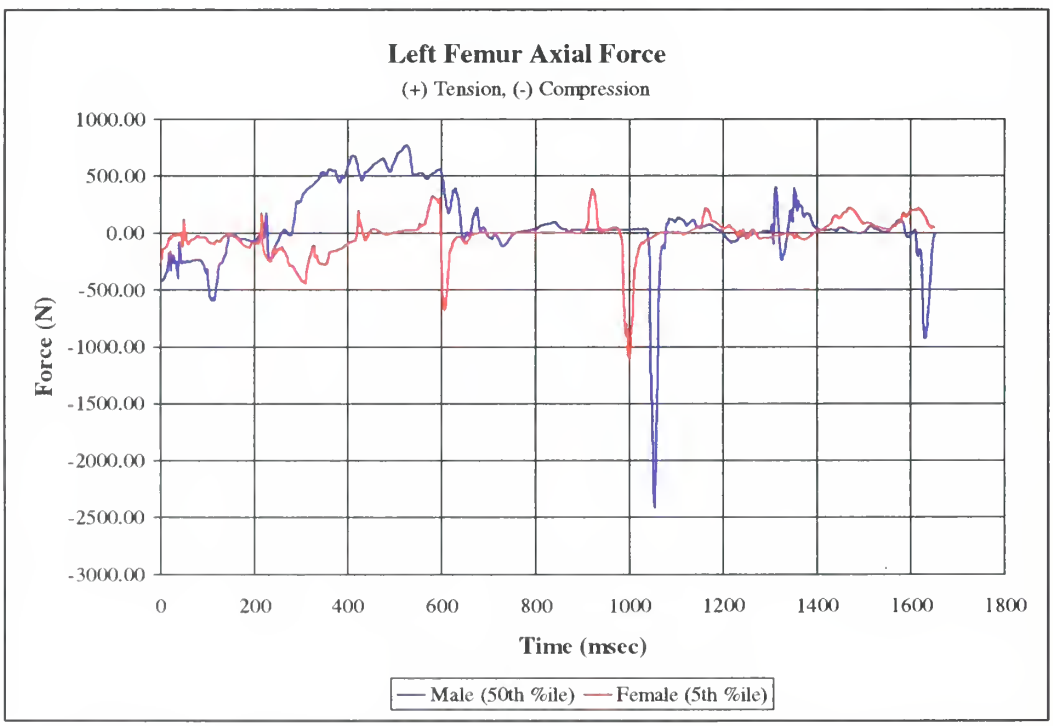

Figure 110. Left Femur Axial Forces for Subjects with Bent Knees

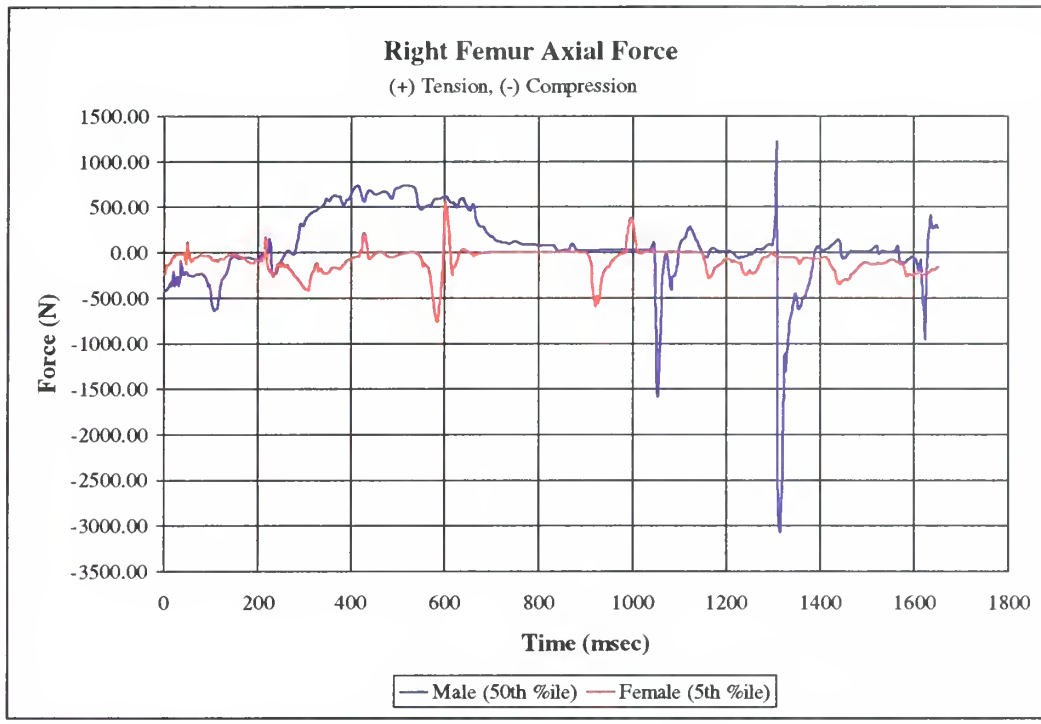

Figure 111. Right Femur Axial Forces for Subjects with Bent Knees

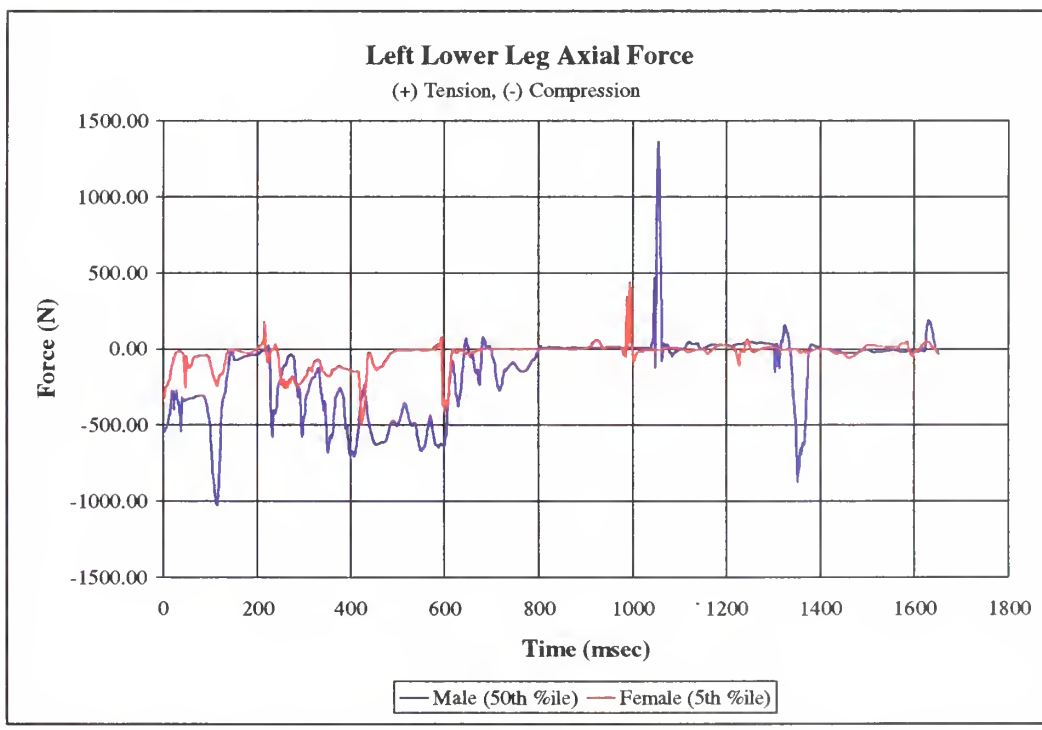

Figure 112. Left Lower Leg Axial Forces for Subjects with Bent Knees

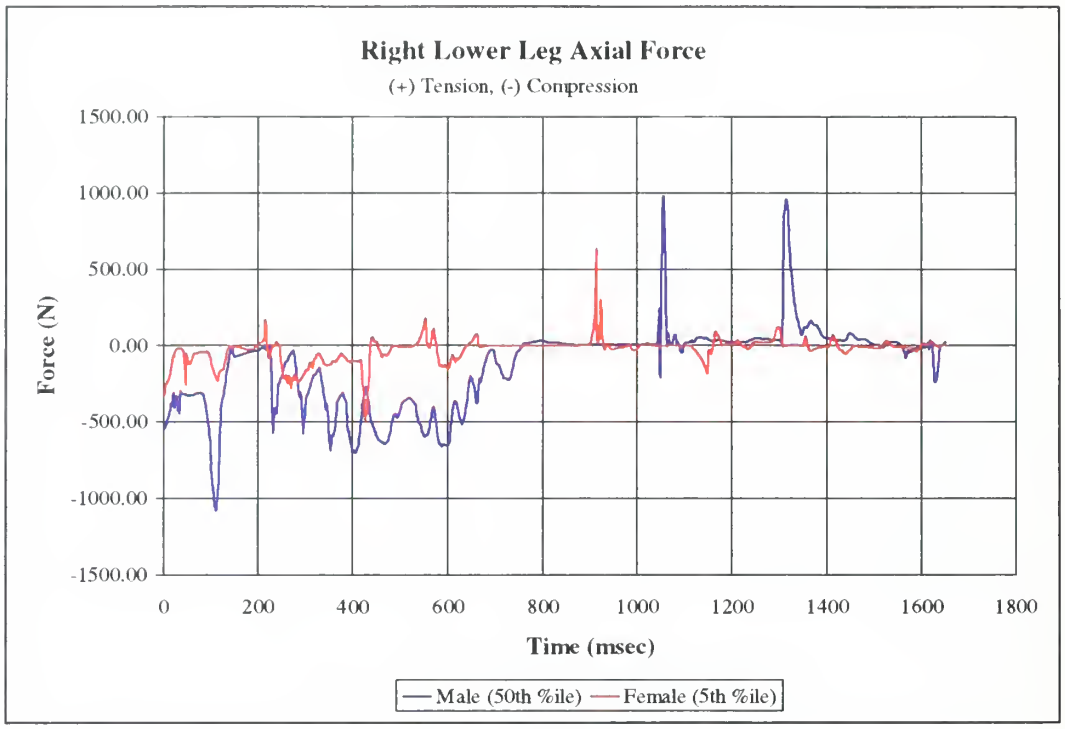

Figure 113. Right Lower Leg Axial Forces for Subjects with Bent Knees

b. Results for the female subject

The gross bodily motion for the female subject with initial bent knees was quite similar to that of the male subject up until the first head contact with the deck. The female subject experienced the head contact at an earlier time and rebounded higher than did the male subject. During the rebound, the female subject's extended arms got between the deck and the upper torso, and thus inhibited further contact between the head or upper torso and the deck.

The HIC was computed using the ATB program to be 205.3, well below the limit of 1113. Thus, no AIS $\geq$ 4 head injury is expected based on the HIC computation. The time interval found to maximize the HIC value was 583 to 604 msec, with an average acceleration of 39.4 g's. The peak linear acceleration of the center of gravity of the head was 49.1 g's, as seen in Figure 103, and it occurred during the initial contact of the head with the deck at 593 msec.

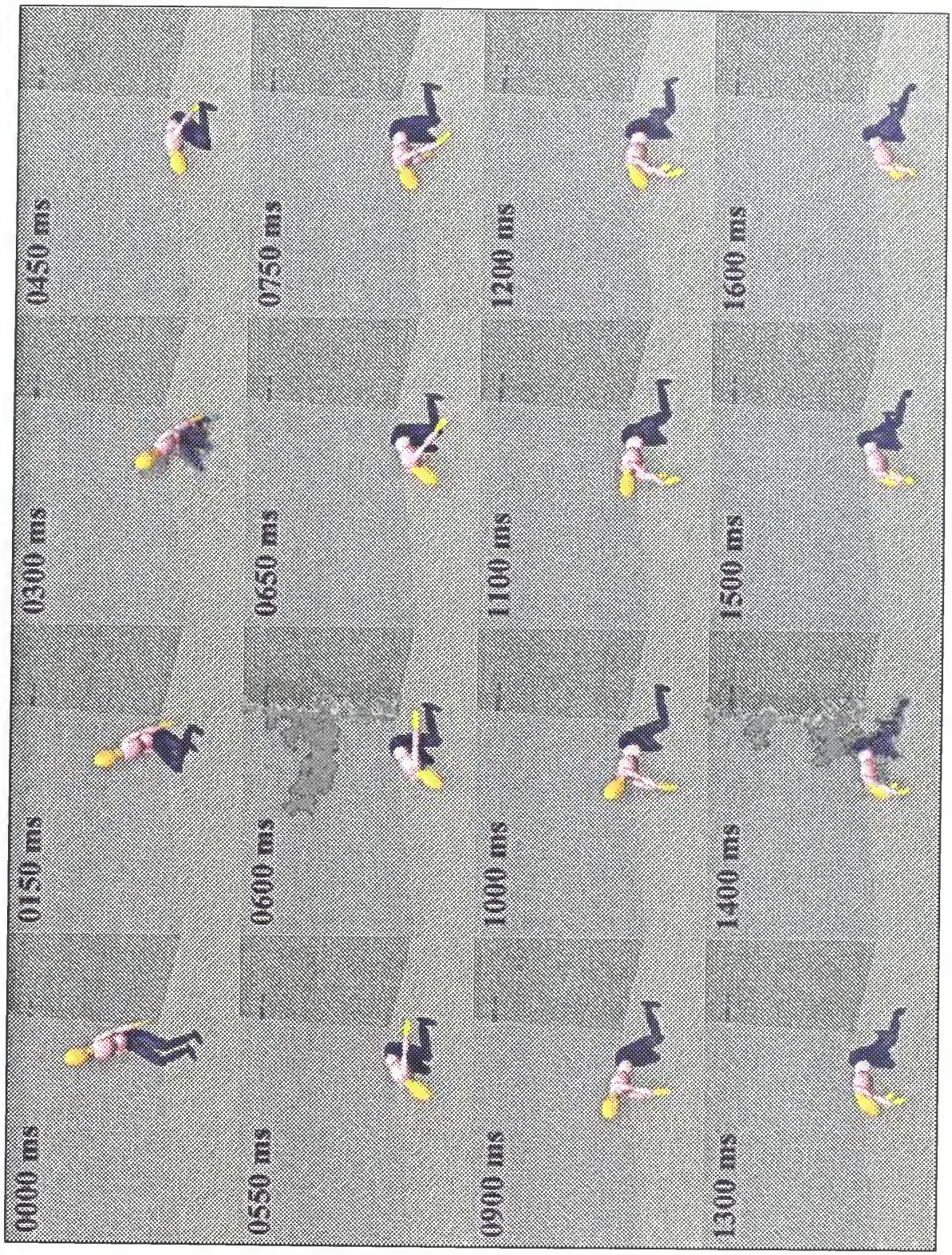

Figure 114. Predicted Motion of the Female Subject with Knees Bent

The head angular accelerations, as seen in Figure 104, and angular velocities, as seen in Figure 105, were examined and compared against the injury criteria. The peak angular acceleration occurred at 601 msec during the initial head strike and had a magnitude of 5597 rad/sec^2. The associated angular velocity was 16.3 rad/sec and it occurred at 607 msec. Although the angular velocity is below the 50 rad/sec tolerance value, the angular acceleration is well above the 1800 rad/sec^2 tolerance value and the female subject would probably receive a cerebral concussion during this head impact.

The head-deck contact forces, shown in Figure 106, were examined in order to make estimates of possible fractures of the bones of the face or skull. The initial head contact with the deck developed a peak force of 1598 lb at 590 msec and occurred between the frontal region of the skull and the deck. This force exceeds the 900 lb tolerance value for the frontal bone and, as such, would possibly result in a fracture of the frontal bone.

Examination of the head angular position with respect to the torso, as shown in Figure 107, revealed no excessive flexion or extension angles. A peak occipital condyle torque of 98.4 ft-lb occurred at 601 msec, as shown in Figure 108. This value exceeds the 65 ft-lb injury threshold value in flexion, but, since the neck is loaded in compression during this period, as can be seen in Figure 109, no whiplash injury is expected.

The peak compressive load in the neck, 10958 N, occurred at 590 msec as seen in Figure 109 and was a result of the initial contact of the head with the deck. This value is well above all of the limits for compression loading of the neck and, as such, would probably result in a significant neck injury. A summary of typical compression injury mechanisms is provided in Table 6.

As for the male subject, the left and right peak femur loads occurred at separate times. The left femur experienced a peak load of 1092 N at 998 msec, as seen in Figure 110, during the second contact of the left knee with the deck. The right femur experienced a peak load of 760 N at 584 msec, as seen in Figure 111, during the first contact between the right knee and the deck. Both peak loads are well below the

tolerance values for compression loading of the femur and no injuries are expected to result.

The peak loads developed in the left and right lower legs, as seen in Figure 112 and Figure 113, respectively, were quite low. The left lower leg experienced a peak load of 497 N at 422 msec and the right lower leg experienced a peak load of 491 N at 426 msec. The is an essentially zero percent probability of injury to the foot-ankle complex associated with these loads, as can be seen in Figure 51.

The injury estimates for both the male and female subjects with initially bent knees are summarized in Table 16.

c. Summary of results for subjects with bent knees

From the summaries of estimated injury potentials for the male and female subjects with initially bent knees provided in Table 16 it is apparent that both subjects are likely to receive significant injuries. In addition, the male subject appears to suffer more severe injuries than does the female subject.

The male subject experiences two probable cerebral concussions, two probable significant neck injuries due to axial loading, possible fractures to the frontal and zygomatic bones, and possible, but not likely, whiplash injury. The female subject experiences a probable cerebral concussion, probable significant neck injury, and possible fracture of the frontal bone.

Table 16. Summary of Results for Subjects with Bent Knees

	Time (msec)	Parameter	Value	Limit	Source (Ref. #)	Outcome
50th Percentile Male	1082	Head Ang. Accel.	6863 r/s^2	1800 r/s^2	19	Probable cerebral concussion
	1315	Head Ang. Accel.	4212 r/s^2	1800 r/s^2	19	Probable cerebral concussion
	1053	Head Cont. Force	1697 lb	900 lb	20	Possible fracture of the frontal bone
	1320	Head Cont. Force	588 lb	225 lb	20	Possible fracture of the zygomatic bone
	493	Head Ang. Position	83.5 deg. (flexion)	58 deg.	13	Possible whiplash injury (not likely)
	1053	Neck Axial Force	10895 N	2000 N	23	Probable significant neck injury
	1614	Neck Axial Force	3837 N	2000 N	23	Probable significant neck injury
5th Percentile Female	601	Head Ang. Accel.	5597 r/s^2	1800 r/s^2	19	Probable cerebral concussion
	590	Head Cont. Force	1598 lb	900 lb	20	Possible fracture of the frontal bone
	590	Neck Axial Force	10958 N	6000 N	23	Probable significant neck injury

3. Summary of Results for Extensions of the Standing Simulation

From the summary of estimated injury potentials for all of the standing subjects provided in Table 17, several similarities and differences can be noted. The male and female subjects suffer similar injuries within each case. In general, the male subject suffers more injuries than does the female subject. The only cases for which leg injuries are expected to occur are the two cases where the subject's knees were initially locked. In neither case was there a possibility of the female subject receiving a whiplash injury, but the male subject could have received one in each of the cases. In all cases, the subject is likely to receive at least one cerebral concussion, fracture to one or more bones of the face and skull, and at least one significant neck injury.

Table 17. Summary of Injury Estimates for Standing Subjects

	Subject	Summary of Injury Estimates
Knees Locked	50th %-ile Male	Probable cerebral concussion (four counts) Possible fracture of the zygomatic bone Probable whiplash injury Possible significant neck injury (three counts) Possible fracture of the left femur 70% likely fracture in the left foot-ankle complex 70% likely fracture in the right foot-ankle complex
	5th %-ile Female	Probable cerebral concussion Probable fracture of the zygomatic bone Possible, but not likely, whiplash injury (two counts) Probable significant neck injury 33% likely fracture in the left foot-ankle complex 18% likely fracture in the right foot-ankle complex
Knees Bent	50th %-ile Male	Probable cerebral concussion (two counts) Possible fracture of the frontal Possible fracture of the zygomatic bone Possible, but not likely, whiplash injury Probable significant neck injury (two counts)
	5th %-ile Female	Probable cerebral concussion Possible fracture of the frontal bone Probable significant neck injury

E. OVERALL SUMMARY OF RESULTS

From the summaries of injury estimates for the seated subjects provided in Table 13 and those for the standing subjects provided in Table 17, it is clear that the standing subjects are likely to receive more serious injuries than the seated subjects. The injuries experienced by the seated subjects tended to be whiplash, cerebral concussion, and fractures of the bones of the face. Those experienced by the standing subjects tended to be cerebral concussion, fractures of the bones of both the face and skull, and significant neck injuries. In addition, the standing subjects with initially locked knees tended to receive injuries to the legs, in particular the bones in the foot-ankle complex. With the

exception of the simulation of the subjects seated at a computer, the female subject tended to receive less severe injuries than did the male subject.

VII. CONCLUSIONS AND RECOMMENDATIONS

A. CONCLUSIONS

On the basis of the results presented in the previous chapter, the following conclusions are drawn:

1. The Articulated Total Body program is a viable tool for simulating both male and female personnel, seated and standing, in shipboard environments during underwater explosion events.

2. Standing subjects tended to experience more significant injuries than did seated subjects. This correlation is not entirely conclusive since the two simulation used different shock excitations.

3. Female subjects, with the exception of the simulation of subjects seated at a computer, tended to experience less severe injuries than did the male subjects.

4. Significant injuries can be expected for both seated and standing personnel in a shipboard environment subjected to a shock induced excitation.

5. The selection and application of injury criteria to predicted motion is extremely complex.

B. RECOMMENDATIONS

The following are recommendations for further research in this area:

1. Future shock testing of test vessels should include a detailed plan for measuring the response of anthropomorphic test devices in a variety of positions. In particular, the ATD's should be instrumented with not only triaxial linear accelerometers in the head, thorax and pelvis, but with neck and chest load sensors, sternum deflection sensors, femur load sensors, lower leg load sensors, and angular accelerometers. Collection of this data would facilitate evaluation of the injury potential for a given underwater explosion event by allowing direct comparison of recorded data against the appropriate injury criteria.

2. Future shock testing involving ATD's should use high speed film, and sufficient lighting, to record the motion of the dummy. The use of high speed film, as opposed to standard videotape, would provide a clearer image as well as a definite time reference and would greatly facilitate validation of a model.

3. Further analysis and simulation of both seated and standing personnel should be conducted for various shock conditions and shipboard environments. This study examined the effects of only two underwater explosion events on two ATD's although video and accelerometer data exists for many more cases.

4. Further investigation should be performed into the application of injury criteria in acceleration induced trauma and impact loading as applied to the ship shock environment. In particular, very little information concerning the injury tolerances for female subjects was found.

5. An attempt should be made to use the ATB program as a design tool. For example, simulated modifications to the operator's chair could be modeled and the effects on predicted injuries noted. Thus, the ATB program could be used in an iterative manner to determine what chair properties would minimize the injury potentials for male and female subjects of varying sizes.

LIST OF REFERENCES

1. Oglesby, D.B. and Y.S. Shin, *ATB Program and Its Applications to Biodynamic Response Simulation of Underwater Explosion Events*, Technical Report NPS-ME-98-002, Naval Postgraduate School, Monterey, CA, March 1998.

2. Obergefell, L.A., et. al., *Articulated Total Body Model Enhancements Volume 2: User's Guide*, AAMRL-TR-88-043, 1988.

3. Fleck, J.T., and F.E. Butler, *Validation of the Crash Victim Simulator, Volume I: Engineering Manual, Part I: Analytical Formulation*, DOT-HS-806279, Vol. 1., Part 1., 1981.

4. Cheng, H., et. al., *Generator of Body Data (GEBOD) Manual*, AL/CF-TR-1994-0051, 1994.

5. Leetch, B.D. and W.L. Bowman, *Articulated Total Body (ATB) "VIEW" Program Software Report, Part II, User's Guide*, AAMRL-TR-81-111, Vol. 2., 1983.

6. Sides, T.J., *Submarine Shock Test Vehicle (SSTV)*, 1997.

7. Naval Surface Warfare Center Carderock Division Underwater Explosions Research Department.

8. *Anthropomorphic Dummies for Crash and Escape System Testing*, AGARD Advisory Report 330, 1996.

9. Backaitis, S.H. and H.J. Mertz, eds., *Hybrid III: The First Human Like Crash Test Dummy*, Society of Automotive Engineers, Warrendale, PA, 1996.

10. Marieb, E.N., *Human Anatomy and Physiology*, The Benjamin/Cummings Publishing Company, Inc., Redwood City, CA, 1991.

11. Thomas, C.L., ed., *Taber's Cyclopedic Medical Dictionary*, F.A. Davis Company, Philadelphia, PA, 1993.

12. Calais-Germain, B., *Anatomy of Movement*, Eastland Press, Seattle, WA, 1993.

13. Panjabi, M.M. and A.A.White III, "Biomechanics of Spinal Injuries" in A. Sances, Jr., et. al., eds., *Mechanisms of Head and Spine Trauma*, Aloray, Goshen, NY, 1986, pp. 237-264.

14. Kallieris, D., et. al., "Considerations for a Neck Injury Criterion" in *The 35th Stapp Car Crash Conference Proceedings*, Society of Automotive Engineers, Warrendale, PA, 1991, pp. 401-417.

15. Levine, R.S., "Musculoskeletal Injuries of the Cervical Spine" in R.S. Levine, ed., *Head and Neck Injury*, Society of Automotive Engineers, Warrendale, PA, 1994, pp. 157-173.

16. Mertz, H.J. and L.M. Patrick, "Strength and Response of the Human Neck" in S.H. Backaitis, ed., *Biomechanics of Impact Injury and Injury Tolerances of the Head-Neck Complex*, Society of Automotive Engineers, Warrendale, 1993, pp. 821-846.

17. Stakes, J.D., et. al., *The Abbreviated Injury Scale 1980 Revision*, American Association for Automotive Medicine, Morton Grove, IL, 1980.

18. Sances, A., Jr. and N. Yoganandan, "Human Head Injury Tolerance" in A. Sances Jr., et. al., eds., *Mechanisms of Head and Spine Trauma*, Aloray, Goshen, NY, 1986, pp. 189-215.

19. Ommaya, A.K., et. al., "Comparative Tolerances for Cerebral Concussion by Head Impact and Whiplash Injury in Primates" in S.H. Backaitis, ed., *Biomechanics of Impact Injury and Injury Tolerances of the Head-Neck Complex*, Society of Automotive Engineers, Warrendale, PA, 1993, pp. 265-274.

20. Allsop, D., "Skull and Facial Bone Trauma: Experimental Aspects" in A.M. Nahum and J.W. Melvin, eds., *Accidental Injury: Biomechanics and Prevention*, Springer, New York, NY, 1993, pp. 247-267.

21. Porta, D.J., "Introduction to Head and Neck Anatomy" in R.S. Levine, *Head and Neck Injury*, Society of Automotive Engineers, Warrendale, PA, 1994, pp. 1-38.

22. McElhaney, J.H. and B.S. Myers, "Biomechanical Aspects of Cervical Trauma" in A.M. Nahum and J.W. Melvin, eds., *Accidental Injury: Biomechanics and Prevention*, Springer, New York, NY, 1993, pp. 311-361.

23. Sances, A., Jr., et. al., "Spinal Injuries with Vertical Impact" in A. Sances Jr., et. al., eds., *Mechanisms of Head and Spine Trauma*, Aloray, Goshen, NY, 1986, pp. 305-348.

24. King, J.J., et. al., "Femur Load Injury Criteria—A Realistic Approach" in *The 17th Stapp Car Crash Conference Proceedings*, Society of Automotive Engineers, Warrendale, PA, 1973, pp. 509-524.

25. Yoganandan, N., et. at., "Dynamic Axial Tolerance of the Human Foot-Ankle Complex" in *The 40th Stapp Car Crash Conference Proceedings*, Society of Automotive Engineers, Warrendale, PA, 1996, pp. 207-218.

26. Crandall, J.R., et. al., "Biomechanical Response and Physical Properties of the Leg, Foot, and Ankle" in *The 40th Stapp Car Crash Conference Proceedings*, Society of Automotive Engineers, Warrendale, PA, 1996, pp. 173-192.

INITIAL DISTRIBUTION LIST

		No. Copies
1.	Defense Technical Information Center 8725 John J. Kingman Rd., STE 0944 Ft. Belvoir, VA 22060-6218	2
2.	Dudley Knox Library Naval Postgraduate School 411 Dyer Rd. Monterey, CA 93943-5101	2
3.	Professor Y.S. Shin, Code ME/Sg Department of Mechanical Engineering Naval Postgraduate School Monterey, CA 93943	5
4.	Professor Y.W. Kwon, Code ME/Kw Department of Mechanical Engineering Naval Postgraduate School Monterey, CA 93943	1
5.	Naval/Mechanical Engineering Curricular Office (Code 34) Department of Mechanical Engineering Naval Postgraduate School Monterey, CA 93943	1
6.	LT Douglas B. Oglesby 1225 B General Street Virginia Beach, VA 23464	1
7.	Robert Bowser NAVSEA 03P3, NC4-Rm. 374 Naval Sea Systems Command 2531 Jefferson Davis Highway Arlington, VA 22242	1
8.	Dana Johansen NAVSEA 03P4, NC4-Rm. 438 Naval Sea Systems Command 2531 Jefferson Davis Highway Arlington, VA 22242	1

9. Mark Lotz — 1
National Biodynamics Laboratory
P.O. Box 29407
New Orleans, LA 70189-0407

10. Dr. Salvadore Guccione — 1
National Biodynamics Laboratory
P.O. Box 29407
New Orleans, LA 70189-0407

11. Michael Riley — 1
Naval Surface Warfare Center, Carderock Division
Underwater Explosions Research Department
1445 Crossways Blvd.
Chesapeake, VA 23320

12. Michael Winnette — 1
Naval Surface Warfare Center, Carderock Division
Underwater Explosions Research Department
1445 Crossways Blvd.
Chesapeake, VA 23320

13. Fred Costanzo — 1
Naval Surface Warfare Center, Carderock Division
Underwater Explosions Research Department
1445 Crossways Blvd.
Chesapeake, VA 23320

14. Tom Sides — 1
Naval Surface Warfare Center, Carderock Division
Underwater Explosions Research Department
1445 Crossways Blvd.
Chesapeake, VA 23320

15. Dr. Louise Obergefell — 1
Armstrong Laboratory – AL/CFBV
2610 Seventh Street
WPAFB, OH 45433-7901

DUDLEY KNOX LIBRARY
3 2768 00366782 5